OBITUARY

Rear Admiral Sir Philip Clarke, K.B.E., C.B., D.S.O., C.Eng., M.I.E.R.E. died at his home at Christchurch, Hampshire, on 13th November 1966. Sir Philip had achieved distinction both as a naval officer and as professional engineer: he was President of the Institution from 1955 to 1956.

Born in December 1898, he entered the Royal Navy as a Cadet in 1911 and went to sea as a Midshipman from 1914 to 1917, during which time he saw action in the Channel, the Dardanelles and with the Grand Fleet. On promotion to Sub-Lieutenant he served with the Dover Patrol. In the period between the wars he qualified as a Specialist Torpedo Officer and successfully completed the course at the Royal Naval Staff College. He was promoted to Captain in 1938. In December 1943 he was made a Companion of the Distinguished Service Order in recognition of gallantry in action with enemy destroyers and he was twice mentioned in despatches.

Sir Philip was appointed Director of Manning at the Admiralty from 1946 to 1948 and was promoted to Rear Admiral in January 1948; he served as Flag Officer Malta and Admiral Superintendent Malta until August 1950. He was made a Companion of the Most Honourable Order of the Bath in the Birthday Honours List in 1949. Admiral Clarke retired from the Royal Navy in May 1951 but was called back to be Director of the Naval Electrical Department in August 1951; his work in this appointment was recognized in 1954 when he was created a Knight Commander of the Most Excellent Order of the British Empire. He finally retired from the Royal Navy in 1955.

Sir Philip Clarke gave a great deal of his time and energies to the Institution, particularly after his retirement from the Royal Navy. He served on the Professional Purposes Committee and as a Trustee of the Institution's Benevolent Fund; he was elected to be a Vice-President in 1952.

The Council has sent a message of sympathy to Lady Clarke and the Institution was represented at the funeral service.

INSTITUTION NOTICES

Conference on Solid State Devices

The Institute of Physics and The Physical Society jointly with the Institution of Electrical Engineers, the Institution of Electronic and Radio Engineers and the Institute of Electrical and Electronics Engineers, United Kingdom and Eire section, is arranging a conference of about three days' duration in the period 4th to 8th September 1967, to be held at the University of Manchester Institute of Science and Technology.

The object of the conference is to provide a forum for the presentation of applied research work in the physics and characterization of solid-state devices, together with associated technologies.

The I.E.R.E. representative on the joint organizing committee is Professor F. J. Hyde, D.Sc. (Member). Members wishing to receive information on the submission of contributions and attendance should write to the Institution at 9 Bedford Square, London, W.C.1.

Air Traffic Control Systems

'Air Traffic Control Systems Engineering and Design' is the subject of a Conference to be held at the London headquarters of the Institution of Electrical Engineers, from 13th to 17th March 1967. It is being sponsored by the I.E.E. Electronics Division and the I.E.R.E.

The Conference will cover:

Information Services (including communications, navigational aids, primary and secondary radar systems and equipment); and

Data Handling and Displays (including display for air traffic control, methods of character production and presentation, tracking systems and automatic tracking, transmission and storage of radar information, the role of the computer in air traffic control.

Registration forms and other details are available from the I.E.R.E., 9 Bedford Square, London, W.C.1.

U.K.A.C. Control Convention

A second U.K.A.C. Control Convention, on 'Advances in Computer Control', will be held at the University of Bristol from 11th to 14th April, 1967. It is being organized by the Institution of Electrical Engineers in conjunction with the other Engineering Institutions and Societies of the United Kingdom Automation Council.

The theme of the Convention is intended to illustrate the impact of computers on techniques and applications of automatic control. Papers will be grouped under the following main headings:

Theory of computer control, including modelling; applications in utilities; materials forming and handling; process industries; food, petroleum, chemical, extractive industries, etc.; transport—communications and control; scientific and medical applications.

Application forms and further information may be obtained from the U.K.A.C. Secretariat, Institution of Electrical Engineers, Savoy Place, London, W.C.2.

U.D.C. 621.396.62.029.45

A Spectrographic Receiver for V.L.F. Transmissions

By

G. L. JONES, B.Sc.,†

R. A. MORRIS, B.Sc.†

AND

N. R. POLETTI, N.Z.C.S.†

Presented at the New Zealand National Electronics Conference sponsored jointly by the New Zealand Section of the I.E.R.E. and the New Zealand Electronics Institute, Inc., in Auckland in August 1966.

Summary: This paper describes a multiple filter spectrograph for recording the spectrum of a radio signal in the v.l.f. band. The primary use of the equipment is in recording the Doppler shift of v.l.f. signals received via the whistler mode. There are other uses in narrow-band filtering applications.

1. Introduction

The multiple filter spectrograph was developed[1] in the light of results obtained in earlier work by F. A. McNeill and A. H. Allan.[2] They used a 'swept frequency' receiver to record the frequency spectrum of man-made v.l.f. transmissions received via the whistler mode. (Further information on whistler mode propagation can be obtained from references 3, 4 and 5.) In their equipment the band covered was $\pm 0{\cdot}5$ Hz about the nominal frequency, 18·6 kHz, of Station NPG at Seattle. Because of the long time-constants involved, one complete sweep occupied a time of 30 minutes and information on rapid variations of the whistler mode signals was lost. The present instrument was designed to overcome this limitation by recording simultaneously the outputs of 25 narrow-band filters spaced symmetrically about the centre frequency. It is possible to shift the centre frequency to coincide with the carrier frequency of any transmitter in the v.l.f. band without upsetting the relative spacing of the filters.

2. General Description

The spectrograph has a channel spacing of 0·05 Hz and the bandwidth of each filter is 0·007 Hz. The amplitude of the voltage at the output of each filter is recorded continuously on 35 mm film moving at a speed of 1 inch/hour.

As shown in the block diagram (Fig. 1) the incoming signal is received by a tuned loop antenna (1) and amplified in a number of tuned stages (2). For convenience the signal is then shifted in frequency to another part of the v.l.f. band. In the particular case considered the incoming frequency (18·6 kHz from NPG) is mixed with a local signal of $33{\cdot}\dot{3}$ kHz and the difference of $14{\cdot}7\dot{3}$ kHz selected (3). This signal is supplied in parallel to 25 phase-sensitive detectors (4) whose reference frequencies are supplied by a unit called the micro-frequency synthesizer (5). Each detector is followed by a direct-coupled amplifier (6) with an integrating time constant of 22 seconds. Such a combination of phase-sensitive detector and low-pass filter has the properties of a band-pass filter with the centre frequency equal to that of the reference frequency, and a bandwidth equal to twice that of the low-pass filter.

The 25 frequencies from the micro-frequency synthesizer are spaced symmetrically about a frequency of $14{\cdot}7\dot{3}$ kHz at increments of 0·05 Hz. They are derived from the centre frequency electro-mechanically. Both the centre frequency, $14{\cdot}7\dot{3}$ kHz, and the local signal, $33{\cdot}\dot{3}$ kHz, are synthesized (7) from a frequency standard having a stability of a few parts in 10^{10} per week.

The 25 outputs of the instrument are displayed (8) on a cathode ray tube, and photographed on 35 mm film. The outputs are presented as 25 evenly spaced spots along the Y axis of a 23 in television picture tube, with no X deflection. The positions of the spots are shifted in proportion to the output voltages of the 25 amplifiers. A 35 mm camera (9), with continuously moving film, views the tube with the Y axis of the tube perpendicular to the direction of film travel.

3. Equipment Details

3.1. *Aerial and Receiver*

For reception of whistler mode signals from NPG, the loop aerial is orientated for minimum sub-ionospheric reception. Any strong sub-ionospheric signal would overload the central channel of the spectrograph, and spill over into adjacent channels, and this would cause loss of information on the desired whistler mode signal.

The receiver is of a conventional design with three tuned stages.

† Physics and Engineering Laboratory, Department of Scientific and Industrial Research, New Zealand.

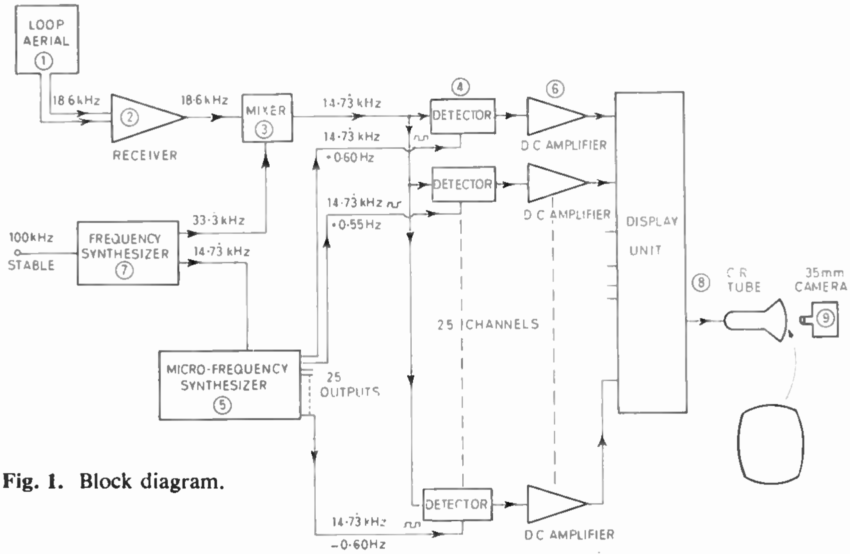

Fig. 1. Block diagram.

3.2. *Frequency Synthesis* (Fig. 2)

3.2.1. Synthesis of 33·3̇ kHz

The stable input (1) of 100 kHz is shaped to a square wave (2), and then frequency-divided by three, using a three-state counter (3). The output pulses from this counter are applied to a sharply tuned filter (4) so as to produce a 33·3̇ kHz sine wave, which is passed to the receiver mixer (5) and to the 14·73̇ kHz synthesizer.

3.2.2. Synthesis of 14·73̇ kHz

The 100 kHz square wave is divided by 500, using three commercial decade dividers (6), one of which is modified to divide by 5. The 200 Hz square wave output is differentiated and amplified. The short pulses that result are applied to a sharply tuned circuit (7) resonant at 600 Hz. The 'ringing' of this circuit gives a 600 Hz sine wave. This sine wave is shaped to a square wave (8) and then frequency-multiplied by 31 to give 18·6 kHz. As before, the square wave is differentiated, amplified, and applied to a sharply resonant tuned circuit (9), which is a 'Q-multiplier' with $Q = 850$.

The 18·6 kHz is now fed to a mixer (10) where it is mixed with the 33·3̇ kHz wave. The difference frequency of 14·73̇ kHz (12) is extracted using a filter (11).

3.3. *The Micro-frequency Synthesizer* (Fig. 3)

This operates on the principle that a constant rate of change of phase is equivalent to a frequency shift.

$$f = \frac{1}{2\pi}\frac{d\phi}{dt}$$

where f is in Hz, ϕ is in radians. This principle is implemented by the use of magslips.

There are 24 magslips in the micro-frequency synthesizer, since there is no shift in the central channel. The stator windings of these magslips are fed with a three-phase 14·73̇ kHz signal. The magslips are driven in pairs in steps of 0·05 revolutions per second at speeds up to 0·60 rev/s and the members of

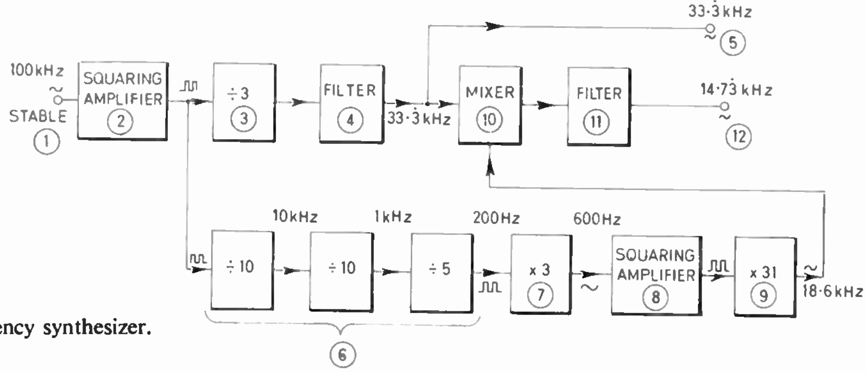

Fig. 2. Frequency synthesizer.

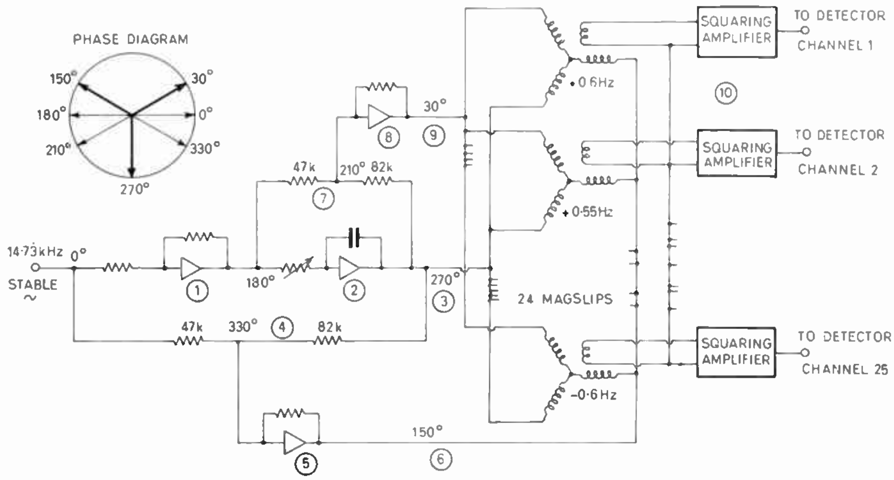

Fig. 3. Micro-frequency synthesizer.

each pair are rotated in opposite directions. The outputs are taken from the rotor windings of the magslips. Thus the input signal is changed in frequency by amounts varying from $-0{\cdot}60$ Hz to $+0{\cdot}60$ Hz in 0·05 Hz steps.

The three-phase generators are composed of four two-stage feedback transistor amplifiers with complementary emitter followers before each output. The first amplifier (1) has resistive feedback and inverts the input to 180 deg, and this is followed by an amplifier with capacitive feedback (2), forming one of the three phases (3). A resistive divider (4) with a ratio $1 : \sqrt{3}$ is connected between the input (0 deg) and the 270 deg output.

The vector sum of the voltages, which is the output of this divider, has a phase of 330 deg. This output is fed to an amplifier with resistive feedback (5), producing a 150 deg signal for the second phase (6). Similarly there is a divider (7) between the 180 deg and 270 deg points, giving 210 deg, which is phase-inverted (8) to give 30 deg for the third phase (9).

A variable resistor is in series with the input to the amplifier with capacitive feedback, to set the gain of this stage to unity for the frequency used. All the amplifiers then have voltage gains of unity.

Each magslip output is shaped to a square wave (10) for application to the subsequent phase-sensitive detectors.

3.4. *Detectors and D.C. Amplifiers* (Fig. 4)

The square waves produced by the micro-frequency synthesizer are used to switch inverted silicon transistors (1), which act as phase-sensitive detectors for the signal from the receiver. The output signals are

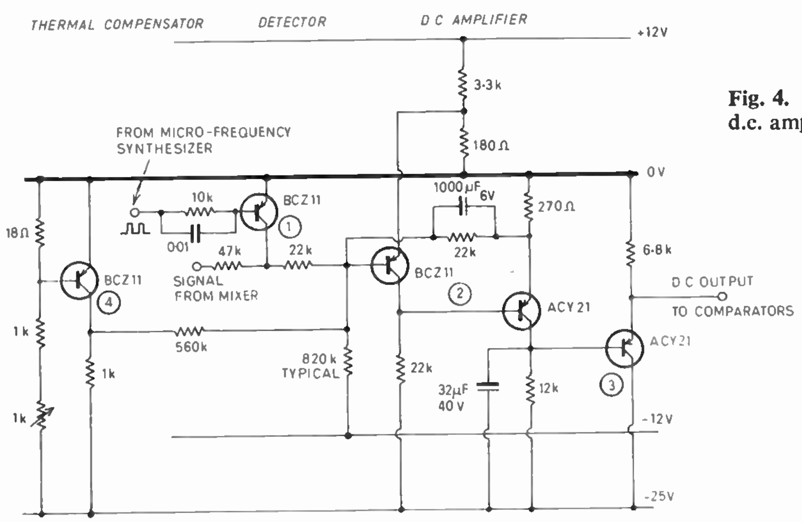

Fig. 4. Detector and d.c. amplifiers.

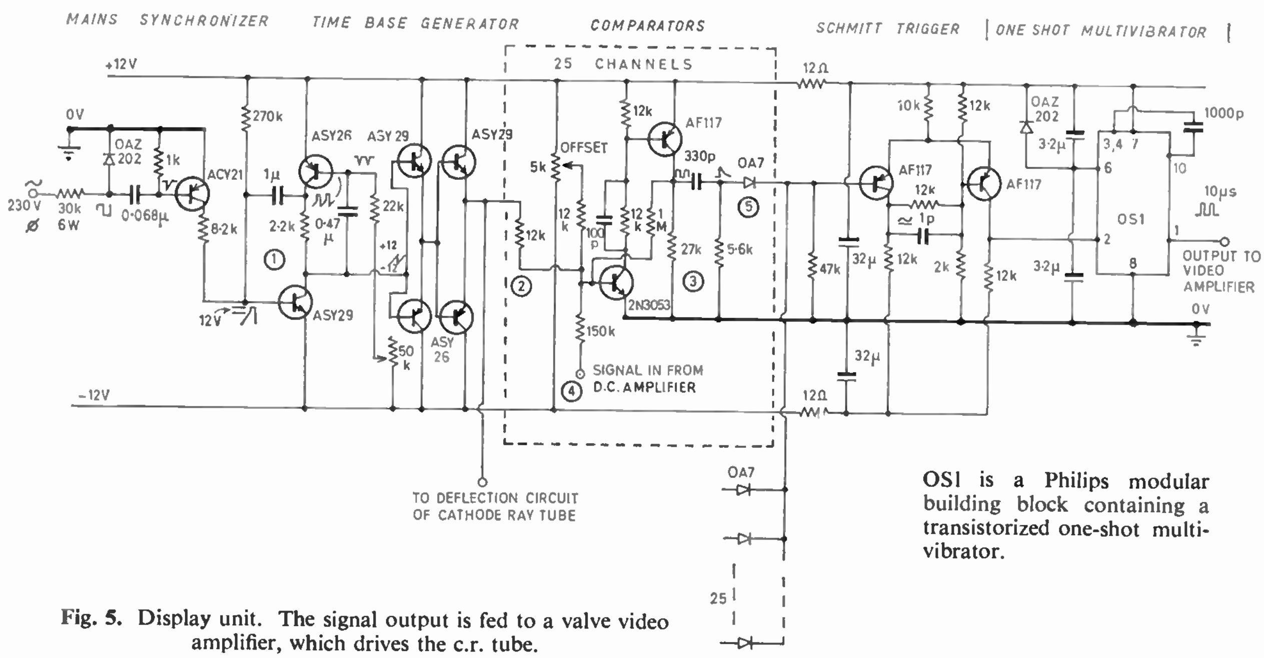

Fig. 5. Display unit. The signal output is fed to a valve video amplifier, which drives the c.r. tube.

then passed through d.c. amplifiers (2) with integrating time-constants of 22 seconds. These transistor amplifiers act as low-pass filters, and the outputs are passed through emitter followers (3) to the display unit. The input stages of the d.c. amplifiers are thermally compensated (4).

3.5. *The Display Unit* (Fig. 5)

A mains-locked time-base generator (1) produces a sawtooth wave of 20 ms period. This sawtooth provides Y deflection of the cathode ray tube, and also drives one input terminal (2) of each of the 25 comparator units (3). The other input terminal (4) of each comparator is fed by the output of one of the d.c. amplifiers of the spectrograph. The comparators are essentially high-gain amplifiers with positive feed-back. When the rising sawtooth voltage on one input overtakes the direct voltage on the other input, there is a sharp voltage change on the output of the comparator. This change is used to generate a 10 μs pulse. It will be seen that the action of the comparator is voltage to time conversion: the direct output voltage of a spectrograph channel is converted to an equivalent pulse, timed with respect to the start of the sawtooth time-base wave.

Given this voltage to time conversion, the remaining operation of the display unit is simple. The 25 d.c. amplifier voltages applied to the comparators are progressively offset by constant amounts, each offset differing from the next by a voltage equivalent to

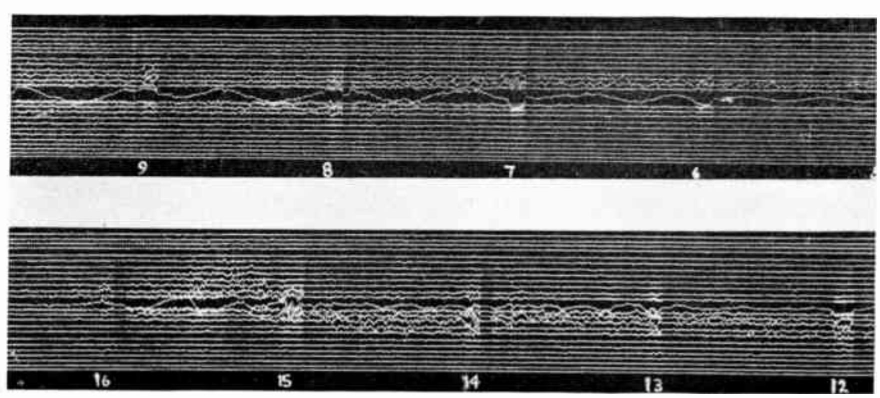

Fig. 6. Examples of signal records. The upper record was obtained on 12th April 1966, and the lower on 25th December 1965. The numbers below each record denote hours U.T.

1/25th of the time-base sweep. Supposing for the moment that each d.c. amplifier has zero output, the 25 comparators will generate 25 pulses, each of 10 μs equally spaced in time along the time-base sweep. These pulses are combined in an OR gate (5) and fed into a video amplifier. The cathode of the c.r. tube is connected to the output of this amplifier, so that as the time-base sweep deflects the beam along the Y axis, the 10 μs pulses produce 25 spots on the face of the 23-in television picture tube. If now outputs of the d.c. amplifiers vary, these spots will undergo proportional shifts along the Y axis. A 35 mm camera records the spot deflections as a 25-track film trace. The film is driven at 1 inch/hour and a clock is illuminated every hour.

4. Records

Two examples of records are shown in Fig. 6. A signal on any channel produces an oscillation on its trace of a greater amplitude than that produced by noise. Oscillations on several adjacent channels imply the existence of a broad band of Doppler shifted signals. The period of the large-amplitude slow-period beat on the centre channel indicates the difference between the carrier frequency, as received, and the local standard. Just before each hour is a short period of 'key up' followed by a period of 'key down'.

5. Conclusion

A spectrographic receiver for v.l.f. transmissions has been described, which has been in operation for one year. By using a tunable receiver and another frequency synthesizer, it is possible to obtain frequency spectra from any v.l.f. station, by adjusting one control in the micro-frequency synthesizer.

The technique of producing narrow-band filters, as described in this paper, could be used to advantage if it is required that a radio signal, of any frequency, be examined in detail. The technique may be able to be applied to other fields of research.

6. Acknowledgments

The authors wish to thank M. B. Forsyth, who constructed the magslip assembly, and the various other workers who helped in the production of the spectrograph.

7. References

1. R. A. Morris and N. Poletti, 'Frequency spectrum of Doppler-shifted whistler-mode signals', *Nature*, **208**, No. 5009, p. 479, 30th October 1965.
2. F. A. McNeill and A. H. Allan, 'Frequency variation of whistler mode signals from NPG Seattle as received in New Zealand', *J. Geophys. Res.*, **69**, No. 19, pp. 3989–94, 1st October 1964.
3. L. R. O. Storey, 'An investigation of whistling atmospherics', *Phil. Trans. Roy. Soc., London*, **A, 246**, pp. 113–141, 1953.
4. M. G. Morgan, H. E. Dinger and G. McK. Allcock, 'Observations of whistling atmospherics at geomagnetically conjugate points', *Nature*, **177**, No. 4497, pp. 29–31, 7th January 1956.
5. D. D. Crombie, F. A. McNeill and G. McK. Allcock, 'Variations in phase path of man-made onehop whistler signals at 18·6 kc/s', *J. Geophys. Res.*, **68**, pp. 6229–35, 1st December 1963.

Manuscript first received by the Institution on 27th May 1966 and in revised form on 10th November 1966. (Paper No. 1080.)

Tests on the Prototype of the UK-3 Satellite

The principal prototype model of *UK-3*, the first all-British satellite, commissioned by the Science Research Council, and which is due to carry five British scientific experiments into space in March/April 1967, has now been sent to the U.S.A. for compatibility tests. It will undergo mechanical and other tests with the actual launch vehicle at Dallas, Texas.

The earlier *UK-1* (*Ariel 1*) and *UK-2* (*Ariel 2*), launched as part of the joint U.S.-U.K. co-operative space research programme, were built by the American National Aeronautics and Space Administration and carried British scientific experiments. It was jointly agreed that the third satellite in the series should be designed, developed and built entirely in the United Kingdom.

UK-3 is a 198-lb (90-kg) satellite and will be launched into a circular orbit some 325 miles above the earth. As well as scientific instruments, the satellite will carry a data handling and storage system, a command receiver and telemetry system for relaying information back to ground stations including the Radio and Space Research Station and an array of thousands of solar cells.

Co-ordination of this most significant British project in space has been undertaken by the Space Research Management Unit of the Science Research Council, together with the Ministry of Aviation. The Space Department at the Royal Aircraft Establishment at Farnborough was nominated as the research, development and design authority and the two main contracts were let to the British Aircraft Corporation, Stevenage, and G.E.C. Electronics, Portsmouth. B.A.C.'s responsibility has been to design, develop and test the structure and to integrate and test the complete satellite with all the installed equipment. G.E.C. has developed and tested the electronics systems.

The design aim is that the satellite should transmit experimental data for a year. The five experiments the satellite will be carrying will:

measure the characteristics of radio frequency emissions from natural terrestrial sources, such as thunderstorms (the Radio and Space Research Station);

study the vertical distribution of molecular oxygen in the Earth's atmosphere at about 150 km (the Meteorological Office);

study the spatial and temporal characteristics of v.l.f. radiation (1–20 kHz) above the Earth's ionosphere (Sheffield University);

effect a world-wide survey of the ionosphere by measuring the electron density and temperature at frequent points along the path of the satellite (Birmingham University); and

measure the emission of radio noise from sources in the galaxy at frequencies too low to be observed on the ground (Jodrell Bank).

The Engineering of the Satellite

After an extensive series of mechanical and electrical development tests on two full-scale satellite models (*D1* and *D2*), manufacture of the prototype (*P1*) was begun late in 1965. *P1* was built to full flight standard.

In order to ensure both high reliability and a satisfactory external thermal control finish, all processes were carried out in special areas under scrupulously clean conditions. Operators were given training in assembly techniques, and the wearing of protective clothing in the clean areas was made compulsory. Inspection of every part and process was undertaken by B.A.C.'s inspectorate under the supervision of resident and visiting D.G.I. staff. Wiring of the built-in cable harness was subject to similar controls; one joint in every ten made by each wireman was destructively tested to ensure that quality was being maintained.

Achievement of electronic compatibility in *UK-3* has been very difficult because of the highly sensitive nature of several of the experiments: any stray signals tend to be picked up by the experiment receivers. The early trials on the *D2* model had shown the need for unusually stringent filtering, screening and earthing methods.

Design Qualification Testing

The spacecraft was accurately weighed and balanced using a new machine installed at B.A.C., Stevenage. Moments of inertia were also measured to check that the satellite would maintain a stable attitude in orbit. Functional tests were then performed at −30°C, to simulate storage conditions on the ground, and at −15°C and +60°C, to represent operational temperatures, for up to 12 hours each. A centrifuge test at 33 *g*, using B.A.C.'s new satellite spin facility, was performed to apply loads 50% greater than those experienced during launch acceleration. The vibration test levels were 50% higher than those expected during launch and comprised excitation by both sine and random waveforms in three mutually perpendicular planes.

P1 was then taken to R.A.E., Farnborough, to be mounted in the 2½-metre space simulation chamber. Solar illumination tests at a pressure of approximately 10^{-6} torr were performed, using carbon-arc sources at one end of the chamber, while the satellite was spun and made to present different faces to the artificial sun. The vacuum tests continued with temperature cycles designed to represent the worst possible orbit conditions.

Reliability of the electronic equipment has been assured by the use of redundant circuitry and components and, in the case of the telemetry, by duplication of the whole transmitter. All assembly was carried out at Portsmouth in air conditioned clean rooms, and the test environments available there included such extremes as a thermal vacuum of one thousand millionths of an atmosphere and random motion thrusts of twenty thousand pounds.

Two papers† describing the satellite and its ground check-out equipment were presented at an Institution meeting in London last April and, brought up to date to include the latest equipment modifications, will be published in *The Radio and Electronic Engineer* early in 1967.

The information in this article has been supplied by the Government Departments and industrial organizations responsible for the satellite.

† F. P. Campbell, 'The *UK-3* satellite and its ground check-out equipment'; W. M. Lovell, 'Electronic systems of the *UK-3* satellite'.

U.D.C. 621.375.9

The Effect of the Upper Sideband on the Performance of a Parametric Amplifier

By

K. L. HUGHES, B.Sc., Ph.D.†

AND

J. D. PEARSON, M.Sc., C.Eng.†

Summary: The equations which represent the effect of the upper sideband in a conventional parametric amplifier are derived in detail. It is then shown that the effect of the upper sideband is to present a positive conductance to the signal circuit and partly to nullify the negative resistance associated with the idler circuit. The noise figure expression is derived and shows that noise is introduced into the amplifier at the upper sideband and is converted to signal circuit, degrading the noise figure of the amplifier.

List of Symbols

C_1 maximum amplitude of change in capacitance
C_0 junction capacitance at the working voltage
r diode base resistance
f_q signal frequency
G_0 total conductance at ω_q
G_1 diode conductance at ω_q
G_{-1} total conductance at $(\omega_p - \omega_q)$
G_{+1} total conductance at $(\omega_p + \omega_q)$
G_s source conductance
G_L load conductance
Ω_1 $\omega_q/(\omega_p - \omega_q)$
Ω_2 $\omega_q/(\omega_p + \omega_q)$
$\gamma = C_1/C_0$
i_0 current at ω_q
i_{-1} current at $(\omega_p - \omega_q)$
i_{+1} current at $(\omega_p + \omega_q)$
Q_0 Q-factor of signal circuit
Q_{+1} Q-factor of upper sideband circuit
Q_{-1} Q-factor of idler circuit
B_0 susceptance of signal circuit
B_{+1} susceptance of upper sideband circuit
B_{-1} susceptance of idler circuit
ω_c diode cut-off frequency $\times$ 2π at zero volts

$$K = \tfrac{1}{2}\gamma \frac{1}{\omega_q C_0 r} = \text{diode figure of merit}$$

$\omega_q = 2\pi \times$ signal frequency (f_q)
$\omega_q' = 2\pi \times$ resonant signal frequency (f_q')
$\omega_p = 2\pi \times$ pump frequency (f_p)

$$\delta = \frac{\omega_q' - \omega_q}{\omega_q}$$

† Ferranti Ltd., Wythenshawe, Manchester.

1. Introduction

A negative resistance parametric amplifier is designed to support and effectively to separate the three frequencies present in the amplifier, i.e. the signal, idler and pump. To utilize the full potential of improved varactor diodes, parametric amplifiers are being pumped at higher frequencies. This means that the bandwidth of the idler circuit is larger and increases the possibility of the upper sideband being supported in that circuit.

A further possibility of course is that a separate circuit capable of supporting the upper sideband is present by accident.

It is the purpose of this paper to derive the expressions which show the effect of the presence of the upper sideband on the performance of such a parametric amplifier.

2. Derivation of the Basic Equations

It is assumed here that the pump voltage is much greater than any signal voltages present so that the varactor can be considered as a time-varying capacitance with a fundamental angular frequency ω_p. There is now no need to consider the presence of the pump frequency further.

Figure 1 shows a circuit representation of a parametric amplifier supporting the upper sideband and

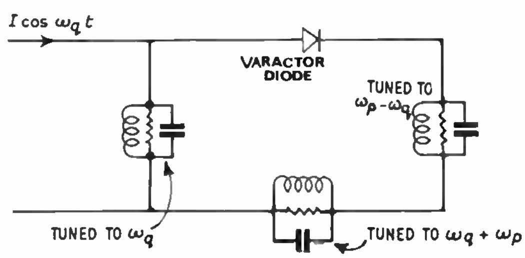

Fig. 1. Circuit representation of a parametric amplifier supporting the upper sideband.

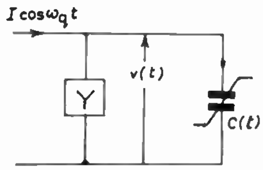

Fig. 2. Equivalent circuit of Fig. 1.

Fig. 2 shows an equivalent circuit. The small signal currents, $i(t)$ and the small signal voltages, $v(t)$, are then related by

$$i(t) = \frac{d}{dt}[C(t).v(t)] + Y.v(t) \qquad \ldots\ldots(1)$$

In general, the voltage $v(t)$ will contain components at all possible modulation frequencies $n(\omega_p \pm \omega_q)$ and can be written as

$$v(t) = \sum_{m=-\infty}^{\infty} v_m[\cos(\omega_q + m\omega_p)t + \theta_m] \qquad \ldots\ldots(2)$$

It has been shown elsewhere† that the phase angle always carries the same subscript as the voltage magnitude, so that if the voltages v_m are considered as vector quantities the phase angle can be dropped. The time-varying capacitance can be represented by the Fourier series

$$C(t) = \sum_{n=0}^{\infty} C_n \cos n\omega_p t \qquad \ldots\ldots(3)$$

By manipulating eqns. (1), (2) and (3) and allowing voltages to exist only at frequencies ω_q, $(\omega_p - \omega_q)$ and $(\omega_p + \omega_q)$ we arrive at equations for currents at three frequencies:

At frequency ω_q

$$I_0 = v_0\{Y_0 + j\omega_q C_0\} + v_{+1}\left\{j\omega_q \frac{C_1}{2}\right\} + v_{-1}\left\{j\omega_q \frac{C_1}{2}\right\} \qquad \ldots\ldots(4)$$

† D. G. Tucker, 'Circuits with time-varying parameters', *The Radio and Electronic Engineer*, 25, No. 3, p. 263, March 1963.

At frequency $(\omega_q + \omega_p)$

$$0 = v_0\left\{j(\omega_q + \omega_p)\frac{C_1}{2}\right\} + v_{+1}\{Y_{+1} + j(\omega_q + \omega_p)C_0\} + v_{-1}\left\{j(\omega_q + \omega_p)\frac{C_2}{2}\right\} \qquad \ldots\ldots(5)$$

At frequency $(\omega_q - \omega_p)$

$$0 = v_0\left\{j(\omega_q - \omega_p)\frac{C_1}{2}\right\} + v_{+1}\left\{j(\omega_q - \omega_p)\frac{C_2}{2}\right\} + v_{-1}\{Y_{-1} + j(\omega_q - \omega_p)C_0\} \qquad \ldots\ldots(6)$$

3. Derivation of the Gain Equation

It is theoretically possible to produce a time-varying capacitance with $C_2 = 0$ so that for the sake of simplicity this case will be considered here.

$$v_0 = \frac{I_0(G_{+1}+jB_{+1})(G_{-1}+jB_{-1})}{(G_0+jB_0)\{(G_{+1}+jB_{+1})(G_{-1}-jB_{-1})\} - j\omega_q\frac{C_1}{2}\left\{j(\omega_q+\omega_p)\frac{C_1}{2}(G_{-1}+jB_{-1})\right\} + j\omega_q\frac{C_1}{2}\left\{+j(\omega_p-\omega_q)\frac{C_1}{2}(G_{+1}+jB_{+1})\right\}} \qquad \ldots\ldots(7)$$

Thus

$$\frac{v_0}{I_0} = \frac{1}{(G_0+jB_0) + \dfrac{\omega_q(\omega_p+\omega_q)}{(G_{+1}+jB_{+1})}\dfrac{C_1^2}{4} - \dfrac{\omega_q(\omega_p-\omega_q)}{(G_{-1}+jB_{-1})}\dfrac{C_1^2}{4}} \qquad \ldots\ldots(8)$$

$$= \frac{1}{\left[G_0 + \dfrac{\omega_q(\omega_p+\omega_q)}{(G_{+1}^2+B_{+1}^2)}\dfrac{C_1^2}{4}G_{+1} - \dfrac{\omega_q(\omega_p-\omega_q)}{(G_{-1}^2+B_{-1}^2)}\dfrac{C_1^2}{4}G_{-1}\right] + j\left[B_0 - \dfrac{\omega_q(\omega_p+\omega_q)}{(G_{+1}^2+B_{+1}^2)}\dfrac{C_1^2}{4}B_{+1} + \dfrac{\omega_q(\omega_p-\omega_q)}{(G_{-1}^2+B_{-1}^2)}\dfrac{C_1^2}{4}B_{-1}\right]} \qquad \ldots\ldots(9)$$

This can be written in the form

$$\frac{v_0}{I_0} = \frac{1}{a+jb} \qquad \ldots\ldots(10)$$

so that the gain given by $4G_L G_s\left|\frac{v_0}{I_0}\right|^2$ is

$$\text{gain} = \frac{4G_L G_s}{a^2+b^2} \qquad \ldots\ldots(11)$$

The frequency of maximum gain is when

$$b = 0 \qquad \ldots\ldots(12)$$

i.e.

$$B_0 - \frac{\omega_q(\omega_p+\omega_q)}{(G_{+1}^2+B_{+1}^2)}\frac{C_1^2}{4}B_{+1} + \frac{\omega_q(\omega_p-\omega_q)}{(G_{-1}^2+B_{-1}^2)}\frac{C_1^2}{4}B_{-1} = 0 \qquad \ldots\ldots(13)$$

In the general case it is possible to express B_0, B_{+1} and B_{-1} in terms of the Q factors and frequency deviations of their particular circuits and find the frequency at which maximum gain is achieved. This will then yield expressions for the positive and negative conductances generated by the varactor actions and the effective degradation in the amplifier circuit can then be calculated.

A particular case will be examined here, where the idler bandwidth is sufficiently large to support the upper sideband. In this case we can write

$$G_0+jB_0 = G_0(1+2j\delta Q_0) \qquad \ldots\ldots(14)$$

$$G_{-1}+jB_{-1} = G_{-1}\left(1+2j\delta Q_{-1}\frac{\omega_q'}{\omega_p-\omega_q'}\right) \qquad \ldots\ldots(15)$$

$$G_{+1}+jB_{+1} = G_{-1}\left(1+2j\delta Q_{-1}\frac{\omega_q'}{\omega_p-\omega_q'}+ +4j\frac{\omega_q'}{\omega_p-\omega_q'}Q_{-1}\right) \qquad \ldots\ldots(16)$$

These equations can now be substituted into eqn. (13). If it is assumed that δ is small, we have

$$2\delta Q_0 G_0 - \frac{\omega_q(\omega_p+\omega_q)\dfrac{C_1^2}{4}\left(1+\dfrac{4\omega_q' Q_{-1}}{\omega_p-\omega_q'}\right)}{G_{-1}\left(1+\dfrac{16\omega_q'^2 Q_{-1}^2}{(\omega_p-\omega_q')^2}\right)} + \frac{\omega_q(\omega_p-\omega_q)}{G_{-1}}\frac{C_1^2}{2}Q_{-1}\frac{\omega_q'\delta}{\omega_p-\omega_q'} = 0 \qquad \ldots\ldots(17)$$

$$\delta\left\{2Q_0G_0+\frac{\omega_q(\omega_p-\omega_q)C_1^2}{2G_{-1}}\cdot Q_{-1}\frac{\omega_q'}{\omega_p-\omega_q'}\right\} = \frac{\omega_q(\omega_p+\omega_q)C_1^2\left(1+\dfrac{4\omega_q' Q_{-1}}{\omega_p-\omega_q'}\right)}{4G_{-1}\left(1+\dfrac{16\omega_q'^2 Q_{-1}^2}{(\omega_q-\omega_p')^2}\right)} \qquad \ldots\ldots(18)$$

Under the condition where eqn. (18) applies, the gain A becomes

$$A = \frac{4G_L G_s}{\left[G_0 - \dfrac{\omega_q(\omega_p-\omega_q)C_1^2}{4G_{-1}} + \dfrac{\omega_q(\omega_p+\omega_q)C_1^2}{4G_{-1}\left(1+\dfrac{16\omega_q'^2 Q_{-1}^2}{(\omega_p-\omega_q')^2}\right)}\right]^2} \qquad \ldots\ldots(19)$$

where the amplifier is fitted with a circulator, $G_L = G_s$ and the gain becomes

$$A = \frac{4(G_s/G_1)}{\left[\dfrac{G_0}{G_1} - \dfrac{\omega_q(\omega_p-\omega_q)C_1^2}{4G_{-1}G_1} + \dfrac{\omega_q(\omega_p+\omega_q)C_1^2}{4G_{-1}G_1\left(1+\dfrac{16\omega_q'^2 Q_{-1}^2}{(\omega_p-\omega_q')^2}\right)}\right]^2} \qquad \ldots\ldots(20)$$

The third term in the denominator of eqn. (20) can be identified as a positive conductance produced by the presence of the upper sideband, while the second term is the negative conductance associated with the idler. The signal circuit loading is normally such that the first term in the denominator is approximately equal to the negative conductance. However, the presence of the upper-sideband component introduces a positive conductance and the maximum value of the loading (G_0/G_1) is reduced.

An alternative view is that the mixing action of the varactor is such that the total negative conductance available is reduced.

In the case where a resonant circuit is present at the upper sideband it is clear from eqn. (19) that the positive resistance is of comparable magnitude to the negative resistance associated with the idler circuit. In these circumstances it would be very difficult to achieve any gain at all.

For an ideal idler circuit, where the bandwidth has its maximum value, the idler Q is given by $\omega_c/(\omega_p-\omega_q)$. If G_n and G_p are the negative and positive conductances produced by the varactor action, Table 1 shows their relative values for ideal idler circuits.

Table 1

f_q GHz	(f_p-f_q) GHz	(f_p+f_q) GHz	Q_{-1}	G_p/G_n
3	6	12	10	0·005
3	15	21	6·7	0·05
1·5	15	18	6·7	0·17
3	30	36	3	0·50
0·4	8	8·8	12·5	0·15

Clearly the effect of the upper-sideband can be quite disastrous in certain circumstances, e.g. in the 3 GHz amplifier pumped at 36 GHz.

4. Derivation of Noise Figure

If the Johnson noise currents entering the amplifier at frequencies ω_q, $(\omega_p-\omega_q)$ and $(\omega_p+\omega_q)$ are $\mathscr{I}_0$, $\mathscr{I}_{-1}$ and $\mathscr{I}_{+1}$ then the noise output voltage v_0, can be derived from eqns. (4), (5) and (6) as follows:

$$v_0 = \frac{\mathscr{I}_0\{(G_{+1}+jB_{+1})(G_{-1}+jB_{-1})\} - \mathscr{I}_{+1}\left\{j\omega_q\dfrac{C_1}{2}(G_{+1}+jB_{+1})\right\} - \mathscr{I}_{-1}\left\{j\omega_q\dfrac{C_1}{2}(G_{-1}+jB_{-1})\right\}}{\Delta_1} \qquad \ldots\ldots(21)$$

where Δ_1 is the determinant formed by the coefficients of eqns. (4), (5) and (6). Hence,

noise output power N_0

$$= \frac{|\mathscr{I}_0|^2(G_{+1}^2+B_{+1}^2)(G_{-1}^2+B_{-1}^2) + |\mathscr{I}_{+1}|^2\dfrac{\omega_q^2C_1^2}{4}(G_{+1}^2+B_{+1}^2) + |\mathscr{I}_{-1}|^2\dfrac{\omega_q^2C_1^2}{2}(G_{-1}^2+B_{-1}^2)}{|\Delta_1|^2} \qquad \ldots\ldots(22)$$

Since δ is small, B_{-1} approaches zero and N_0 becomes

$$N_0 = \frac{|\mathscr{I}_0|^2 G_{-1}^2 (G_{+1}^2 + B_{+1}^2) + |\mathscr{I}_{+1}|^2 \frac{\omega_q^2 C_1^2}{4} \times (G_{+1}^2 + B_{+1}^2) + |\mathscr{I}_{-1}|^2 G_{-1} \frac{\omega_q^2 C_1^2}{4}}{|\Delta_1|^2} \qquad \text{......(23)}$$

where

$$|\mathscr{I}_0|^2 = 4kT\Delta f(G_1 + G_s) \qquad \text{......(24)}$$

$$|\mathscr{I}_{+1}|^2 = 4kT\Delta f G_{+1} \qquad \text{......(25)}$$

$$|\mathscr{I}_{-1}|^2 = 4kT\Delta f G_{-1} \qquad \text{......(26)}$$

The noise figure of the amplifier given by

$$F = \frac{N_0}{kT\Delta f \times \text{gain}} \qquad \text{......(27)}$$

becomes

$$F = 1 + \frac{G_1}{G_s} + \frac{\omega_q^2 C_1^2}{4G_s G_{-1}} + \frac{\omega_q^2 C_1 G_{-1}}{4G_s[G_{+1}^2 + B_{+1}^2]} \qquad \text{......(28)}$$

$$= 1 + \frac{G_1}{G_s} + \frac{\omega_q^2 C_1^2}{4G_s G_{-1}} + \frac{\omega_q^2 C_1^2}{4G_s G_{-1}\left[1 + \frac{16\omega_q^2}{(\omega_p - \omega_q)^2} Q_{-1}^2\right]} \qquad \text{......(29)}$$

But if it is assumed that the circuit losses are small compared with the diode losses, then,

$$G_{-1} = (\omega_p - \omega_q)^2 C_0^2 r. \qquad \text{......(30)}$$

Hence

$$F = 1 + \frac{G_1}{G_s} + \frac{G_1}{G_s}\Omega^2 K^2 + \frac{G_1}{G_s}\Omega^2 K^2 \cdot \frac{1}{\left[1 + \frac{16\omega_q^2 Q_{-1}^2}{(\omega_p - \omega_q)^2}\right]} \qquad \text{......(31)}$$

The fourth term in eqn. (31) represents the noise contribution due to the presence of the upper sideband, so that not only is the effective quality of the diode reduced but there is also an additional noise term.

Equation (20) can be rewritten as

$$A = \frac{4(G_s/G_1)^2}{\left[\frac{G_0}{G_1} - \Omega K^2 + \Omega K^2 \cdot \frac{1}{\left[1 + \frac{16\omega_q^2 Q_{-1}^2}{(\omega_p - \omega_q)^2}\right]}\right]^2} \qquad \text{.....(32)}$$

Thus, for the amplifier still to oscillate,

$$\frac{G_0}{G_1} = \Omega K^2 \left[1 - \frac{1}{\left[1 + \frac{16\omega_q^2 Q_{-1}^2}{(\omega_p - \omega_q)^2}\right]}\right] \qquad \text{......(33)}$$

and

$$F = 1 + \frac{1}{\left[\Omega K^2\left\{1 - \frac{1}{1+x}\right\} - 1\right]} \times \left\{1 + \Omega^2 K^2 \left[1 + \frac{1}{1+x}\right]\right\} \qquad \text{......(34)}$$

where

$$x = \frac{16\omega_q^2 Q_{-1}^2}{(\omega_p - \omega_q)^2} \qquad \text{......(35)}$$

Where no upper sideband exists

$$F = 1 + \frac{1}{(\Omega K^2 - 1)}\{1 + \Omega^2 K^2\} \qquad \text{......(36)}$$

If eqn. (34) is called F_A and eqn. (36) is called F_B, Table 2 compares the theoretical temperatures of amplifiers where the upper sideband exists and where it is eliminated.

Table 2

f_q GHz	$(f_p - f_q)$ GHz	Q_{-1}	F_A °K	F_B °K
3	6	10	186	183
3	15	6·7	93	91
1·5	15	6·7	52	42
3	30	3	202	91
0·4	8	12·5	23	17

5. Conclusions

In the design of parametric amplifiers using wide-band idler circuits it is necessary to consider the contribution to the noise figure due to the presence of the upper sideband in the idler circuit. In certain cases this effect can seriously increase the amplifier overall noise figure and make it necessary to use a narrower band idler circuit.

In the case of an amplifier using a narrow-band idler circuit the presence of a resonant circuit at the upper sideband can, under some circumstances, prevent gain being obtained.

Manuscript first received by the Institution on 19th July 1966 and in final form on 14th October 1966. (Paper No. 1081.)

U.D.C. 621.396.677

Some New Studies of Angular Resolution for Linear Arrays

By

D. E. N. DAVIES, Ph.D., C.Eng.
(*Associate Member*)†

AND

I. D. LONGSTAFF†

Summary: This paper studies the limitation on the angular resolving power of linear aerial arrays. It is shown that there are some fundamental differences between the resolving powers of arrays, depending upon whether they are mechanically rotated or undergo electronic beam-scanning and this leads to a new approach to superdirectivity for arrays employing continuous mechanical rotation. It is shown that a super-directive array can be used with electronic scanning but this process requires discontinuous changes in the array excitation. The ultimate resolving power of a fixed linear array in the absence of noise is studied in terms of its ability to determine separately the angular location of a number of point sources. It is shown that the maximum number of such sources that can be independently located by an n-element array is given by $(n-1)$. It is further shown that the use of multiplicative signal processing or any other form of non-linear processing on the output of the array can produce no improvement over this limit. The change in the resolving power of arrays from the noise-free case to the noise-limited case is also discussed.

1. Introduction

Several authors have discussed different aspects of angular resolution in arrays.[1-3] They have adopted several different approaches to resolution ranging from a comparison with optical resolving power to the ability of a radar to distinguish small targets located near to much larger targets. The conclusions are broadly in agreement but differ considerably in detail owing mainly to the adoption of differing criteria of resolution. In radar practice, for instance, there may be a good case for the adoption of quite different criteria of resolution for different target environments.

The criterion of resolution to be discussed later in this paper relates to the maximum number of independently time varying signal sources that can be located and whose signal strength can be independently measured by a receiving array in the absence of noise. This approach to resolution is analysed in terms of the location of the zeros of the directional pattern of the receiving array and results in a very simple picture of resolution, which is used to obtain some new results.

The analysis developed in the paper is quite general and applies to linear arrays of equi-spaced elements receiving either electromagnetic or acoustic waves. The discussions will assume that a receiving array is used to produce a map of the far-field distribution of signal sources, but the results also apply to the case of locating a number of point targets using a two-way directional pattern of a radar aerial array. In this context it may be mentioned that the two-way directional pattern of a radar need not be the square of the one-way pattern, owing to the use of either separate aerials for transmission and reception or the use of non-reciprocal devices in the array. In fact this gives greater freedom in design of the directional pattern.

† Department of Electronic and Electrical Engineering, University of Birmingham.

Several previous discussions of resolution use the concept of ambiguity functions;[2, 4] these are derived from expressions for the mean square difference between a waveform and a displaced form of the same waveform. Although ambiguity functions give a very useful insight into the resolution performance and limitations of a system they do so only for the case where there are two targets. Also ambiguity functions only give a qualitative estimate of resolution performance and take no account of the demodulation systems used.

2. Mechanically Rotated Arrays

2.1. *Scanning as a Filtering Process*

A useful concept for analysing the output of an array which scans across the far-field distribution of sources is to relate scanning to the process of filtering a waveform with a conventional time-invariant filter. This concept was introduced by Bracewell.[5] Consider a mechanically rotating array with a directional pattern given by $E(\theta)$. The output of the array due to each far-field signal source will be a voltage waveform proportional to $E\left(\theta - \frac{2\pi t}{T}\right)$, where T represents the period of one revolution. Let the far-field distribution of target amplitudes and phases be represented as a complex function of bearing and given by $G(\theta)$, then the instantaneous output of the array $V(t)$ will be given by the convolution function:

$$V(t) = \int_{-\pi}^{+\pi} E\left(\theta - \frac{2\pi t}{T}\right) G(\theta)\,\mathrm{d}\theta \qquad \ldots\ldots(1)$$

The convolution theorem for periodic functions shows that the Fourier series coefficients $v(n)$ of the output $V(t)$ is given by

$$v(n) = e(n).g(n) \qquad \ldots\ldots(2)$$

$n = 0, 1, 2 \ldots =$ harmonic number

where $e(n)$ are the Fourier series coefficients of the directional pattern and $g(n)$ the Fourier series coefficients of the far-field target distribution function. If the far-field distribution varies during the rotation period, the above equations may be rewritten in terms of the Fourier transform. The fundamental frequency of the voltage output depends on the scanning rate and is given by $1/T$ Hz.

Thus the output waveform may be regarded as the far-field target distribution function 'filtered' by the Fourier series representation of the array directional pattern. This leads to the concept of the array acting as a 'spatial filter' on the far-field target distribution. Theoretically the output can again be filtered, this time with a real filter at the output of the array, and the directional pattern can be effectively changed to some other form. In practice it is not usually possible to control the shape of directional patterns in this way because of the difficulties of making a filter with the correct frequency response. For instance an array rotating uniformly at say 6 rev/min would have a fundamental output frequency of 0·1 Hz. Electronically scanned arrays, mentioned later, can scan at much faster rates and so beam-shaping with a passive filter is more practical in this case.

Even when this type of beam shaping is practically possible, signal/noise requirements may limit, or dictate, the shape of the beam to be synthesized. Because of these difficulties, no existing systems appear to use this technique. Instead, of course, they rely on the unfiltered output of an array designed to produce a narrow beam with low side-lobes.

2.2. *Spatial Harmonic Response of Mechanically Rotated Arrays*

Consider a linear array of $2n-1$ elements rotating about its own centre at $1/T$ rev/s. The directional pattern is given by the vectorial sum of the received signals from a source at some angle θ and may be represented by the sum of $(2n-1)$ terms:

$$E(\theta, t) = \sum_{a=-n}^{a=+n} A_a \exp\left[\frac{\mathrm{j}2\pi\, \mathrm{d}a}{\lambda}\cos\left(\theta - \frac{2\pi t}{T}\right)\right] \qquad \ldots\ldots(3)$$

where A_a is the complex weighting function of the ath element and d is the element spacing.

Now the Bessel function[6] expansion of the above gives

$$E(\theta, t) = \sum_{a=-n}^{a=+n} A_a \sum_{q=-\infty}^{q=+\infty} (\mathrm{j})^q \mathrm{J}_q\left(\frac{2\pi\, da}{\lambda}\right) \exp[\mathrm{j}q(\theta - 2\pi t/T)] \qquad \ldots\ldots(4)$$

where $\mathrm{J}_q(\ )$ is a Bessel function of order q.

The coefficients of $\exp[\mathrm{j}q(\theta - 2\pi t/T)]$ are the amplitudes of the components of the line spectrum.

Thus each element of the array contributes to the effective far-field filter a line spectrum with a frequency spacing of $2\pi/T$ radians per second, and with the amplitude of the qth harmonic given by

$$A_a(\mathrm{j})^q \mathrm{J}_q\left(\frac{2\pi\, da}{\lambda}\right)$$

This is the spectrum of a sinusoidal frequency modulated wave with a modulation index of $m = 2\pi da/\lambda$. It is also the spectrum that an observer in the far-field would see if that particular element was radiating. The rotation about the centre of the array would change the phase distance between the element and the observer cosinusoidally, producing a sinusoidal frequency modulation on the received signal. Thus if the array is rotated about its centre element each of the remaining $2n$ elements will produce a frequency modulation spectrum and the modulation index of the component spectrum of each element is proportional to the distance of the element from the array centre.

Although the bandwidth of sinusoidal f.m. is theoretically infinite it is well known that the amplitudes of the spectral components become very small beyond a certain finite bandwidth. Therefore if we consider the spectrum of the array output to be band-limited this results in there being a minimum time duration to the pulse corresponding to the main beam of the directional pattern of the array in the corresponding voltage–time waveform. The above statement therefore represents the well-known relationship between beamwidth and array length in wavelengths.

An estimate of the beamwidth obtainable can be derived from equation (4). The elements producing the widest bandwidth (i.e. having the highest f.m. index) are the end pair (with $a = \pm n$ in (4)). The combined spectrum of this pair is given by

$$E_n(\theta, t) = \sum_{q=-\infty}^{+\infty} (\mathrm{j})^q \mathrm{J}_q\left(\frac{\pi L}{\lambda}\right) \exp[\mathrm{j}q(\theta - 2\pi t/T)]$$

$$= \mathrm{J}_0\left(\frac{\pi L}{\lambda}\right) + \sum_{r=-\infty}^{r=+\infty} 2\,\mathrm{J}_{2r}\left(\frac{\pi L}{\lambda}\right) \exp[\mathrm{j}2r(\theta - 2\pi t/T)] \qquad \ldots\ldots(5)$$

where L = length of array.

Thus the amplitude of $2r$th harmonic is given by

$$J_{2r}\left(\frac{\pi L}{\lambda}\right)$$

Now in general the Bessel coefficient $J_n(x)$ is very small if n is greater than x and usually large for n less than x. So although the spectrum of the array output is infinite the highest usable harmonic $\hat{r}$ is given by:

$\hat{r} \simeq$ array length in wavelengths

where $\hat{r}$ is an integer. ....(6)

and the corresponding approximate beamwidth by $2\pi/\hat{r}$, giving the well-known expression:

beamwidth (in radians) $\simeq$ wavelength/array length.

The harmonics greater than r can be used to make the beam narrower, but only with difficulty and providing that these harmonics are significant compared with the noise level in the receiver. An array using these harmonics would be superdirective.

This section has primarily served to demonstrate that the directional properties of arrays may be studied in terms of the time waveform and signal spectrum received by an array while it is undergoing a process of continuous rotation (or scanning). It will subsequently be shown that this approach is of value in showing up some important differences between electronic and mechanical beam scanning and in suggesting a new approach to superdirectivity.

2.3. *Superdirectivity*

It was first shown by Bouwkamp and De Bruijn[7] that a finite aperture could theoretically produce any desired radiation pattern in the far field. Superdirective aerial arrays can produce beams which are significantly narrower than λ/L (L = aperture or array length) without the necessity for large side-lobes. Such aerials are characterized by aperture weighting functions with repeated phase reversals and by close element spacings. They also generally have a highly reactive radiation impedance, a narrow band of operation and high ohmic losses in the array elements, associated with the high reactive currents. Superdirective arrays are usually quite impracticable for these reasons, with the important exception of arrays whose length is not greater than about one or two wavelengths long.

Methods of synthesizing superdirective arrays and apertures have been well documented in the literature.[8, 9] However the performance in terms of the effective filter spectrum does not seem to have been reported. It should be sufficient for our purposes just to explain, without going into mathematical details, how the effective filter bandwidth is increased.

2.4. *Mechanically Rotated Superdirective Arrays*

It was shown in Section 2.2 that the spectrum of the directional pattern of a mechanically rotating array was infinite, although it was attenuated sharply after the harmonic corresponding to equation (6). To obtain superdirectivity the spectral components must be redistributed and the lower harmonics attenuated in some manner so that they are of the same magnitude as the desired high order spectral lines. One method of achieving this is to increase the number of elements and to weight the output so that the lower harmonics of the added elements almost cancel out the lower harmonics produced by the original elements. In fact if there are $2n+1$ elements it is possible to design any directional pattern with n harmonics, independent of the array length. To show this suppose the desired directional pattern has a spectrum where B_r is the complex amplitude of the rth harmonic. From equation (5) this will be given by the sum of the rth harmonics from each element, i.e.

$$B_r = \sum_{a=-n}^{+n} A_n \left[(j)^r J_r\left(\frac{2\pi da}{\lambda}\right) + (j)^{-r} J_{-r}\left(\frac{2\pi da}{\lambda}\right)\right]$$

If $A_a = A_{-a}$ then

$$B_r = A_0 J_r(0) + 2A_1 J_r\left(\frac{2\pi d}{\lambda}\right) + 2A_2 J_r\left(\frac{4\pi d}{\lambda}\right) + \ldots$$

$$\ldots + 2A_n J_r\left(\frac{2\pi nd}{\lambda}\right) \qquad \text{......(7)}$$

Similarly

$$B_{r+1} = A_0 J_{r+1}(0) + 2A_1 J_{r+1}\left(\frac{2\pi d}{\lambda}\right) \ldots \qquad \text{......(8)}$$

If n such equations were written starting with B_0, there would be n equations and n unknowns. It would therefore be possible to solve these simultaneous equations to find the desired element weighting functions (A's) necessary to produce a pattern with the given harmonic amplitudes (B's).

This method of designing a superdirective array is not normally used; however the process of cancelling out the lower harmonics to make them the same as the higher harmonics is inherent in the methods which are used. To demonstrate this, a superdirective array using a Dolph-Chebychev[10] directional pattern was taken from a text book.[11] The array was of total length one-quarter wavelength and the number of elements was five. It was found that a narrow beam with low side-lobes was produced with element weightings of: 1 : −3·7680 : 5 : −3·7680 : 1. Figure 1 shows the spectral lines from each element, the unweighted sum of these spectra and the weighted sum. The unweighted sum shows that only two lines are of the same order and the weighted sum shows three lines—suggesting the narrower beam obtained.

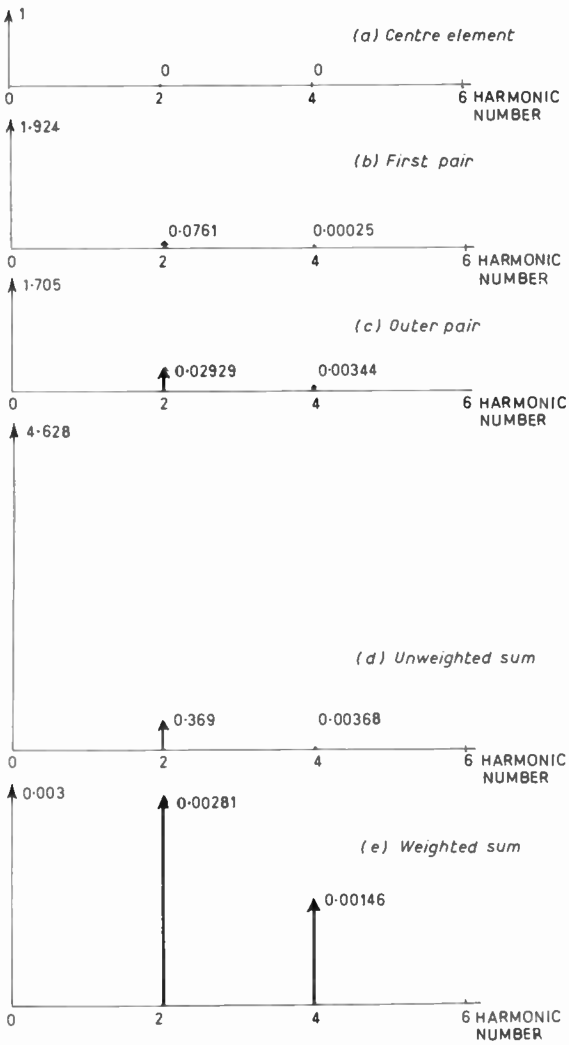

Fig. 1. Spatial harmonics of a five-element array.

It is interesting to note that although the method of designing an array by solving *n* simultaneous equations is not used for linear arrays, it appears to be the basis of certain methods available for synthesizing directional patterns for circular arrays.[12, 13]

2.5. *A New Approach to Superdirectivity for Mechanically-rotating Arrays*

If an array is rotating at a constant angular velocity the output frequency spectrum due to a single constant frequency signal source in the far field is identical to the 'spatial frequency response' of the array. Therefore for such an example there is no need to control the amplitude and phase of each element in order to control the directional pattern, the same effect can be obtained merely by passing the output of the array through a conventional electrical filter with a specified frequency response. This filter may also be designed to convert the output of a conventional array to that of a superdirective array. In this case the filter would reduce the amplitude of the lower spectral components in order that they might be comparable with some of the higher-order spectral components whose effects are normally negligible. As mentioned earlier such a filter might be very difficult to produce, though an optical signal processing system[14] could possibly be designed to perform the necessary filtering.

This particular approach to superdirectivity involves several marked differences to the former method of synthesizing directional patterns. It was shown in Section 2.2 that the frequency spectrum received from each element of a mechanically-rotating array corresponds to the spectrum of sinusoidal f.m. and is therefore infinite in extent. Consequently for a mechanically rotating superdirective array it is only necessary to employ one element rotating about a centre other than its own and to design some suitable filter to equalize the amplitude and phase of a specified number of spectral harmonies.

An important constraint on this process is the fact that a few harmonics may have zero amplitude corresponding to zeros of the appropriate Bessel functions.

It can clearly be seen from the above that several of the usual disadvantages of superdirectivity do not apply to the above case; for example the necessity to employ many elements with very close inter-element electrical spacing is removed since only one element is necessary. The extreme accuracy necessary in specifying the relative weightings of the output of each element is also obviated. However in place of these disadvantages we inherit the problem of synthesizing the necessary equalizing filter to produce

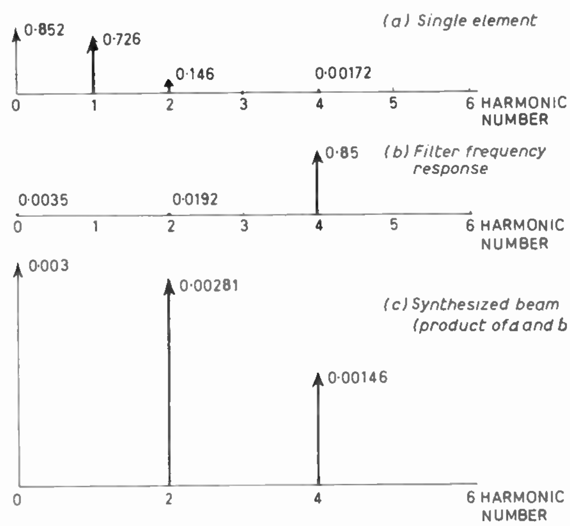

Fig. 2. Harmonics of a synthesized single-element superdirective array.

the superdirectivity. This can involve accurate control of both amplitude and phase in the filter response.

As an example of the use of this technique, it is shown how the superdirective pattern obtained with a five-element array of length $\lambda/4$ can be synthesized from the output of one single element rotating about a diameter of $\lambda/5$. The harmonic content of the output of a single element is shown in Fig. 2(a). The frequency response of the required beam shaping filter is shown in Fig. 2(b). This is multiplied by the signal spectrum to produce the spectrum of Fig. 2(c) which is identical to the spectrum of the five-element superdirective array of Fig. 1.

The fact that there are only even harmonics means that the far field pattern repeats itself twice in the range of real angles. Thus the front lobe is equal to the back lobe. The array, or rotating element can be made unidirectional by utilizing both odd and even harmonics.

A pattern of the form $\sin n\theta/n \sin\theta$ can be synthesized from a single rotating element if the first n spatial harmonics of the element output are adjusted to be all the same size. The filter necessary to do this would have a frequency response with relative amplitudes of

$$\frac{1}{J_0\left(\frac{2\pi r}{\lambda}\right)},\ \frac{1}{J_1\left(\frac{2\pi r}{\lambda}\right)},\ \frac{1}{J_2\left(\frac{2\pi r}{\lambda}\right)},\ldots,\ \frac{1}{J_{n-1}\left(\frac{2\pi r}{\lambda}\right)}.$$

at frequencies of $0, f, 2f\ldots(n-1)f$, where r is the radius of rotation and f the frequency of rotation.

3. Electronically-scanned Fixed Arrays

3.1. *Spatial Harmonic Response*

An n-element electronically-scanned array is shown in Fig. 3. The output from the mth element is weighted in amplitude and phase by $a_{m-1}\exp(j\alpha_{m-1})$ and added to the weighted outputs of all the other elements.

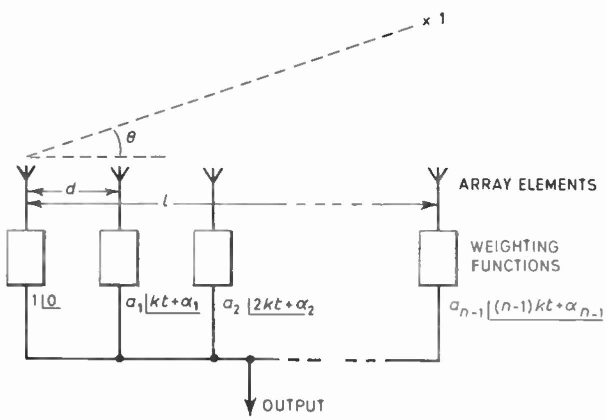

Fig. 3. Electronically-scanned array.

The signal from a target in the far field at an angle θ radians to the line of the array will cause a signal in the mth element of $k\exp(2\pi d/\lambda\cos\theta)$

where k = constant depending on target size,

d = element spacing,

λ = signal wavelength.

The amplitude of the array output as a function of $\cos\theta$ gives the directional pattern on a $\cos\theta$ scale

$$E(\theta) = \left|1 + a_1\exp\left[j\left(\frac{2\pi d}{\lambda}\cos\theta + \alpha_1\right)\right] + a_2\exp\left[j\left(\frac{4\pi d}{\lambda}\cos\theta + \alpha_2\right)\right] + \ldots + a_{n-1}\exp\left[j\left(\frac{2(n-1)\pi d}{\lambda}\cos\theta + \alpha_{n-1}\right)\right]\right| \quad \ldots\ldots(9)$$

$$= |1 + a_1\exp[j(p+\alpha_1)] + a_2\exp[j(2p+\alpha_2)]\ldots + a_{n-1}\exp[j(n-1)p + j\alpha_{n-1}]| \quad \ldots\ldots(10)$$

where $p = 2\pi d/\lambda\cos\theta$.

A directional pattern is formed by fixing the a's and α's to predetermined values. For instance a pattern of the form $\sin np/n\sin p$ is obtained if all the a's are unity (or equal) and all the α's zero. The beam can be deflected along the p scale uniformly with time if the phase weightings are changed with time according to:

$$\alpha_1 = kt,\quad \alpha_2 = 2kt \quad\ldots\quad \alpha_{n-1} = (n-1)kt.$$

The directional pattern remains unchanged under translation along the p scale (as opposed to the θ scale); thus the convolution integral which describes scanning (equation (1)) must be written in terms of p with the far-field target distribution re-defined in terms of p:

$$V(t) = \int_{-\pi}^{+\pi} G_0(p)E_0(p - 2\pi t/T)\,dp$$

giving the amplitude of the nth harmonic of the output as:

$$v_0(n) = g_0(n).e_0(n)$$

The subscript 0 denotes that the functions relate to variations on a $\cos\theta$ scale.

Thus the equivalent 'filter' which filters the far field is the Fourier series representation of the directional pattern in p. It is well known that the directional pattern in p is given by the Fourier series transform of the aperture weighting function. Thus a plot of the aperture weighting against distance along the array is identical in form to the frequency response of the effective filter which filters the far-field target distribution. The spectrum will be a line spectrum since the scanning is repetitive and the aperture weighting function will be delta functions at positions corresponding to the isotropic receiving elements.

3.2. *The Location of the Zeros of a Directional Pattern*

Schelkunoff[15] has described a synthesis technique for linear arrays based upon the location of the zeros of the directional pattern. Using the substitutions $Z = e^{jp}$ and $A = a\,e^{jx}$ in equation (10) gives the directional pattern in the form of a polynomial:

$$E = 1 + A_1 Z + A_2 Z^2 + A_3 Z^3 + \ldots A_{(n-1)} Z^{n-1} \quad \ldots\ldots(11)$$

Such a polynomial may be represented by the product of $n-1$ factors

$$(Z-a_1)(Z-a_2)(Z-a_3)\ldots(Z-a_n) \quad \ldots\ldots(12)$$

each such factor represents a zero of the directional pattern which may be plotted on the unit circle of the complex function $z = e^{jp}$. Since an n element array is represented by a polynomial of order $(n-1)$ there will be no more than $(n-1)$ zeros in one repetition period of the directional pattern; this exactly corresponds to the range of real angles in space for an element spacing of $\lambda/2$.

If a larger element spacing is used there will be at least partial repetition of this pattern over the range of real angles. Schelkunoff showed that it is possible to synthesize directional patterns by choosing the locations of the zeros of the pattern. The technique is also applicable to superdirective arrays; in this case it is first necessary to employ element spacings less than $\lambda/2$, this results in some of the zeros of the pattern residing outside the range of real angles. The effect of superdirectivity is then obtained by altering the array excitation in order to move these zeros into the range of real angles. This also results in a directional pattern with a very large response (which may be many times greater than the main lobe) in the range of imaginary angles (i.e. the range of p for which $|\sin\theta| > 1$).

3.3. *Superdirective Arrays with Electronic Scanning*

If the value of the progressive phase shift along a linear array is made to vary uniformly with time, the directional pattern is translated along the p scale at a uniform rate. Also since a uniform rate of change of phase represents a constant frequency it is evident that the frequency spectrum of the output of such an array when illuminated by a single plane wave will consist of one frequency per element of the array; a result that must be true for superdirective or non-superdirective patterns.

This situation draws attention to some rather interesting fundamental differences between the resolving properties of arrays employing mechanical and electronic beam scanning. The fundamental reason for these differences may be understood by the following simple distinction: the directional properties of a mechanically-rotating array arise from a series of measurements of the received field made with the same array in differing physical positions while the directional properties of a fixed array correspond only to the effect of different combinations of the signals received at each array element.

It is clear from former sections that in order to produce high degrees of superdirectivity it is necessary to increase the spatial frequency spectrum of the output of the array. But the spatial spectrum of a linear array with continuous electronic beam scanning just consists of one line per array element and the width of the spectrum is directly proportional to the length of the array. There is therefore an apparent anomaly: although it is possible to produce a narrow beam by means of a superdirective excitation it does not seem possible to increase the bandwidth of the spatial spectrum of the array. Electronic deflection of a superdirective pattern is limited by the large responses in the range of imaginary angles and can only be accomplished by the suitable design of that range of the pattern which enters the range of real angles. However if we consider the case of uniform continuous movement of the pattern along the p scale, the large imaginary angle responses are bound to enter the range of real angles and thus destroy the superdirectivity.

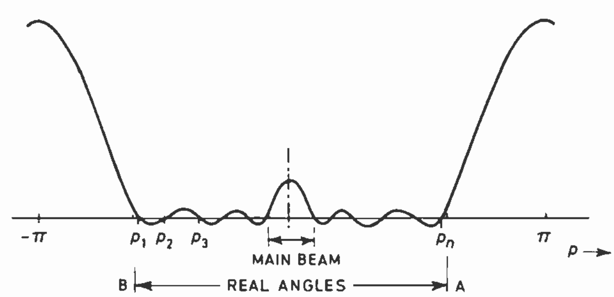

Fig. 4. Typical superdirective pattern in terms of p.

It will now be shown that it is possible to approximate to a process of uniform continuous deflection of the pattern along the p scale; but such a process requires discontinuous changes of both amplitude and phase of the array excitation. Figure 4 shows a typical superdirective directional response in the range of both real and imaginary angles. The zeros of the pattern $p_1 p_2 p_3 \ldots p_{n-1}$ are all in the range of real angles. If the pattern is deflected a small amount to the left by the application of a linear progression of phase shifts then p_1 will move just inside the region of imaginary angles. Further deflection of the pattern is precluded by the intrusion of the large response into the range of real angles.

However it is quite feasible to change the excitation of the array such that the location of p_1 is transferred to the point A. This change of excitation is clearly discontinuous and results in the generation of a wide bandwidth frequency spectrum. The relocation of the zero enables the superdirective pattern to be deflected in the usual way until p_2 moves out of the range of real angles when it too must be transferred to the location A.

Thus although the directional pattern in the range of real angles may be caused to move in an apparently uniform manner the movement of parts of the pattern outside this range must be discontinuous. Furthermore it is the wide-band spectrum so generated that provides the necessary high-order spectral harmonics necessary for the production of a superdirective pattern.

To summarize the result of this section: the process of continuous uniform angular deflection of a superdirective pattern cannot be achieved by the usual variation of element phase shifts as used for non-superdirective patterns. The process of continuous angular deflection of such a pattern by variations of array excitation must involve discontinuous changes in both the amplitude and phases of the array excitation. The important condition that it is essential to maintain for this process is the conservation of the zeros of the pattern in the range of real angles.

3.4. *The Maximum Resolving Power of a Fixed Array in the Absence of Noise*

The synthesis technique described by Schelkunoff has shown that an n element array can produce a directional pattern with not more than $(n-1)$ independent zeros. The location of these zeros may be independently controlled to correspond to any desired direction in space. The ability to control the location of the zeros of a directional pattern suggests a new technique for the determination of the positions of a distribution of signal sources in the far field of the array.

If the far field contains a distribution of fluctuating point sources of signal then the output of the array will only be continuously zero if at least one zero of the directional pattern corresponds to the direction of each source. Thus by controlling the location of the $(n-1)$ zeros of an n element array it is possible to determine the positions of no more than $(n-1)$ different sources. The amplitude and fluctuations of any given source may be measured by removing the particular zero corresponding to that source. If the targets are not fluctuating then zero outputs can occur with zeros at other positions than as defined above. These ambiguous positions can only be resolved if the number of zeros is greater than 3/2 times the number of non-fluctuating sources.[16, 20]

As might be expected, a system such as this would have difficulty resolving one target which was close to another. When a zero is placed in the direction of one target the amplitude of the directional pattern on either side of this zero will be low. If another target should exist in this region the signal obtained from it would be correspondingly low. If noise was present and greater than this low signal, then the second target could go undetected.

Even though this system may not be practical it does show that there is a maximum number of targets which a fixed array can possibly resolve. This number is one less than the number of elements of the array (i.e. the number of degrees of freedom of the array). Also, in the absence of noise, this resolution is independent of the array size. The only restriction on the array is that the element spacing should be less than $\lambda/2$; otherwise one zero on the unit circle in Z can produce more than one zero in the range of real angles, so causing ambiguities in the system. It is worth recalling however that this limit of resolution does not apply to mechanically-rotated arrays since these can form even superdirective patterns with only one element.

3.5. *The Maximum Resolving Power of a Fixed Array in the Presence of Noise*

If the directional pattern of a linear receiving array is caused to scan the far-field distribution of sources by electronic means in a time T, the resulting output waveform from the array may be said to contain a quantity of information I (bits) about the location of these sources. The maximum possible information content in such a waveform is given by the relationship:[17]

$$I = WT \log_2 \left(1+\frac{S}{N}\right) \qquad \ldots\ldots(11)$$

where W is the bandwidth of the received signal and S/N the r.m.s. signal/noise power ratio.

The above relationship relates to the maximum possible information content of the waveform assuming some optimum noise-like coding technique. In the above example the actual method of coding is beyond the control of the aerial designer, it is independent of the choice of directional pattern and is merely given by the convolution of the 'message' with the directional pattern. It is therefore necessary to introduce a constant K into this equation to account for the non-optimum coding:

$$I = WT \log_2 K\left(1+\frac{S}{N}\right)$$

If the rate of amplitude fluctuations of the far-field sources is slow compared with the output bandwidth then the bandwidth due to the spectral harmonics of the directional pattern with uniform scanning is given by:

$$W = \frac{L}{\lambda T}$$

where L = length of array. This gives the value of I:

$$I = \frac{L}{\lambda} \log_2 K\left(1+\frac{S}{N}\right) \qquad \ldots\ldots(12)$$

The significance of this information content may be regarded as information relating to the occupancy of I possible bearing cells.

Using the results from this and the previous section it is possible to draw a graph representing the ultimate resolving power of a fixed electronically-scanned array. The resolving power is represented as the maximum number of targets or resolution cells which the array can process and this is plotted against the received signal/noise power ratio in Fig. 5, curve A.

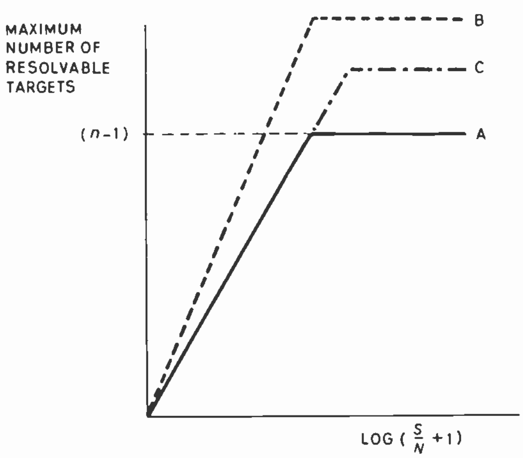

Fig. 5. Resolving power of a fixed array as a function of signal/noise ratio, showing:

A a given array.

B effect of increasing array length by adding elements and keeping spacing constant.

C effect of adding elements but keeping array length constant.

The implications of this rather crude graph is that for poor signal/noise ratio the resolving power is determined by the received information, and for good signal/noise ratio it is not possible to utilize all the information available as resolution information. However, information about target amplitudes is available.

The slope of the graph below the corner point is given by the length of the array in wavelengths (L/λ). Thus an increase in array length with a proportional increase in the number of array elements (so keeping the element spacing constant) will produce a proportional increase in the resolving power (see Fig. 5, curve B). This increase in resolving power is obtained without the necessity of increasing the received signal to noise power ratio.

However if the length of the array is kept constant then resolving power can only be improved by increasing the logarithm of ($S/N+1$). If the corner point is reached then an increase in the number of array elements is also required as in Fig. 5, curve C. This technique will in general produce a super-directive array.

4. Some Theoretical Aspects of the Effect of Demodulation on Resolution

At this stage it is convenient to show the effects of the different types of demodulation on the theoretical limits of performance as discussed previously. The most conventional form of demodulation system is to pass the received signal through a square-law diode followed by a low-pass filter. This system can optimize the probability of detection[18] if post-detector integration is used. An alternative technique is to divide up the array in such a way that two or more different outputs are obtained, multiplied together and then low-pass filtered. Previous workers have shown that such arrays can give an improved resolution performance compared with square-law detection for situations involving only two closely-spaced targets.

A particular characteristic of this multiplicative signal processing technique is that the demodulated response of the array can have more than the normal ($n-1$) zeros. It would therefore appear that such arrays might be able to resolve more than ($n-1$) separate point targets; however it can easily be shown that this is not so.

To demonstrate this consider the general form of a multiplicative array of n elements. By taking a number N (usually 2 in practice) of weighted outputs from each array element and adding as shown in Fig. 6, it is possible to synthesize a number of directional patterns. If the outputs from such patterns are multiplied together the resultant directional pattern E_m will then be given by the product of the individual directional patterns:

$$\begin{aligned}E_m = (1+a_1Z+a_2Z^2+\ldots+a_{n-1}Z^{n-1})\times \\ (1+b_1Z+\ldots+b_{n-1}Z^{n-1})(\;)(\;)\ldots \\ \ldots(\;)(\;)(1+N_1Z+\ldots+N_{n-1}Z^{n-1}) \qquad \ldots\ldots(13)\end{aligned}$$

This is a polynomial of order ($n-1$) which can have ($n-1$) zeros.

This is the response of the system to one target; however, if several targets are present the resulting directional response is not the sum of the displaced single-target directional patterns since superposition does not hold. Suppose there were M fluctuating targets in the far field then the directional response would be, taking $N = 2$ for convenience:

$$\begin{aligned} E_m = {} & [(1+a_1Z_1+a_2Z_1^2+\ldots+a_{n-1}Z_1^{n-1})+\ldots+ \\ & +(1+a_1Z_2+\ldots)+\ldots+(1+a_1Z_M\ldots)]\times \\ & [(1+b_1Z_1+b_2Z_1^2+\ldots+b_{n-1}Z_1^{n-1})+\ldots+ \\ & +(1+b_1Z_2+\ldots)+\ldots+ \\ & +(1+b_1Z_M+\ldots+b_{n-1}Z_M^{(n-1)})] \qquad \ldots\ldots(14) \end{aligned}$$

where Z_1, Z_2, $\ldots Z_M$ represent the positions of the targets in Z.

Thus the output is only zero all the time when the first bracket in (14), (i.e. the first synthesized array) *or* the second bracket, is zero and not otherwise. As the output from one array can only be zero when the number of target is less than, or equal to, $(n-1)$ then we see that the multiplicative array with $2(n-1)$ zero's can still only uniquely detect $(n-1)$ targets. The same is true of a multiplicative array with any multiple of $(n-1)$ zeros.

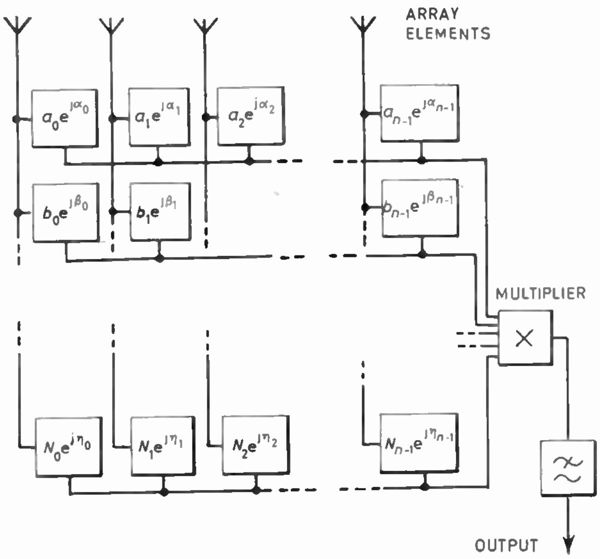

Fig. 6. General form of a multiplicative array.

The square-law detected array can also be considered as a special case of the former multiplicative array with two identical synthesized beams multiplied together. In this case the maximum number of detectable targets is still $(n-1)$. This limitation also relates to any other form of non-linear signal processing since any non-linear law may be approximated by the sum of a number of product terms and such product terms constitute multiplicative processing.

The former arguments show that multiplicative signal processing cannot increase the ultimate resolution capabilities of an array, defined in terms of the maximum number of targets that it can resolve. This result does not contradict previous work[3, 19] on multiplicative arrays relating to their ability to separate two closely-spaced targets, which clearly involves a completely different criterion of resolution.

5. Conclusions

This paper has shown that the maximum number of sources that can be separately resolved by a fixed linear array is given by one less than the number of elements in the array and that this result is independent of the form of signal demodulation. It has also been shown that there are some fundamental differences between the application of superdirectivity to fixed arrays and uniformly-rotating arrays. This has led to a new approach to superdirectivity for rotating arrays which has some interesting possibilities. It removes problems of mutual coupling between elements since it is shown that there is only need for one element in the rotating array. The possible value of this form of superdirectivity is not immediately clear since it depends on the problems involved in the synthesis of the network used to process the output signals, in order to obtain a superdirective directional response. This problem clearly merits further study.

6. References

1. G. Toraldo di Francia, 'Directivity, super-gain and information', *Trans. Inst. Radio Engrs on Antennas and Propagation*, **AP-4**, p. 473, 1955.
2. P. M. Woodward, 'Probability and Information Theory, with Applications to Radar' (Pergamon Press, London, 1953).
3. E. Shaw and D. E. N. Davies, 'Theoretical and experimental studies of the resolution performance of multiplicative and additive aerial arrays', *The Radio and Electronic Engineer*, **28**, No. 4, p. 1, October 1964.
4. B. Elspas, 'A Radar System Based on Statistical Estimation and Resolution Considerations'. Stanford Electronics Laboratories, Stanford University, California. Technical Report No. 361–1, 1st August 1955.
5. R. N. Bracewell and J. A. Roberts, 'Aerial smoothing in radio astronomy', *Aust. J. Phys.*, **7**, p. 615, December 1954.
6. G. M. Korn and T. A. Korn, 'Mathematical Handbook for Engineers', p. 732 (McGraw-Hill, New York, 1961).
7. C. J. Bouwkamp and N. G. De Bruijn, 'The problem of optimum antenna current distributions', *Philips Res. Rep.*, **1**, p. 135, January 1946.
8. P. M. Woodward and J. D. Lawson, 'The theoretical precision with which an arbitrary radiation pattern may be obtained with a source of finite size', *J. Instn Elect. Engrs*, **95**, Part III, p. 363, January 1948.
9. A. Block, R. G. Medhurst and S. D. Pool, 'Superdirectivity', *Proc. Inst. Radio Engrs*, **48**, p. 1164, June 1960.
10. C. L. Dolph, 'A current distribution for broadside arrays which optimizes the relationship between beamwidth and side lobe level', *Proc. I.R.E.*, 34, p. 335, June 1946.

11. E. C. Jordan, 'Electromagnetic Waves and Radiating Systems', p. 444 (Constable, London, 1953).

12. G. Ziehm, 'Optimum directional pattern synthesis of circular arrays', *The Radio and Electronic Engineer*, **28**, p. 341, November 1964.

13. T. T. Taylor, 'A synthesis method for circular and cylindrical antennas composed of discrete elements', *Trans I.R.E. on Antennas and Propagation*, AP-3, p. 251, August 1952.

14. L. J. Cutrona, E. N. Leith, C. R. Palermo and L. J. Percello, 'Optical data processing and filtering systems', *Trans I.R.E. on Information Theory*, **IT-6**, No. 3, p. 386, June 1960.

15. S. A. Schelkunoff, 'A mathematical theory of linear arrays', *Bell Syst. Tech. J.*, **22**, No. 1, p. 80, 1963.

16. I. D. Longstaff, 'Angular Resolution in Radar Systems'. Unpublished Report. University of Birmingham, November 1965.

17. C. E. Shannon, 'Communication in the presence of noise', *Proc. I.R.E.*, **37**, p. 10, January 1949.

18. D. C. Cooper and J. W. R. Griffiths, 'Video integration in radar and sonar systems', *J. Brit. Instn Radio Engrs*, **21**, p. 421, May 1961.

19. A. A. Ksienski, 'Multiplicative processing antenna systems for radar application', *The Radio and Electronic Engineer*, **29**, p. 53, January 1965.

20. V. G. Welsby, 'The angular resolution of a receiving aperture in the absence of noise', *The Radio and Electronic Engineer*, **26**, p. 115, August 1963.

Manuscript first received by the Institution on 5th May 1966, and in final form on 14th July 1966. (Paper No. 1082/RNA56).

U.D.C. 621.396.933.2

New Precision Techniques for I.L.S. Parameter Measurement

By

G. K. LUNN, B.Sc., C.Eng.†

Presented at the Radar and Navigational Aids Group Symposium on 'Monitoring of I.L.S. Ground Equipment for Automatic Landing' held in London on 4th April 1966.

Summary: The accuracy and simplicity of measurement of the four main parameters of the received I.L.S. signal, i.e. centring accuracy, off-course sensitivity, mean modulation depth and relative tone phase, has been greatly improved by the introduction of a new technique based on phase-locked detection of the 90 and 150 Hz tones using a 120 Hz reference frequency. The paper states the principles of the phase-locked system with the aid of vector diagrams.

Basic block diagrams are shown for the various practical systems according to the measurement application, e.g. test equipment calibration, course line monitoring, field use, etc. The particular requirements for measurements in the presence of noise and large unwanted signals are also considered. The performance requirements for the main circuit blocks show that the a.f. circuitry is basically simple and non-critical and is adaptable to micro-miniature techniques.

Finally a comparison is made between phase-locked detection and previous filter methods. In particular a centring accuracy of 0·1 μA, equivalent to 0·05% difference in tone amplitudes, is easily obtained, and this represents an order of magnitude improvement over filter methods taken to the limit of present-day techniques.

Definitions

Mean modulation depth

$$= \frac{m_{150}+m_{90}}{2} \quad \text{or} \quad \frac{m_{150}+m_{90}}{2} \times 100\%$$

True d.d.m.

$$= m_{150}-m_{90} \quad \text{or} \quad (m_{150}-m_{90}) \times 100\%$$

Normalized d.d.m.

$$= \frac{\text{true d.d.m.} \times \text{actual mean modulation depth}}{\text{standard mean modulation depth}}$$

where

m_{150} = 150Hz modulation index

m_{90} = 90Hz modulation index.

1. Introduction

Provisional specifications for a Category III Instrument Landing Systems require the control of four of the major parameters on transmitters as follows:

centring error (zero d.d.m.): 0·00067 d.d.m. (mean standard deviation)

off-course sensitivity: 5% from nominal (mean standard deviation)

mean modulation depth: 0·5% = 2·5% of m

relative phase: 2½° at 150 Hz = 1·5° at 90 Hz.

This paper will show how the new methods of measurement based on phase-locked detection has enabled all four parameters to be measured with improved accuracy, particularly the most important ones of centring error and off-course sensitivity.

Present methods of measurement of these two are based on separation of the 90 and 150 Hz tones by tuned filters.‡ Obviously the critical part of the system is tuned filters and here the various requirements conflict. Tuned filters work at low frequency, requiring iron-cored inductors, yet must operate with very high stability. They must work at high signal levels to overcome diode rectification errors and yet must be compact enough to pack into airborne equipment. They should have high Q for good rejection of the other frequency, but frequency tolerances and stability requirements demand a low Q.

† The Wayne Kerr Company Ltd., Chessington, Surrey.

‡ S. S. D. Jones, 'I.L.S. monitoring—a statement of the problem', *The Radio and Electronic Engineer*, **32**, pp. 287–92, November 1966.

The tolerances on the filters and rectifiers are such that a definite zero d.d.m. point is obtainable only by setting a 'set zero' control. The new phase-locked system has a zero accuracy built into it such that with care in circuit design the error can be made less than 0·01% d.d.m. without zero setting.

Modulation depth measurements are currently made using peak detection of a single tone, and accurate readings of mean modulation depth of the combined tones are not possible. The new method can measure the combined energy in the two tones and thus make measurements over the full range of d.d.m. values. For measurement of relative phase the only reliable method has been observation of the waveform on a c.r.o. which gives a good indication of when the tones are in the exact phase normal condition but gives no quantitative measurement of error from this condition.

2. Phase-locked System Principles

The frequencies 90 Hz and 150 Hz were conveniently chosen by far-sighted engineers in U.S.A., because they happen to be the sidebands of a 120 Hz carrier modulated at 30 Hz and, what is more, 30 Hz is a divisor of all the other three frequencies. If we look at the I.L.S. waveforms with this in mind it becomes immediately obvious (Fig. 1).

So if we apply normal suppressed carrier demodulation techniques, i.e. mixing, multiplication or phase-sensitive rectification (p.s.r.) with the 120 Hz carrier, we extract all the information about the 90 and 150 Hz sidebands as 30 Hz signals.

Consider the simple vector representation (Fig. 2) of the 90 and 150 Hz signals. We shall choose a

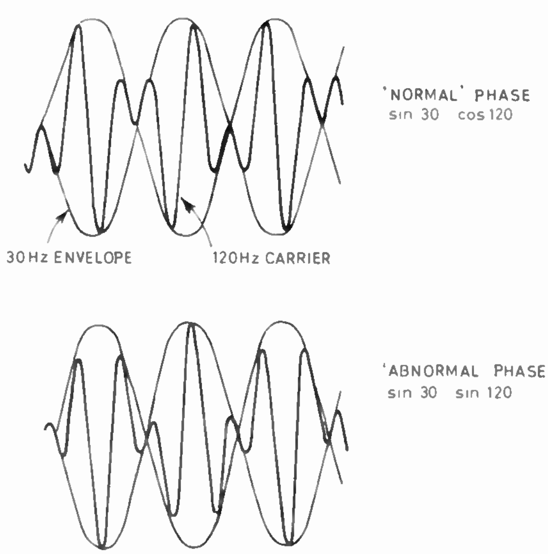

Fig. 1. I.L.S. tones seen as 30 Hz modulation of 120 Hz carrier.

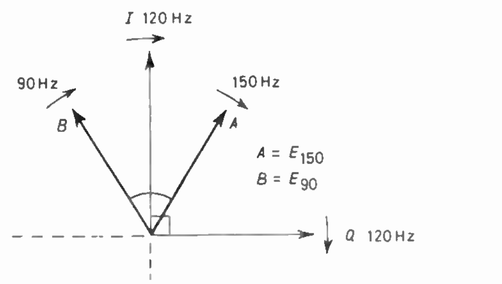

Fig. 2. 90 Hz and 150 Hz vector system with 120 Hz references superimposed.

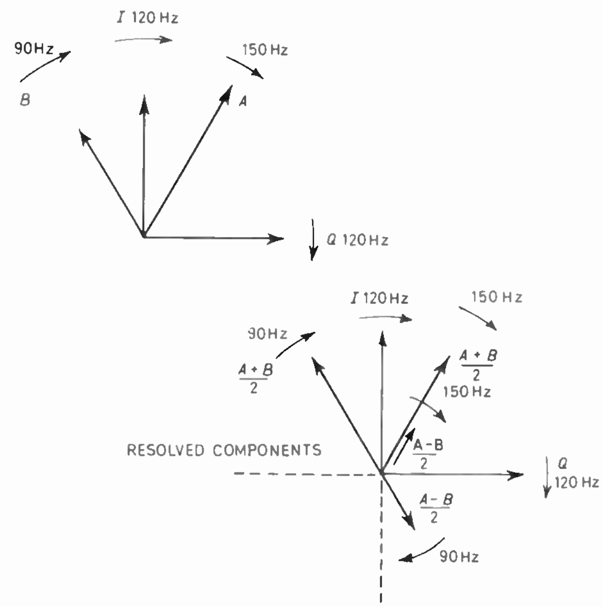

Fig. 3. Resolving vectors of different amplitudes into two vector systems.

120 Hz signal vector which always bisects the angle between the two vectors and will call this the 'in-phase' 120 Hz reference. At right angles to this is the 'quadrature' 120 Hz reference. Now if the 90 and 150 Hz vectors are different (Fig. 3), we can resolve them into two pairs of vectors, one pair of length $(A+B)/2$ and symmetrical about the in-phase reference and the other pair of length $(A-B)/2$ and symmetrical about the quadrature reference. If we stop the rotation of the 120 Hz vectors, which is equivalent to the action of the p.s.r. or multiplier, then the sideband vectors rotate at 30 Hz (Fig. 4). Multiplication by the in-phase reference gives the $(A+B)/2$ vectors and by the quadrature reference gives the $(A-B)/2$ vectors as 30 Hz signal outputs. Thus it can be seen that if the 90 and 150 Hz are exactly equal, there is a null output of the $(A-B)/2$ 30 Hz when multiplied by the quadrature 120 Hz reference and differences in tone amplitudes give proportional

30 Hz outputs. The $(A+B)/2$ 30 Hz always gives the mean tone amplitude which can eventually be used to give a measure of modulation depth.

If these 30 Hz signals are now detected using 30 Hz multipliers or phase-sensitive rectifiers we can obtain two more pieces of information.

Take first the quadrature reference 120 Hz (Fig. 5). Normally the output of the multiplier is amplified and detected by a 30 Hz p.s.r. which has its reference in the same phase as the $(A-B)$ signal, which we shall call the quadrature reference 30 Hz. A second p.s.r. with its reference aligned to the $(A+B)$ 30 Hz should see nothing. However, if the 120 Hz quadrature reference is now exactly in phase with the $(A-B)$ vectors, then a portion of the $(A+B)$ vector pair will be fed to the two p.s.r.'s and will be detected by the in-phase 30 Hz reference. Thus we have a check on the 120 Hz reference phase by observing the output of this p.s.r. and setting it to zero.

In a similar way (Fig. 6), when the in-phase 120 Hz reference is being used, the in-phase 30 Hz p.s.r. will see the $(A+B)$ vector pair and the quadrature 30 Hz p.s.r. should see nothing unless the 30 Hz references are not correctly aligned in phase, in which case a portion of the $(A+B)$ vector pair will be seen. Hence by setting the quadrature 30 Hz p.s.r. output to zero we can correctly align the 30 Hz references.

Thus we have four relationships. Two of them obviously give information about the 90 and 150 Hz signals and two give information about the reference signals. Using a shorthand notation, namely I for in-phase and Q for quadrature components, these four relationships are:

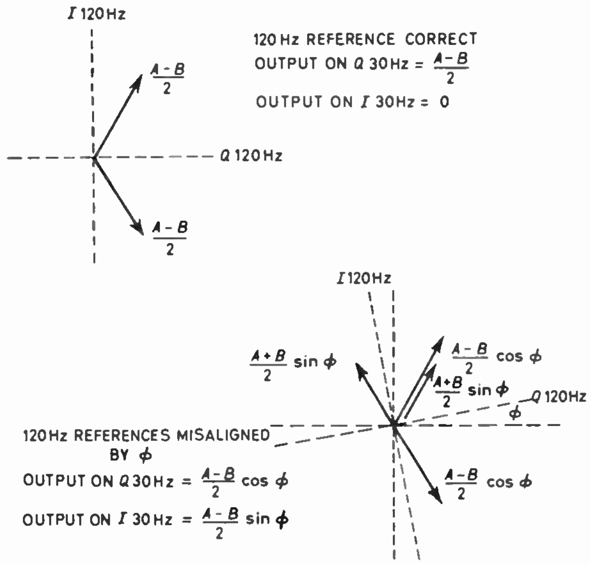

Fig. 4. Splitting of resolved components by I120 Hz and Q120 Hz.

(1) I 120 and I 30 → $(A+B)$ → total modulation depth

(2) Q 120 and Q 30 → $(A-B)$ → difference in modulation depth or d.d.m.

(3) Q 120 and I 30 → 120 Hz reference phase error

(4) I 120 and Q 30 → 30 Hz reference phase error and 90 Hz/150 Hz relative phase.

It is not immediately obvious that (4) gives a bonus of information. In the original 90 and 150 Hz waveform the phase relationship of the tones is really determined by the phase relationship of the 30 Hz modulating waveform with respect to the 120 Hz

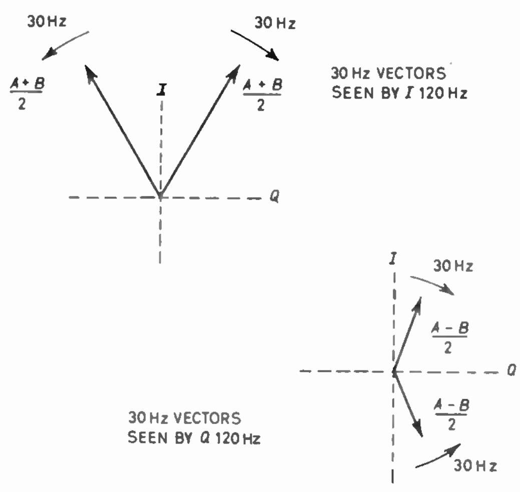

Fig. 5. Effect of phase error in 120 Hz reference.

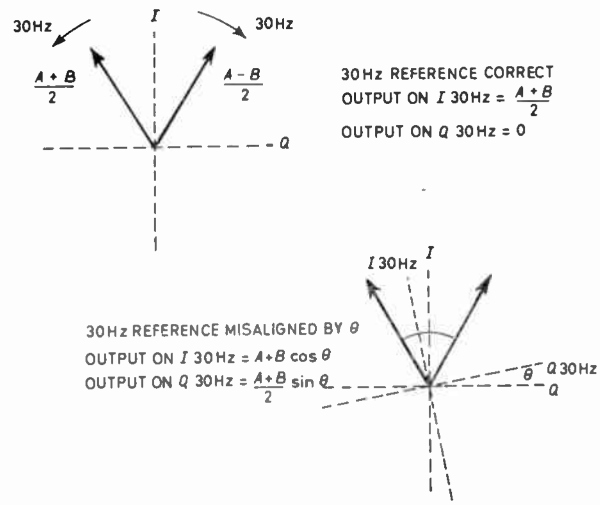

Fig. 6. Effect of phase error in 30 Hz reference.

carrier. The normal phase relationship is given by sin 30 Hz with sin 120 Hz, and the abnormal phase by sin 30 with cos 120 Hz. Thus for a 90° change of 120 Hz phase or a $22\frac{1}{2}°$ change in 30 Hz phase (which amounts to the same thing), the phase relationship changes from normal to abnormal. Now when we produce the 30 Hz reference signals it is convenient to do this by direct division from the 120 Hz reference. If we now introduce a calibrated phase shifter in the divider chain then when the 30 Hz phase is aligned using this phase shifter and eqn. (4), the position of the phase shifter gives a measure of relative phase between the 30 Hz and 120 Hz or by appropriate calibration between 90 Hz and 150 Hz.

So we have all the required information about the I.L.S. tones. Of course, the main advantage of this system is that the information is in the form of 30 Hz signals and may be filtered and amplified without the errors associated with d.c. systems.

The zero d.d.m. may be displayed as a very sensitive and accurate null reading and offset d.d.m.'s give 30 Hz signals linearly related to the difference in amplitudes of the two tones.

3. System Block Diagram

We can now build up a basic block diagram for the measurement (Fig. 7). In this the 30 Hz detectors are shown as multipliers because this is the general case. Ideally pure analogue multipliers would be used in all cases multiplying by the reference fundamental component only, but p.s.r.'s which effectively multiply by all the Fourier components of the reference square wave may be used for simplicity in many cases.

There are many ways of obtaining the 120 and 30 Hz references from the I.L.S. tones but the simplest is to make use of the phase-locked oscillator technique at 120 Hz using binary dividers to obtain the 30 Hz. The phase-locking signal can be obtained from the 120 Hz phase information from eqn. (3) as shown in Fig. 8.

For a simple d.d.m. read-out with constant 90 Hz and 150 Hz relative phase, as might be required for, say, an aircraft receiver, the phase shifter may be set constant and this simple loop may be used.

A high-gain amplifier in the 120 Hz phase-locking loop ensures accurate phasing of the 120 Hz reference with the 90 Hz and 150 Hz signals and no adjustment is required.

Where modulation depth and relative phase measurements are also required the block diagram must be expanded (Fig. 9).

This type of system would be required for monitoring or measurement purposes. When used with clean signals, as in checking of laboratory instruments and test gear, and for basic course-structure measurements, the multipliers may all be of the simple p.s.r. type. In noisy situations such as flight calibration, or critical ones such as course-line monitoring, the circuit must be as discriminating as possible against interference, and pure analogue multipliers with sine wave references must be used at least in the main reference generator loop. In this situation the chief difficulties are caused by Doppler effects or reflected signals which can give interference frequencies in the range 0–100 Hz and propeller modulation in the case of calibration aircraft which can give modulation frequencies around the 300 Hz region. The 120 Hz multiplier must be well balanced so that there is no direct feed-through of frequencies such as 30 Hz and give low distortion to avoid producing 30 Hz outputs with harmonics of the reference signal. All this can be achieved with a fairly simple multiplier, such as a pulse width modulator type.

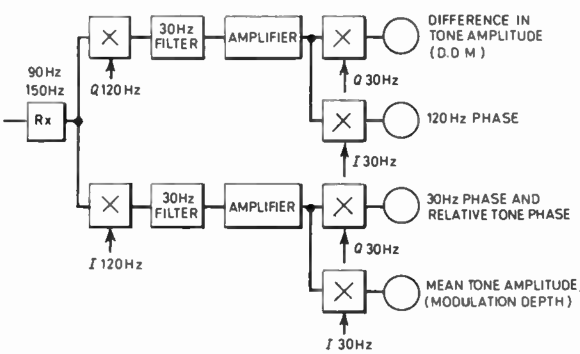

Fig. 7. Basic measurement system.

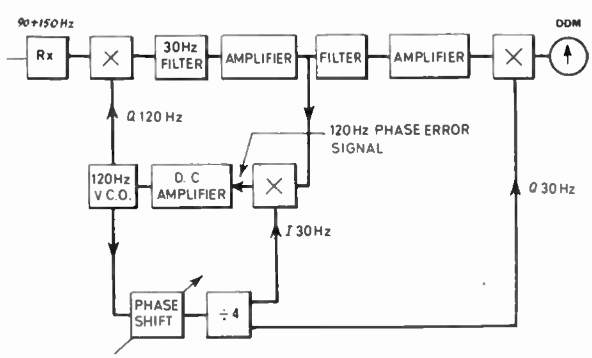

Fig. 8. Reference generator and d.d.m. channel.

The other requirement is for the reference phase-lock loop to lock under noisy conditions and if the signal disappears for a short time it should relock immediately the signal comes back. The systems developed do, in fact, 'flywheel' for a time so that, for short breaks, signal relocking is instantaneous. For longer breaks

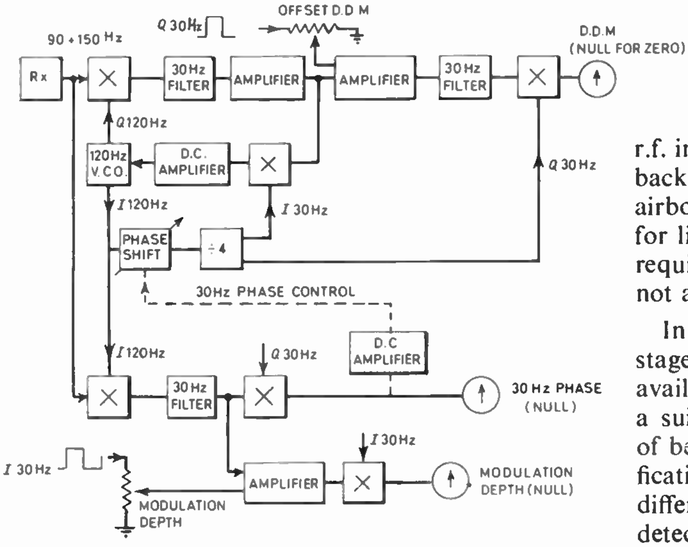

Fig. 9. Complete measurement system.

a rapid lock is possible. The following characteristics have been observed:

Locking-in time: 0·1 s on clean signal

Locking-in time: 1 s on very noisy offset d.d.m. signal (worst case)

Response to change or relative phase both 120 and 30 Hz: 0·1 s

Response to change in d.d.m.: 0·1 s to 95%.

Note the rapid response to change in relative phase. The 30 Hz phase loop can, in fact, give other information; for instance, in the airborne calibration role there is a requirement to distinguish between interference by signals around the tone frequencies and beam bends. Both would give an apparent low frequency oscillation in the d.d.m. outout, but whereas the beam bend is the coherent I.L.S. signal and would have no relative phase movement, the spurious signal would give an apparent movement in the relative phase and hence the 30 Hz phase loop, and the discrepancy can be detected.

It is interesting also that the phase-lock loop locks solidly on a signal buried in noise or spurious signals of two or three times the tone amplitude.

4. Modulation Depth and True D.D.M.

The system so far described gives a very accurate indication of zero d.d.m. and enables one to measure differences in tone amplitude and sum of tone amplitudes as a.f. signals. However, to convert the difference of tone amplitude into difference in depth of modulation, or d.d.m. and the sum of tone amplitudes into mean modulation depth, accurate information about the relationship of the a.f. tones with the v.h.f. carrier must be obtained. Obviously then the v.h.f. receiver which feeds the system plays an important part in the accuracy of these measurements. Basically the receiver must have a very linear transfer characteristic between r.f. input and d.c. detector output, and the a.g.c. feedback must not modify the a.f. characteristics. Standard airborne communications receivers are well designed for linearity in early stages to meet cross-modulation requirements but the output and detector circuitry is not adequate for accurate measurements.

In one particular British receiver when the final i.f. stage is replaced by a low distortion amplifier with an available output swing of 25 V peak-to-peak feeding a suitable d.c. coupled detector, an overall linearity of better than 0·2% is achievable. By suitable modifications to the a.g.c. system, using a high-gain differential amplifier and a stable reference, the detector working point is held stable at a chosen value to better than 0·1% over an r.f. input range from 100μV to 10 mV and similarly over the temperature range −10 to +50°C.

Thus we have a receiver in which we can safely predict that for an effective detector working point of 7·07 V d.c. and with 20% sine wave modulation depth the a.f. output signal will be exactly 1 V r.m.s. with an error no more than 0·3%. The receiver has an a.f. output which depends solely on modulation depth and the a.f. circuitry that follows can now make accurate modulation depth and true d.d.m. measurements by simply measuring tone amplitudes.

The logical development therefore on both d.d.m. and modulation depth measurement is to generate 30 Hz square waves of suitable phase and accurately known amplitude to give null beats with the 30 Hz signals from the $(A-B)$ and $(A+B)$ 120 Hz multipliers, and thus to get null indications of these quantities which are not dependent on the gain accuracy of the 30 Hz filters and rectifiers (Fig. 8). The inherent long term stability of this system is particularly useful in the static or far-field monitoring role.

5. Circuit Requirements

Now let us briefly consider the circuit requirements for a representative system.

The two main measurement channels are shown. If the null method is used for modulation depth and offset d.d.m., then the only elements which are critical of gain are the receiver (which we have discussed), the two 120 Hz multipliers and the two filters which follow.

The filters are simple low-pass types to reduce 210 Hz and 270 Hz components in the waveform and sufficiently high stability can be obtained using polyester capacitors and metal oxide resistors.

The square wave multipliers used for the $(A+B)$ channel have inherently constant gain. The pure multiplier for the $(A-B)$ channel can be of the simple mark-space type and by feedback over the 120 Hz reference input the change in gain can be made less than 1% over the temperature range $-10+50$°C. The d.c. amplifiers in the two phase-feedback loops can be achieved with a simple four-transistor circuit without selection of components. All other blocks are basically non-critical.

The whole system can be made entirely without transformers or chokes and the type of circuitry employed lends itself well to hybrid micro-miniaturization.

6. Conclusions

Much development has been carried out since Gouriet's† original ideas were published two years ago. The system has been shown to stay locked and give excellent results at d.d.m.'s approaching single tone condition and in the presence of enormous amounts of noise and spurious signal. The accuracy and stability obtained on zero d.d.m. is at least an order better than can be obtained with filter techniques. It does not drift with temperature, modulation depth changes, tone frequency, r.f. signal, etc., and in fact, has no zero setting control, nor is there any need for one.

By suitable receiver design and using a.c. null methods, modulation depth and offset d.d.m. can be measured to better than 1% accuracy, the latter being a true d.d.m. measurement and not simply a tone ratio.

Measurement of relative tone phase can give a bonus of information on interference detection.

† G. G. Gouriet, 'A new approach to I.L.S. modulation depth comparison', *Electronic Engng*, 36, p. 2, January 1964.

Finally, a rough comparison of the capabilities of this system compared with best conventional filter methods is given in Table 1.

Table 1

Comparative system performance

	Conventional	Phase locked		Transmitter requirement
		present	future	
Zero d.d.m.	±0·001	0·0001	0·0001	0·00067
Offset d.d.m. (normalized)	—	3%	1%	—
Offset d.d.m. (true)	5%	5%	1%	5%
Mean modulation depth	2% of m (single tone)	2½% of m	1% of m	2½% of m
Relative phase	—	2° at 90 Hz	1° at 90 Hz	1·5° at 90 Hz

7. Acknowledgments

I would like to acknowledge the work of my colleague, Mr. E. J. Grisley, who has contributed much to the material on which this paper is based, and to thank the Royal Aircraft Establishment, Farnborough and The Wayne Kerr Company for permission to publish the paper.

Manuscript received by the Institution on 4th April 1966. (Paper No. 1083/RNA57.)

U.D.C. 621.396.933.23

An Experimental I.L.S. Echo-Monitoring System

By

J. G. FLOUNDERS†

Presented at the Radar and Navigational Aids Group Symposium on 'Monitoring of I.L.S. Ground Equipment for Automatic Landing' held in London on 4th April 1966.

Summary: An experimental system for monitoring on the ground the I.L.S. localizer signals reflected from a landing aircraft is described. Special features of the equipment developed for the monitor, and a selection of the trials' results which give an indication of the correlation obtained between airborne and ground recordings, are included.

1. Introduction

The possibility of using radar-like techniques to try and receive on the ground a reflected replica of the I.L.S. signals being received in the landing aircraft, was first put forward by the Radio Department of Royal Aircraft Establishment, early in 1964. The proposal was particularly attractive in that if it were proved feasible, integrity information would be directly available on the ground in real-time and without the need for additional airborne telemetry equipment. In June 1964 work was started on the design and construction of an experimental system to enable the feasibility of the echo-monitoring principle to be assessed. It was intended to process the reflected signals received by the echo-monitor, in a similar manner to that used in the airborne receiver system, record them, and subsequently correlate them with the signals received in the landing aircraft and similarly recorded.

From the degree of correlation obtained over a statistically significant number of landings it would be possible to define the confidence level to be placed on the device as an integrity monitor for Category III I.L.S. installation.[1, 2] In parallel with the construction of the ground equipment, the B.E.A. fleet of *Vanguard* aircraft were fitted with small portable tape recorders connected to record the I.L.S. localizer guidance signals, together with identification and timing signals to assist the subsequent correlation process, during the latter stages of the landing from the outer marker beacon to touch-down.

At the present time, whilst there have not yet been enough landings monitored to enable the degree of confidence to be defined, early results indicate that the echo-monitor principle is feasible and that guidance and interfering signals received in the aircraft are reproduced in the ground equipment recordings.

† Plessey Radar Limited, Cowes, Isle of Wight.

2. The Equipment Design

Performance calculations based on the well-known 'radar-equation'[3] showed that it would not be difficult to obtain usable echo signal strengths from typical commercial aircraft, and that provided the received noise level could be kept low enough an adequate signal/noise ratio should be obtained at all ranges of interest. Received noise as defined here includes both system thermal noise and transmitter noise. The first of these is readily calculable in terms of noise power per cycle of receiver bandwidth and the noise figure of the receiver input stages. In the echo-monitor equipment the use of a low-noise r.f. preamplifier and narrow-band filters in the receiver and analysis equipment ensured that thermal noise was not a limiting factor in the measurements.

Transmitter noise, however, is not calculable with any accuracy since it depends on the spectral characteristics of the particular I.L.S. localizer transmitter in use; the separation between the transmitting and receiving aerials and nearby reflecting objects; the radiation patterns of the transmitting and receiving aerials, and the receiver characteristics. In order to reduce transmitter noise as much as possible it was necessary to site the echo-monitor well forward of the localizer transmitter, in practice near the runway threshold; to design a receiving aerial with a good front-to-back gain ratio; and to utilize the Doppler shift introduced into the reflected signals by the velocity of the landing aircraft to discriminate against the transmitter signals.

The combination of these techniques resulted in a low enough transmitter noise level to enable good quality recordings to be made at Farnborough, usable echo signals being obtained from aircraft at ranges of 5–7 miles. At London Airport, where the equipment was installed earlier this year, the transmitter noise level was found to be significantly greater and limited the useful range to some 2–3 miles. Investigation showed the high level to be due to the transmitter characteristics, the proximity of large buildings acting as scatterers, and the restricted choice of sites for the monitor aerial. Improvements to the a.f.c. system to accommodate the transmitter frequency characteristics, and the optimization of the band-stop filter characteristics are being incorporated which it is hoped will increase the useful range to the order of 5 miles.

3. The Aerial Array

A number of different aerial systems were considered notably Yagi,[4] slotted,[5] and Sterba[6] arrays but the dipole-fed corner reflector[7] was chosen since it has a good front-to-back gain ratio, has good low elevation angle gain for a modest structure height, and is simple to feed. The initial design was verified by scale model tests (approx. 30 : 1 scale) over an extended ground plane. These tests confirmed that maximum gain at low elevation was obtained with a dipole height of $0{\cdot}75\lambda$. Figure 1 shows the measured vertical radiation pattern of the model. With the design value of corner angle at 90 deg, reflector side lengths of $\lambda/\sqrt{2}$ and dipole to apex spacing of $0{\cdot}35\lambda$, the resonant-dipole impedance is almost exactly 50 ohms. Matching problems were therefore reduced to small adjustments of dipole parameters to compensate for mutual coupling effects between elements.

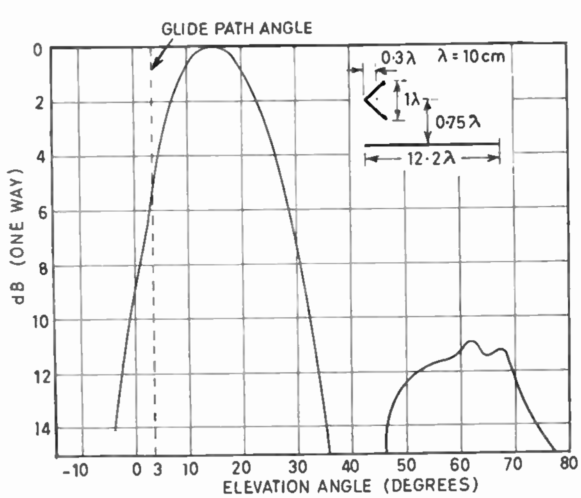

Fig. 1. Vertical radiation pattern of corner reflector above ground plane.

The broadside array of six dipoles was fed by a matched cable network as shown in Fig. 2, the direction of maximum gain in the horizontal plane being controlled by selection of the electrical length of the feed cable to each dipole. The complete array is approximately 33 ft long by 12 ft high and has a

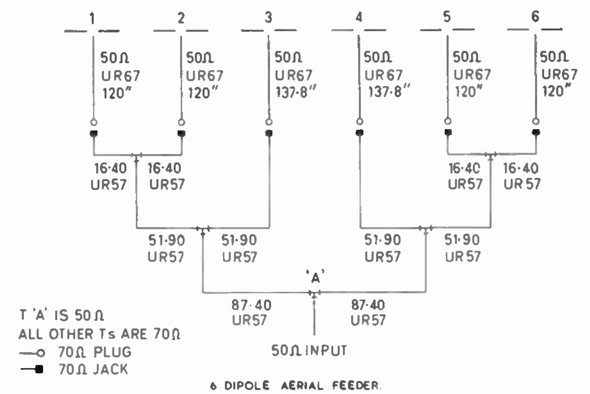

Fig. 2. Six-dipole aerial feeder arrangement.

horizontal beamwidth of 15°. Measurements of front-to-back gain ratio were made both with and without an extra mesh screen behind the corner reflector and gave values of over 30 dB and approximately 20 dB respectively. In view of the need for a low value of transmitter breakthrough, the extra screen was retained in the final design, and can be seen in Fig. 3 which shows the array in position at London Airport.

4. Low Noise Preamplifier

A special low-noise transistor r.f. preamplifier was developed for inclusion in the aerial array feeder cable adjacent to the aerial structure. The preamplifier has a gain of 37 dB, a noise figure of 2·5 dB and a bandwidth of 4 MHz to −3dB points. It is thus suitable for use at any localizer channel frequency in the band 108–112 MHz. The unit is matched into 50 ohm coaxial cable at both input and output and is fed with d.c. power via the output coaxial cable. Using this arrangement it was possible to site the main receiving equipment at any convenient distance from the aerial without degradation of system signal noise performance due to losses in the coaxial cable.

5. The Main Receiver

A block diagram of the main receiver is given in Fig. 4. Two standard airborne localizer receivers type R.1964 were obtained and modified for use in the monitor system. One was used as the main echo signal receiver, and the other as a control receiver for a.f.c. purposes. It will be appreciated that in order to make use of the difference in frequency due to Doppler shift between the localizer transmitter signal and the echo signal, precise control of receiver tuning is necessary, since at normal aircraft landing speeds the Doppler shift is typically only 30–40 Hz.

Both receivers were modified to use common local oscillators and to produce a new third i.f. of 27·8

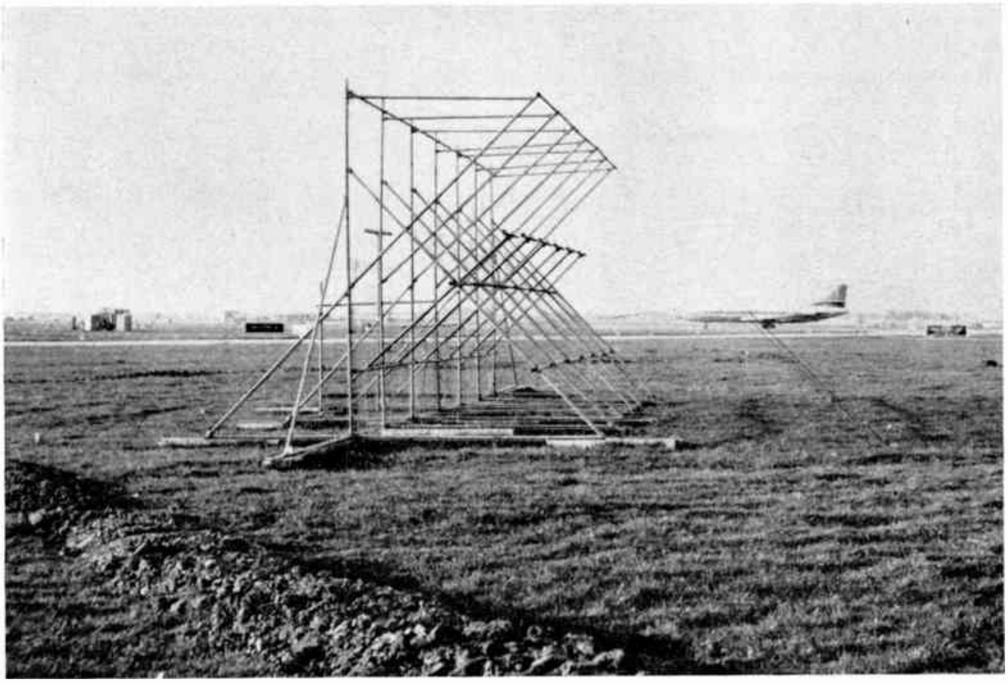

Fig. 3. Completed dipole-fed corner reflector array in position at London Airport.

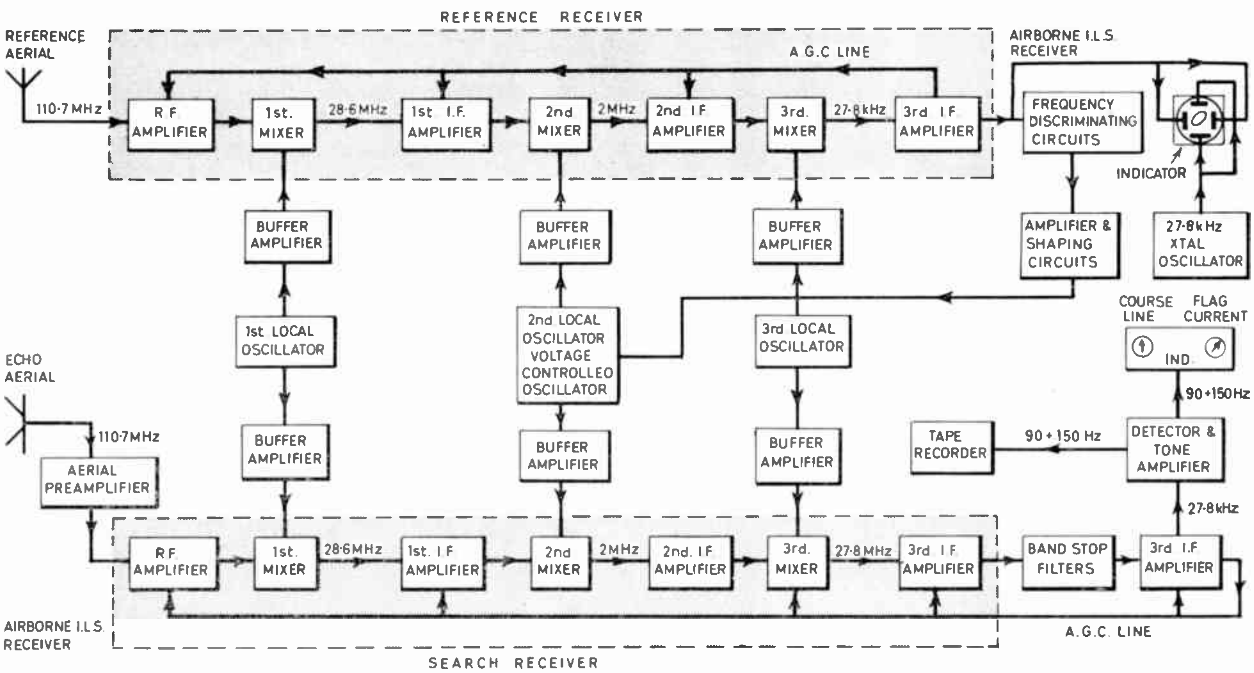

Fig. 4. Block schematic of echo-monitor system.

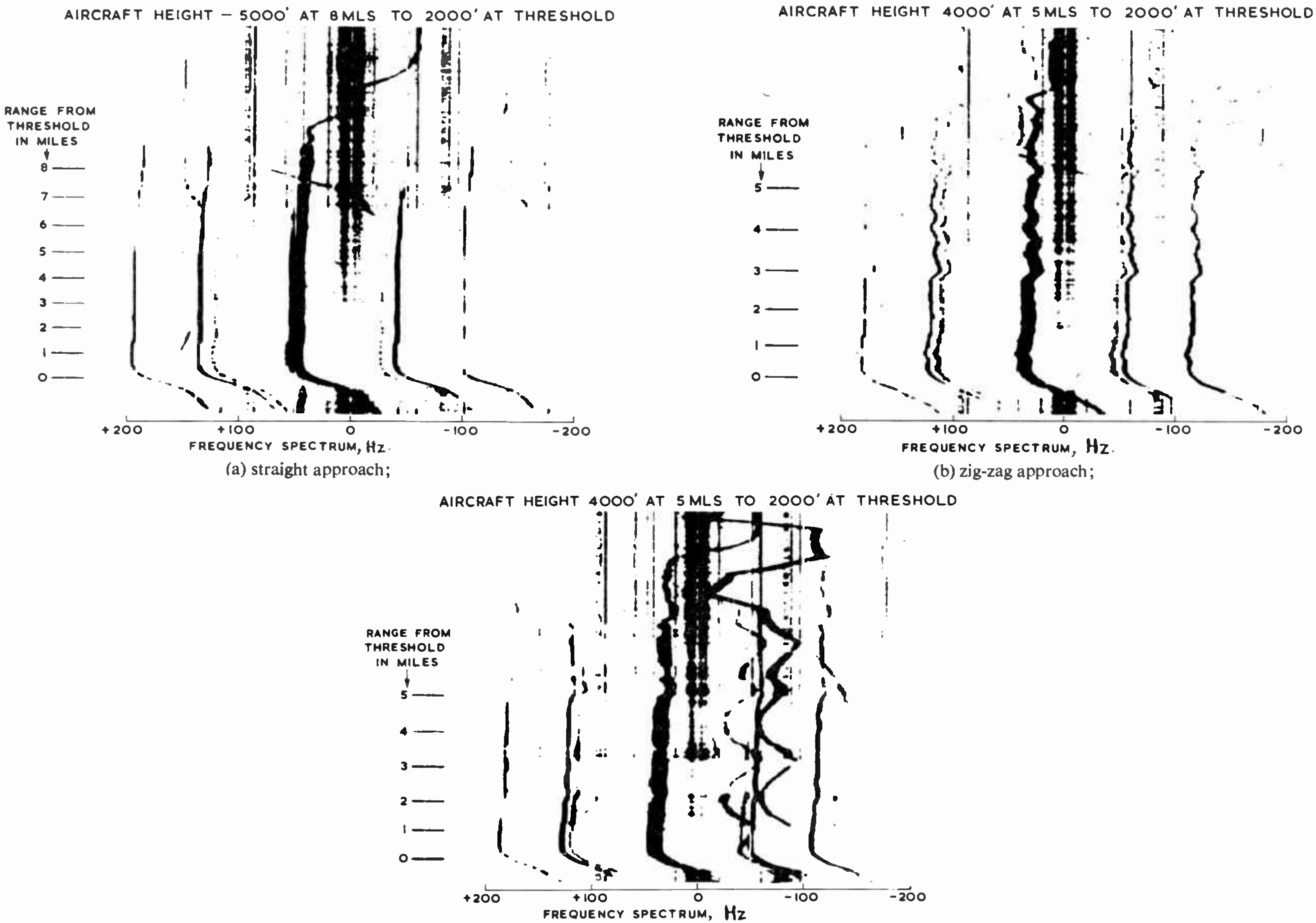

(a) straight approach;

(b) zig-zag approach;

(c) straight approach with interference.

Fig. 5. Reflected I.L.S. signals from an approaching aircraft.

kHz. This frequency was chosen since it matched the frequency-analyser equipment available at R.A.E. and was a convenient frequency for the necessary crystal band stop filters used to attenuate the localizer transmitter carrier and sidebands. The third i.f. output of the control receiver was fed to a frequency discriminator using a pair of crystals with a frequency separation of 4 Hz, centred on 27·8 kHz, and the output error voltage, after d.c. amplification, was used to control a varactor diode coupled to the common second local oscillator circuit.

A second 27·8 kHz crystal-controlled oscillator was used for comparison with the third i.f. output of the control receiver, the two frequencies being fed in quadrature to the X and Y plates of a small oscilloscope c.r.t. Correct tuning is indicated by a stationary circle on the tube.

Voltage controlled tuning by means of a varactor diode was also used as a fine manual control of the first local oscillator in order to bring the receiver tuning within the a.f.c. lock-in range.

It was necessary to improve the linearity of the second i.f. amplifiers in the echo signal receiver, in order to prevent the transmitter break-through signals generating spurious frequencies which would not be rejected by the subsequent band-stop filters. Adequate linearity was obtained by the use of r.f. power pentodes in place of the small signal valves normally used.

After linear amplification the transmitter and echo signals were passed to a set of five band-stop crystal filters tuned to attenuate the transmitter carrier by 50 dB and the ± 90 Hz and ± 150 Hz sidebands by some 30 dB. Each filter had a stop bandwidth of 4 Hz (hence the need for an accurate a.f.c. system), and the filter unit contains buffer amplifiers so that the overall gain is near unity for all other frequencies of interest. After removal of the transmitter signals the echo signals were further amplified and processed in an exactly similar manner to that used in the airborne receiver system to provide outputs to a centre-zero microammeter, for course-line indication, and to a signal strength meter for 'flag current' indication.

Outputs were also provided to feed a standard twin-track audio tape recorder, one track for the guidance signals, and the other for voice recording such information as timing, aircraft identification and range, operator/pilot conversation, etc.

Two types of output analyser were used, the first consisted of a bank of 200 filters each 2 Hz wide, covering the receiver third i.f. of 27·8 kHz $\pm$ 200 Hz. The outputs of these filters were sampled and recorded on a standard 'Mufax' paper recorder, giving a record of the frequencies present in the receiver output. This type of record was particularly useful in identifying the Doppler shifted signals and ensuring that no spurious frequencies were generated in the receiver. Figures 5 (a) to (c) inclusive are typical of the records obtained using the frequency analyser and 'Mufax' equipment.

The second analyser used was a special version of the airborne navigation unit which processed the tape recorded signals and produced a paper record of the angular deviation from course-line and flag current. This equipment was used to process tapes recorded in the echo-monitor equipment and also tapes recorded in the landing aircraft, so that direct comparisons could be made without introducing instrumental errors.

6. Trials Results

The experimental echo-monitor equipment was installed at Farnborough close to the threshold of the main runway and after an initial commissioning period was used for a series of trials to evaluate equipment performance generally and to do comparison trials with a controlled aircraft both with and without deliberate interference present.

The equipment was recently transferred to London Airport and installed adjacent to the threshold of No. 5 runway (28 left) where it is hoped to record sufficient landings to enable a statistical correlation evaluation to be made in the near future.

The results reported here relate to the trials carried out at Farnborough.

Figure 5 (a) shows a typical record of an aircraft making a straight approach to the runway using the frequency analyser and 'Mufax' recorder as mentioned earlier.

Noise sidebands of the transmitter carrier are visible at the top of the record, around 0 Hz Doppler shift, and the reflected carrier and sidebands are clearly visible from some 7 miles range to the overhead position. Automatic gain control derived from the reflected carrier signal can be seen reducing the background noise level as the aircraft approaches. The faint dotted lines visible over the last 3 miles are the sidebands due to modulation of the carrier by aircraft propeller movement.

Figure 5(b) shows the same aircraft making a zig-zag approach, and the small changes in relative velocity due to its changing direction can be clearly seen.

In both the above runs no deliberate interference was present.

In Fig. 5(c) an interference generator radiating 1 watt of unmodulated carrier signal was set up at about 1 mile from the runway centre-line on the opposite side to the echo-monitor and tuned to interfere with the lower 90 Hz sideband of the localizer signal. This interfering line can be seen being tuned on to frequency at the top of the record and then

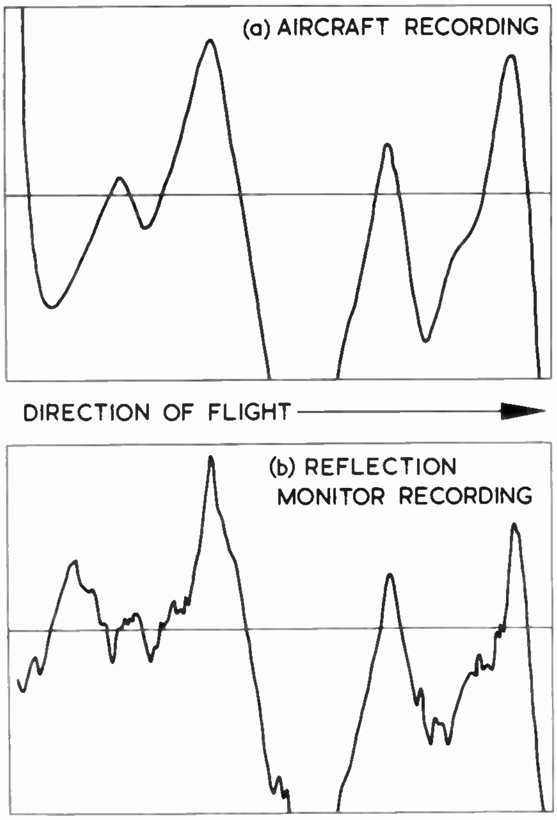

Fig. 6. Comparison of aircraft recording and echo-monitor recording for a zig-zag approach.

drifting slowly around the −90 Hz sideband. The reflected interference line Doppler-shifted by the aircraft can be seen to be a good replica of the interfering signal.

Modulation of the a.g.c. by the interference can be detected and during the approach the pilot reported interruptions in flag current and incorrect and erratic guidance signals in the aircraft.

An example of the comparison of airborne and echo-monitor recordings is shown in Fig. 6. In this case the aircraft was making a zig-zag approach with an angular deviation from the course line of the order of $\pm 3°$. The point where good correspondence between recordings begins is about 5 miles from the runway. In general the correlation is good with the exception of small noise-like modulations present in the echo-monitor record. These were due to imperfections in the flatness of the passbands between the band-stop filters, and the reduced signal strength of the echo signals when the aircraft was at maximum deviation from the correct course line.

7. Conclusions

The experimental echo-monitoring system has demonstrated the principle that information can be obtained on the ground which allows the integrity of the guidance signals being received in the aircraft to be monitored on a real-time basis, without the need for additional airborne equipment or an air-to-ground data link. Further development of the equipment is required to eliminate the remaining instrumental errors and improve the quality of the echo signal recordings. A considerable amount of operational experience and the collection of the necessary quantity of statistical data are needed before it can be confirmed that the high reliability of alarm and low incidence of false alarms, necessary for a Category III monitor system, can be achieved.

8. Acknowledgments

Acknowledgment is made to the Ministry of Aviation who supported this work. The author would also like to thank the members of R.A.E. Radio Dept. for their assistance in the preparation of the results given, Mr. W. F. Winter who conducted most of the trials, and the Directors of Plessey Radar Ltd. and Decca Navigator Co. Ltd. for their permission to publish this paper.

9. References

1. I.C.A.O. Aeronautical Communications Annex 10, Seventh Edition, August 1963.
2. F. R. Gill, 'The Integrity of a Civil Blind Landing System with particular reference to the Azimuth Channel', R.A.E. Technical Report, No. 65022, February 1965.
3. M. I. Skolnik, 'Introduction to Radar Systems' (McGraw-Hill, New York, 1962.)
4. D. G. Reid, 'Gain of an idealized Yagi array', *J. Instn Elect. Engrs*, **93**, Pt. IIIA, p. 564, 1946.
5. Radio Research Laboratory Staff Harvard University, 'Very High Frequency Techniques', Vol. 1. (McGraw-Hill, New York, 1947.)
6. E. J. Sterba, 'Theoretical and practical aspects of directional transmitting systems', *Proc. Inst. Radio Engrs*, **19**, No. 7, p. 1184, July 1931.
7. H. Jasik, 'Antenna Engineering Handbook', Chapter II. (McGraw-Hill, New York, 1961.)

Manuscript received by the Institution on 25th May 1966. (Paper No. 1084/RNA58.)

U.D.C. 517.75 : 621.3.092.53

An Analogue Method of Studying the Angular Spectrum of Radiation Reflected from Rough Surfaces

By

B. WALKER, M.Sc.(Tech.), C.Eng. (*Associate Member*)†

Summary: The approximate analogy between the angular spectrum of radiation reflected from a one-dimensional rough surface and the frequency spectrum of a burst of carrier, phase modulated by an appropriate waveform which is directly related to the surface profile, is described. In each case, and subject to certain approximations, the relationship is a Fourier transform. A simple analogue computer is described and used to justify the principle and demonstrate a convenient means of studying reflection problems approximately for both regular and random rough surfaces. Use of the analogue method allows changes in the surface parameters to be introduced easily so that their effects on the angular spectrum may be observed. The technique is applicable to normal or oblique incidence.

List of Principal Symbols

S	sine of angle of incidence
C	cosine of angle of incidence
$F(S)$	angular spectrum
$z(x)$	surface profile
$g(x)$	field function in the plane of the reflecting surface
$\phi(x)$	phase of $g(x)$
$A(x)$	intensity of $g(x)$
$F(f)$	frequency spectrum
$g(t)$	voltage function of time
$\phi(t)$	phase of $g(t)$
$A(t)$	amplitude of $g(t)$
f_c	carrier frequency
$\rho(\xi)$	field autocorrelation function
$\rho(\tau)$	time autocorrelation function
ξ_0 and τ_0	field and time autocorrelation coefficients
M	modulation sensitivity
λ	radiation wavelength
Λ	wavelength of surface undulations
h	surface height, peak value of sine wave
σ	standard deviation of h
ϕ_0	standard deviation of $\phi(x)$ or $\phi(t)$
l	width of illuminated area

1. Introduction

Problems associated with the reflection of waves from rough surfaces are encountered by engineers in many fields concerned with propagation, e.g., radar,[5,6] radio propagation and ultrasonics. One important property of the reflected radiation is its far-field angular spectrum and the object of this paper is to demonstrate an approximate but convenient method of obtaining this spectrum. The method uses an analogy which has been pointed out by Ratcliffe[1] between the frequency spectrum of a time-varying signal and the angular spectrum of radiation from an aperture: in each case, and subject to certain approximations, the relationship is a Fourier transform. Consequently it is possible to simulate a particular rough surface by an appropriate time-varying signal, obtain the frequency spectrum of this by means of a wave analyser, and hence infer the angular spectrum.

A reflection pattern may be studied directly by illuminating the particular surface and measuring the reflected radiation pattern. This method may be suitable in certain applications but it is laborious and it is not easy to make controlled changes in the surface profile. Alternatively it is possible to relate the radiation pattern to the surface profile mathematically[2] (with approximations), but unfortunately for all but the simplest profiles this approach is also very laborious. Although a solution may be possible for a specific reflector it is again difficult to appreciate the effect of changes in the surface dimensions. The analogue method described here is subject to the same approximations as are frequently made in the mathematical methods but its primary advantage is that subject to these approximations, scatter from any surface profile may be investigated with relative ease, controlled changes in the surface dimensions are readily made, and their effects easily studied. One-dimensional periodic or random rough surfaces may be inspected; in the latter case the statistics of the surface are specified and the angular power density spectrum is obtained. The method may be extended to deal with oblique incidence.

† Formerly at Lanchester College of Technology, Coventry; now at Rutherford College of Technology, Newcastle upon Tyne.

2. The Analogy between a Time-varying Signal and the Reflection from a Rough Surface

2.1. *Reflection from a Rough Surface*

Consider a one-dimensionally rough surface with mean level in the XY plane and rough only in the X direction. The surface is defined by $z(x)$ and suppose the surface to be illuminated by a plane wave having amplitude $A(x)$. Radiation scattered from the surface may be supposed to consist of an angular spectrum of uniform infinite plane waves in the XZ plane. The field due to the reflected radiation at any point in the XZ plane is given by

$$g(x,z) = \int_{-\infty}^{\infty} F(S)\exp\{j2\pi(Sx+Cz)\}\,dS \quad \ldots\ldots(1)$$

S and C are the sine and cosine of the angle formed between the wave normal and the Z axis, $F(S)$ is the complex angular spectrum expressed in terms of S and the quantities x and z are measured in units of wavelength.

In the plane of the reflector

$$g(x,0) = g(x) = \int_{-\infty}^{\infty} F(S)\exp\{j2\pi Sx\}\,dS \quad \ldots\ldots(2)$$

Thus the angular spectrum is related through a Fourier transform to a fictitious field in the plane of the reflector: this field will be known as the field function. If a field function $g(x)$ exists or it generated at $z = 0$, then the angular spectrum $F(S)$ will result with $F(S)$ and $g(x)$ mutual Fourier transforms, i.e.

$$F(S) \rightleftharpoons g(x) \quad \ldots\ldots(3)$$

Since the angular spectrum is associated with a field function and also with a particular rough surface, it is evident[3] that a close relationship exists between the field function $g(x)$ and the surface profile $z(x)$. In fact, it is shown in Appendix 1 that the reflector behaves approximately as a phase changing screen with

$$g(x) = g_0 A(x)\exp\{-j4\pi z(x)\} \quad \ldots\ldots(4)$$

It will be useful to nominate the phase function

$$\phi(x) = 4\pi z(x) \quad \ldots\ldots(5)$$

to denote the phase of $g(x)$, i.e.

$$g(x) = g_0 A(x)\exp\{-j\phi(x)\} \rightleftharpoons F(S) \quad \ldots\ldots(6)$$

2.2. *The Signal Analogue*

The frequency spectrum $F(f)$ of a time varying voltage $g(t)$ is given by its Fourier transform,

$$F(f) = \int_{-\infty}^{\infty} g(t)\exp\{-j2\pi ft\}\,dt \quad \ldots\ldots(7)$$

$$F(f) \rightleftharpoons g(t) \quad \ldots\ldots(8)$$

If the signal is a carrier, amplitude modulated by $A(t)$ and phase modulated by a function $\phi(t)$ then

$$g(t) = V_0 A(t)\exp\{j2\pi f_c t + j\phi(t)\} \quad \ldots\ldots(9)$$

so

$$F(f) = \int_{-\infty}^{\infty} V_0 . A(t) . \exp j\{2\pi f_c t + \phi(t) - 2\pi ft\}\,dt \quad \ldots\ldots(10)$$

and at zero carrier frequency,

$$F(f) = \int_{-\infty}^{\infty} V_0 . A(t) . \exp j\{\phi(t) - 2\pi ft\}\,dt \quad \ldots\ldots(11)$$

Now eqn. (6), expressing an angular spectrum, may be written as

$$F(S) = \int_{-\infty}^{\infty} g_0 A(x)\exp j\{\phi(x) - 2\pi Sx\}\,dx \quad \ldots\ldots(12)$$

The similarity between eqns. (11) and (12) is the basis for the analogue. In principle the angular spectrum of radiation from a particular rough surface may be provided by obtaining the frequency spectrum of an appropriate time-varying signal and this is generally possible using simple electronic circuit techniques. The quantities f and t are analogous to S and x respectively and the relationship between them may be established as follows. Consider a simple reflection system consisting of a smooth surface uniformly illuminated over a width x_1, then eqn. (12) reduces to:

$$F(S) = g_0 \int_{-x_1/2}^{x_1/2} \exp\{-j2\pi Sx\}\,dx \quad \ldots\ldots(13)$$

with solution

$$F(S) = g_0 . x_1 . \frac{\sin 2\pi S \frac{x_1}{2}}{2\pi S \frac{x_1}{2}} \quad \ldots\ldots(14)$$

and the analogue is

$$F(f) = V_0 \int_{-t_1/2}^{t_1/2} \exp\{-j2\pi ft\}\,dt \quad \ldots\ldots(15)$$

$$= V_0 . t_1 . \frac{\sin 2\pi f \frac{t_1}{2}}{2\pi f \frac{t_1}{2}} \quad \ldots\ldots(16)$$

These spectra are shown in Fig. 1. It may be seen that if t seconds represent x wavelengths, then $f = 1/t$ cycles per second will represent an angle given by $S = 1/x$. The equivalence may thus be defined by the equation

$$\frac{t}{x} = \frac{S}{f} \quad \ldots\ldots(17)$$

Several extensions to these basic ideas are necessary before the analogue becomes a useful tool. Firstly, eqn. (12) yields a spectrum having both positive and negative values of S and correspondingly eqn. (11) yields one having positive and negative values of frequency which in practice will be inseparable by the frequency analyser circuits. It is therefore necessary to translate the whole frequency spectrum so that it is disposed about a carrier rather than about zero frequency. This is achieved by arranging for the function $\phi(t)$ to phase-modulate a carrier as suggested by eqn. (9); this is in any case a more practical electronic proposition than modulating zero frequency and the analogue remains with the same relationships. The actual carrier frequency chosen is not important provided that it is high compared with the spectrum widths to be investigated.

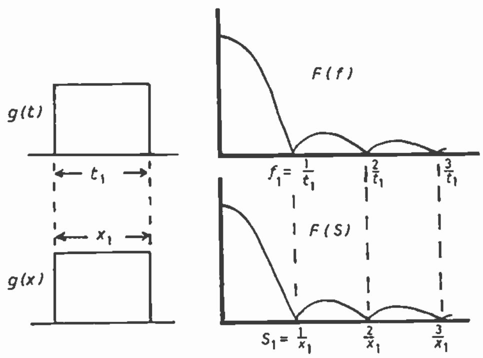

Fig. 1. Time–distance and angle–frequency relationships. (S is the sine of the angle of incidence.)

Secondly, the angular spectrum is confined to values of S between $+1$ and -1. Components outside this range correspond to evanescent waves which do not propagate, consequently we only have interest in the frequency range corresponding to

$$-1 < S < +1$$

It is known that if a very large rough surface is uniformly illuminated the spectrum is determined entirely by the nature of the surface. As the illuminated area is reduced, however, the term $A(x)$ in eqn. (12) becomes increasingly important and the spectrum is modified by edge effects. In simple cases this may correspond to a $(\sin x)/x$ function superimposed corresponding to the radiation pattern from a limited aperture, and this will be referred to as the aperture effect. In the former large surface case the analogue is simply a continuous time-varying signal, but a limited surface corresponds to a burst of signal which in isolation would be impossible to frequency-analyse; consequently the appropriate burst is repeated continuously. The aperture effects now appear as the envelope of a line spectrum with the line spacing equal to the reciprocal of the pulse repetition frequency. Choice of p.r.f. does not affect the spectrum but care is necessary to ensure that the lines are sufficiently close so that the envelope is defined without confusion with genuine spectrum fine structure.

2.3. *Application of the Analogue to a Random Rough Surface*

The Wiener-Khintchine theorem may be stated thus,

$$\rho(\xi) \rightleftharpoons |F(S)|^2 \qquad \text{......(18)}$$

$$\rho(\tau) \rightleftharpoons |F(f)|^2 \qquad \text{......(19)}$$

The right-hand side represents a power density spectrum and the left-hand side is the auto-correlation function of $g(x)$ and $g(t)$ respectively.[4] The auto-correlation function is a statistical measure indicating the average shape of irregularities in the function and is particularly useful in the case of random variables which cannot be specified exactly. It may be defined thus

$$\rho(\xi) = \lim_{X \to \infty} \frac{1}{X} \int_0^X g(x) . g(x+\xi) \, dx \qquad \text{......(20)}$$

or

$$\rho(\tau) = \lim_{T \to \infty} \frac{1}{T} \int_0^T g(t) . g(t+\tau) \, dt \qquad \text{......(21)}$$

Alternatively,

$$\rho(\tau) = \text{average}\,[g(t) . g(t+\tau)] \qquad \text{......(22)}$$

As τ increases, the correlation between $g(t+\tau)$ and $g(t)$ decreases and $\rho(\tau)$ falls to zero. The value of τ at which $\rho(\tau)$ has fallen to $1/e$ is known as the auto-correlation coefficient, τ_0, and similarly for ξ_0.

The similarity between the two systems is evident. A large illuminated surface is simulated by a continuous signal consisting of a carrier, phase modulated with noise having the appropriate autocorrelation function. The frequency power density spectrum may be obtained electronically and interpreted as an angular power density spectrum, relationships between the variables may be chosen as in Section 2.2.

The effects of limiting the illuminated area in the case of a random rough surface are twofold.[3] The spectrum is modified by an aperture effect as discussed in Section 2.2 and also a sampling effect is introduced. For a limited rough surface, X in eqn. (20) is not infinite so $\rho(\xi)$ and therefore $|F(S)|^2$ will deviate from the infinite surface value. If the rough surface is time varying but statistically stationary, a sea surface for instance, or if an assembly of statistically similar surfaces is available, the average angular spectrum obtained will be the large surface value of $|F(S)|^2$, modified by the aperture effect. This average spectrum may be obtained using the analogue by gating the signal to form bursts having duration appropriate to the surface length. The spectrum will fluctuate and a time average value is required at each frequency so a long time-constant detector may be necessary. The aperture effects again appear as a line spectrum and the envelope must be inserted. In this case the scatter components are incoherent, whilst the aperture effect components are coherent. Consequently if the signal energy is changed by increasing the p.r.f., the two sets of components will not increase in the same manner, and it is necessary to make both spectra incoherent in practice so that the overall spectrum is independent of the p.r.f. This could be done by jittering the p.r.f. slightly.

3. Experimental Justification of the Analogue

3.1. *Equipment and Technique*

A simple computer has been assembled to demonstrate the feasibility of applying the analogue to rough-surface scatter problems. A block diagram is presented in Fig. 2.

The function generator produces the phase function analogue $\phi(t)$ which is used to phase-modulate an oscillator. This modulated signal is gated by an adjustable square wave whose generating signal also triggers the function generator so that the gate and the modulating function are synchronized. The resulting burst of phase-modulated carrier is analysed by a wave analyser fitted with a motor drive so that the spectrum could be swept and displayed on a slow time-base oscilloscope or an automatic recorder.

The parameters of the system were chosen to suit the properties of the wave analyser and the function generator. The latter is a standard c.r.o. used as a curve follower (see Appendix 2), for this to be effective the time-base speed was limited, a suitable value for this equipment being 0·5 ms/cm which implies a pulse length of about 3 ms and an aperture effect lobe width of 1·7 kHz on the spectrum. The spectrum lobes must be defined by sufficient lines, so the pulse repetition time was chosen to be 30 ms and the timer circuit set to operate at this rate. The line spacing is therefore 33 Hz and this falls well within the resolution of the wave analyser, quoted as ± 20 Hz to 45 dB. The wave analyser operates to 50 kHz so the f.m. oscillator frequency was chosen to be about 30 kHz allowing an adequate spectrum width to be observed. Finally the sweep speed was chosen to suit the response time of the wave analyser and the recorder. There is some flexibility in the choice of these values and of course different equipment might impose quite different conditions.

The phase modulation is achieved by first differentiating the phase function by means of a simple CR circuit and then using the result to frequency-modulate an oscillator. The oscillator is a free-running multivibrator and the modulating signal is applied as the common base return potential. Since the wave analyser selects the fundamental of the multivibrator output a low-pass filter is unnecessary. The overall performance of the phase modulator was tested by applying a sine-wave modulating signal to give a phase deviation of about 0·8 radians and obtaining the spectrum for a range of modulating frequencies. The spectrum deteriorates as its bandwidth spreads and Table 1 shows an error rising to about 10% for components ∓ 5 kHz from the carrier; this error is due to the nonlinearity of the simple differentiator circuit. The deviation characteristic of the frequency modulator alone was found to be substantially linear from 20 kHz to 40 kHz. With this equipment, quantitative investigation has been limited to spectra having bandwidths less than 10 kHz; thus the error in the amplitude of spectral components rises from zero close to the carrier to 10% for extreme components. Finally the overall modulation sensitivity of the phase modulator (M-radians per volt) was obtained by applying a sine-wave modulating

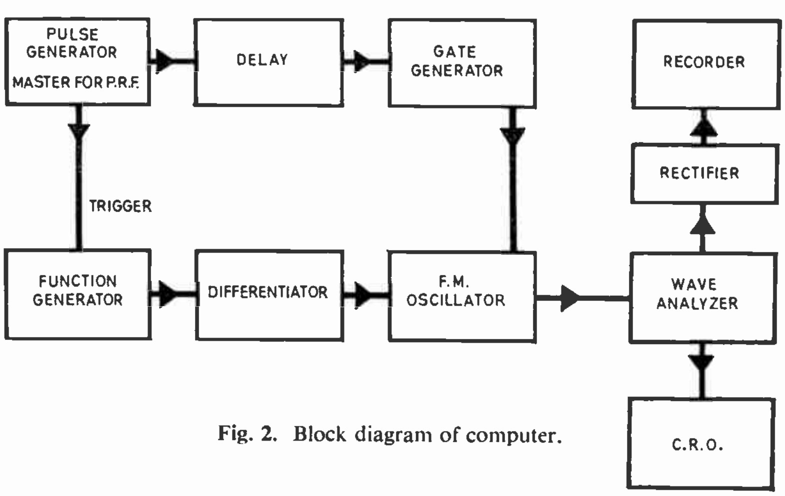

Fig. 2. Block diagram of computer.

Table 1

Fidelity of phase modulator with increasing bandwidth

Modulating frequency f_m	500 Hz	% error	1 kHz	% error	2 kHz	% error	4 kHz	% error	6 kHz	% error	8 kHz	% error
Carrier amplitude (volts)	0·52	0	0·52	0	0·52	0	0·53	+2	0·55	+6	0·56	+8
Amplitude of 1st side-band at ($f_c \mp f_m$)	0·26	0	0·26	0	0·26	0	0·24	−8	0·23	−13	0·22	−18
Amplitude of 2nd side-band at ($f_c \mp 2f_m$)	0·063	0	0·063	0	0·060	−5	0·055	−14	0·050	−25	0·040	−57

signal of known amplitude. In this case

$$\phi(t) = M \,.\, V \cos 2\pi f_m t \qquad \ldots\ldots(23)$$

and

$$F(f) = \int_{-\infty}^{\infty} V_0 \exp j[M \,.\, V \,.\cos 2\pi f_m t - 2\pi f t]\, dt \qquad \ldots\ldots(24)$$

and the solution is

$$F(f) = (j)^n \,.\, J_n(M \,.\, V) \quad \text{for integral } n \ \ldots\ldots(25)$$

where J_n is the Bessel function of the first kind and order n. The value of M was obtained from the spectrum by comparison with published values of Bessel functions and was found to be $M = 39$ rad/V for this equipment. These measurements were made with the gate generator disconnected so that the signal was continuous; in this way accuracy was improved since more energy was concentrated into a sharper spectrum.

3.2. *Reflection Pattern from a Limited Sinusoidal Surface*

The application of the analogue was tested by using it to investigate a reflecting surface whose reflection angular spectrum is simple and known. A limited sinusoidal surface is suitable and a surface consisting of 3 cycles of sinusoidal form with surface wavelength $\Lambda = 5\lambda$ was specified. The angular spectrum was obtained, the surface length being made an integral number of wave lengths (Λ) to eliminate edge effects. A 1 kHz sine wave was applied to the modulator (rather than use the function generator for such a simple waveform a signal generator was used and the gate p.r.f. trimmed to obtain a stationary waveform in the gate) and the gate width was adjusted to include three cycles of the modulating signal. Under these conditions with the surface wavelength specified as 5λ and the modulating signal time period equal to 1 ms, the time–distance relationship is 0·2 ms per unit wavelength (λ). In the resulting spectrum the angle–frequency relationship is, from eqn. (17),

$$\text{grazing incidence } (S = 1) \equiv 5 \text{ kHz}$$

The amplitude of the modulating signal was set to a series of values to simulate several surface heights as indicated in Table 2. The relationship between

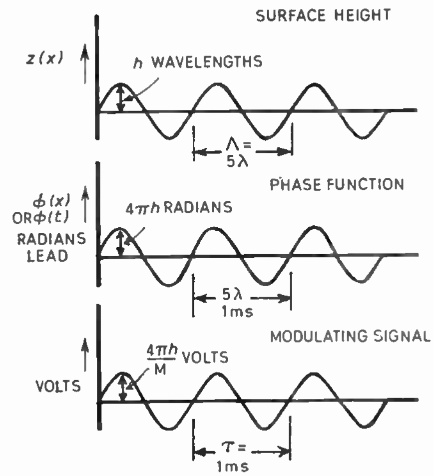

Fig. 3. Relationship between surface, phase function and modulating signal.

surface, field function and modulating signal is summarized in Fig. 3 and the recorded spectra are reproduced in Fig. 4. It is of course the envelope of the line spectrum which corresponds to the angular spectrum.

The spectrum for this type of surface is (within the approximations) the spectrum for an infinite sinusoidal surface with each line broadened into a $(\sin x)/x$ function corresponding to the limited aperture. This predicted spectrum is shown with the experimental result for the case of zero height variation and in the remaining results the theoretical maximum is shown for each lobe. A useful agreement is obtained but it is noticeable in Fig. 4 that the smaller lobes

Table 2

Values of modulation and corresponding surface height

Peak-to-peak modulating signal (volts)	0	0·05	0·1	0·2
Phase function, peak-to-peak range of $\phi(x)$ (radians) ($M =$ 43·5 radians/volt)	0	2·18	4·35	8·7
Surface profile, peak-to-peak range of $z(x)$ (wavelengths)	0	0·18	0·35	0·70

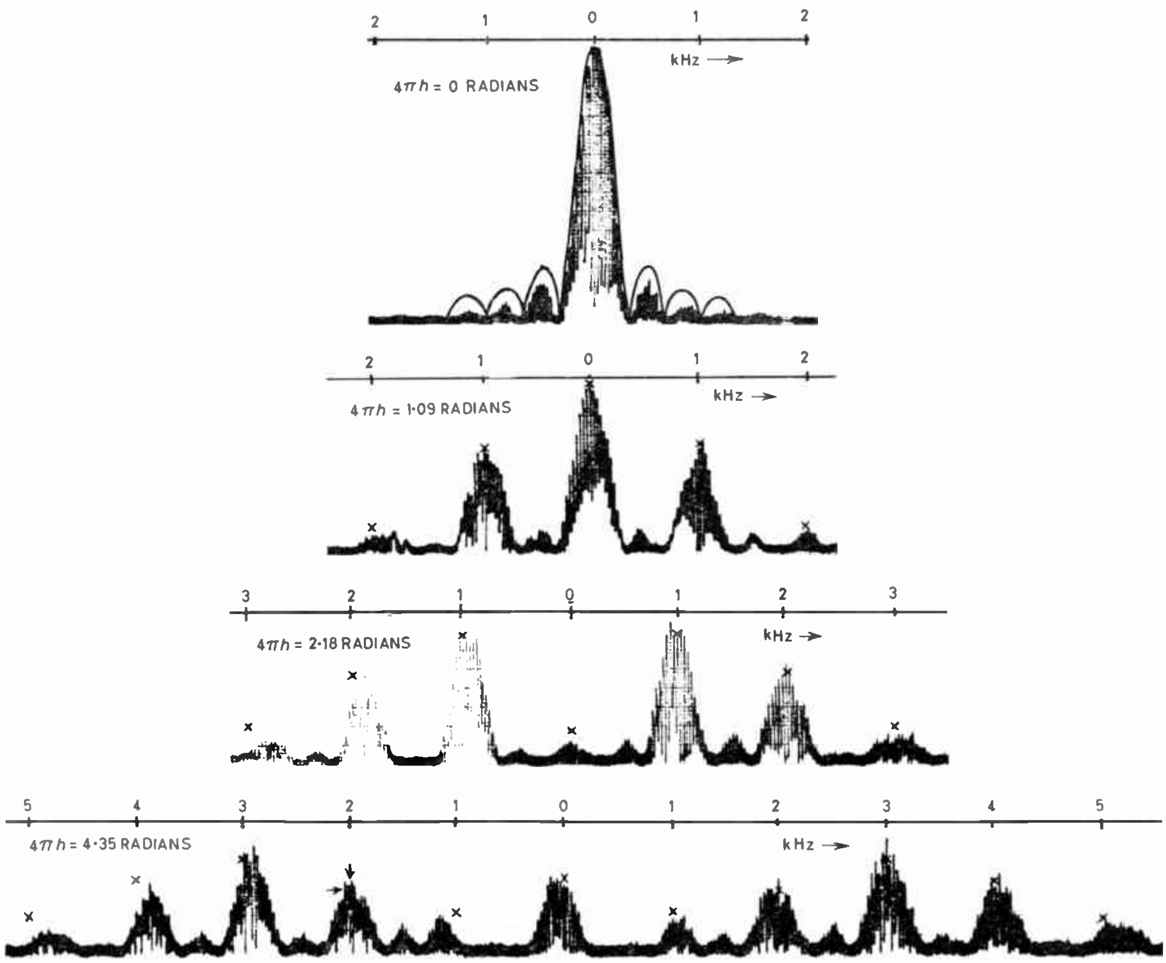

Fig. 4. Results of gated sine wave experiment.

appear falsely low in the experimental results. This is due to the non-linearity of the detector unit between the wave analyser and the recorder and the error is not present when the wave analyser output is plotted manually.

3.3. *Reflection Pattern from a Random Rough Surface*

The particular case of a uniformly-illuminated rough surface having Gaussian height distribution has received some attention,[2,3] and the analogue has been used to obtain results for a large surface of this form. The surface autocorrelation coefficient ξ_0 wavelengths defines the scale of the surface in the X direction and the spectrum was obtained for various values of the height standard deviation σ.

The analogue is a continuous phase-modulated carrier with modulating function consisting of band-limited white noise. The bandwidth was chosen as 2 kHz corresponding to a time autocorrelation coefficient of 0·5 ms so that the time–distance equivalence is, in this case,

$$0{\cdot}5 \text{ ms} \equiv \xi_0 \text{ wavelengths}$$

The r.m.s. amplitude of the noise generator output was set to provide a suitable range of values of phase function standard deviation and hence σ. The spectrum was obtained in each case by plotting the wave analyser r.m.s. output using a slow response instrument; the frequency was adjusted manually and readings taken point by point. The results are shown in Fig. 5(a) together with the spectrum of the noise modulating signal, Fig. 5(b). Since r.m.s. values are plotted the curves show root power density or modulus intensity $|F(S)|$ against S.

For the surface specified above it may be shown that the angular power spectrum is given approximately by

$$|F(S)|^2 = \exp(-\phi_0^2)\,.\left\{\frac{\sin^2 \pi l S}{\pi l S} + \right.$$
$$\left. + \sum_{n=1}^{\infty} \frac{\xi_0 \sqrt{(\pi)}\phi_0^{2n}}{n!\sqrt{n}} \exp\left[\frac{-\pi^2 \xi_0^2 S^2}{n}\right]\right\} \quad \ldots\ldots(26)$$

where ϕ_0 is the r.m.s. value of the phase deviation and is related to the r.m.s. value (standard deviation) of surface height by

$$\phi_0 = 4\pi\sigma \qquad \ldots\ldots(27)$$

The quantities l, ξ_0 and σ are measured in wavelengths. This equation is in general unmanageable (hence the value of the analogue) but it has been discussed by several authors [1-3] and certain simplifications are possible. The first term is the aperture effect $(\sin x)/x$ function which reduces to a single specular reflection when the surface width l is large and decreases in magnitude with increasing ϕ_0. The experimental results show a corresponding carrier component when the depth of modulation is small. The second term in eqn. (26) expresses the scattered radiation. When $\phi_0 \ll 1$ a small fraction of the radiation is scattered and its spectrum shape may be visualized by remembering that for small deviation the shape of a phase-modulation spectrum is the same as the amplitude modulation spectrum and reproduces the spectrum of the modulating signal on each side of the carrier. The spectrum of the noise modulating signal in Fig. 5(b) shows a close similarity to the side-band of the spectrum with $\phi_0 = 0{\cdot}3$. As ϕ_0 is increased, the fine structure becomes blurred and the proportion of scattered energy increases. The experimental results support Ratcliffe's theory in that the angular extent is determined by ϕ_0/ξ_0 and is ϕ_0 times larger than in the case $\phi_0 \ll 1$.

When a specific value is given to ξ_0 the angle–frequency equivalence may be established and the spectrum may be drawn as a function of angle. Only values of $S < 1$ contributes to the spectrum. There is not complete freedom of choice of ξ_0 and σ, the limitations on surface slope and curvature must not be exceeded if the results are to be valid.

4. Further Applications of the Analogue

The application of the analogue to oblique incidence problems is under consideration. Oblique incidence may be simulated by rotating the surface template on the face of the c.r.o. function generator. If the scaling of the template is properly chosen, i.e. horizontal wavelengths per cm must be the same as vertical wavelengths per cm and the phase deviation sensitivity must correspond, then the template angle will correspond exactly to angle of incidence, changes of angle are easily made and measured and the effects on the spectrum may be observed. For this to be generally useful an improved computer is necessary which will accommodate the large total phase shift associated with the slope of the surface whilst still remaining sensitive to relatively small phase shifts arising from surface irregularities.

The effects of non-uniform and non-plane incident radiation may be studied by superposing an appropriate amplitude or phase function on to the modulated carrier.

5. Conclusions

An analogue exists between the frequency spectrum of time-varying signals and the angular spectrum of radiation reflected from a rough surface. This analogue affords a convenient means of studying many reflection problems approximately since changes in the surface parameters may easily be introduced and their effects on the angular spectrum are readily observed. Results obtained using mainly inexpensive laboratory test equipment show that this technique is a practical proposition.

6. Acknowledgments

The author is grateful for the facilities for undertaking this work at The Lanchester College of Technology, Coventry. He also wishes to acknowledge useful discussions with members of the Electrical Engineering Department, particularly with Mr. K. Foster.

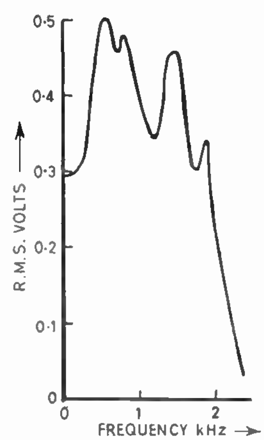

Fig. 5.
(a) Results of random surface experiment.

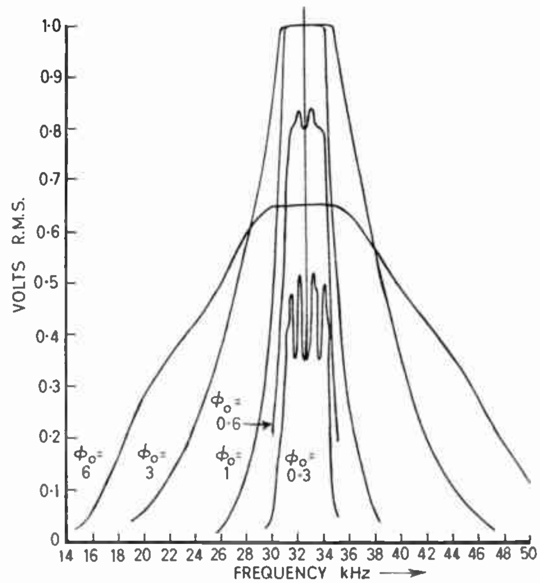

Fig. 5. (b) Spectrum of noise modulating signal.

7. References

1. J. A. Ratcliffe, 'Some aspects of diffraction theory and their application to the ionosphere', *Rep. Prog. Phys.*, **19**, p. 188, 1956.
2. P. Beckmann and A. Spizzichino, 'The Scattering of Electromagnetic Waves from Rough Surfaces' (Pergamon Press, London, 1963).
3. R. H. Clarke, 'Theoretical characteristics of radiation reflected oblique from a rough conducting surface', *Proc. Instn Elect. Engrs*, **110**, No. 1, p. 91, January 1963. (I.E.E. Paper No. 3998E.)
4. W. R. Bennett, 'Methods of solving noise problems', *Proc. Inst. Radio Engrs*, **44**, p. 609, May 1956.
5. W. H. Peake, 'Theory of radar returns from terrain', *I.R.E. Nat. Conv. Rec.* 7, Pt. 1, pp. 27–41, 1959.
6. A. F. Harvey, 'Microwave Engineering' (Academic Press, London, 1963).

8. Appendix 1

Relationship between surface profile and field function

Consider a vertically polarized plane wave of complex amplitude g_0 at the origin and having amplitude defined by $A(x)$. The wave is incident normally upon a rough surface. The incident field at any point in the XZ plane is

$$g(x,z)_i = g_0 A(x)\exp[-\mathrm{j}2\pi z] \qquad \ldots\ldots(28)$$

and the reflected field is given by

$$g(x,z)_r = \int_{-\infty}^{\infty} F(S)\exp[\mathrm{j}2\pi(Sx+Cz)]\,\mathrm{d}S \ldots\ldots(29)$$

At the conducting surface $z(x)$ the magnetic field is continuous so that

$$g(x,z(x))_r = g(x,z(x))_i \qquad \ldots\ldots(30)$$

i.e.

$$\int_{-\infty}^{\infty} F(S)\exp[\mathrm{j}2\pi(Sx+Cz(x))]\,\mathrm{d}S = g_0 A(x)\exp[-\mathrm{j}2\pi z(x)] \ldots\ldots(31)$$

Now consider the approximation $C = 1$ in eqn. (31). Geometrical considerations show that this is good if either the surface height variation is small (say less than λ) or if the spectrum is not unduly broad (see Fig. 6); in other words, the surface must not contain many steep slopes. This condition is also imposed by the fact that the method makes no attempt to consider multiple reflections or shadowing. The analogue method is only accurate therefore for a limited range of surfaces, but it is presented as an approximate technique and it must be emphasized that the analytical techniques make similar approximations in most cases. We therefore rewrite eqn. (31) thus:

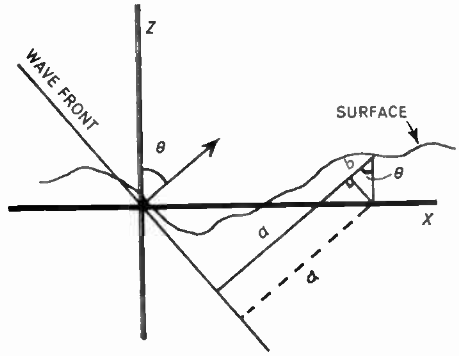

Fig. 6. Justification of approximation in eqn. (31).

$$S.x + C.z(x) = a + b$$
$$\simeq a + \frac{b}{C} = S.x + z(x)$$

provided θ or $z(x)$ is small.

$$\exp[\mathrm{j}2\pi z(x)]\int_{-\infty}^{\infty} F(S)\exp[\mathrm{j}2\pi Sx]\,\mathrm{d}S = g_0 A(x)\exp[-\mathrm{j}2\pi z(x)] \qquad \ldots\ldots(32)$$

But

$$g(x) = \int_{-\infty}^{\infty} F(S)\exp[\mathrm{j}2\pi Sx]\,\mathrm{d}S. \qquad \ldots\ldots(33)$$

Therefore

$$g(x) = g_0 A(x)\exp[-\mathrm{j}4\pi z(x)] \qquad \ldots\ldots(34)$$

and so the surface may be represented as a phase-changing screen. A surface height variation of z_1 wavelengths causes a phase change of $4\pi z_1$ radians in the emergent wave front.

For the case of horizontal polarization

$$g(x,z(x))_r = -g(x,z(x))_i \qquad \ldots\ldots(35)$$

at the conducting surface and

$$g(x) = g_0 A(x)\exp[-\mathrm{j}4\pi z(x)+\mathrm{j}\pi] \qquad \ldots\ldots(36)$$

9. Appendix 2

Description of the curve follower

A template representing the field function is fitted over the screen of a c.r.o. which is then masked and viewed by a photocell. The photocell output is applied to the c.r.o. Y amplifier and when in correct adjustment constrains the spot to follow the line of the template across the screen. The Y amplifier signal may be sampled and reproduces the template as a voltage-time function.

Manuscript first received by the Institution on 6th January 1966 and in final form on 7th June 1966. (Paper No. 1085/RNA 5G.)

U.D.C. 557.508.5 : 621.316.825

A Portable Integrating Omnidirectional Anemometer

By

R. A. MORRIS, B.Sc.,†

A. R. MORMAN (*Student*),†

AND

D. SCOTT, Ph.D.‡

Presented at the New Zealand National Electronics Conference sponsored jointly by the New Zealand Section of the I.E.R.E. and the New Zealand Electronics Institute, in Auckland in August 1966.

Summary: A portable lightweight instrument developed to investigate the effect of total wind flow on plant growth is described. The sensing device is a directly-heated thermistor bead. From the cooling effect of the wind on the bead the electronic circuits produce a voltage that varies linearly with respect to speed over the range of 1–30 miles/hour. This voltage is integrated by a d.c. motor with an attached revolution counter to give the wind flow over a time determined by the operator. The reading is sufficiently independent of direction to be useful in the intended application.

1. Introduction

The instrument was developed for the Plant Physiology Division of the New Zealand Department of Scientific and Industrial Research to assist investigations of the effect on growth of the micro-climate surrounding a plant. In such studies the concept of wind direction has little meaning because of the dominance by turbulent processes caused both by the turbulent heat loss from leaves and by the break up of air movement by leaves and stems. The concept of air movement or rate of air changes at a point are more relevant to the study of processes influencing plants within a vegetation. This accounts for the small sensing element and omnidirectional characteristics required for the instrument. The ventilation at different heights within a pasture is given in Fig. 1 and shows the relative uniform ventilation at the lower levels in the vegetation. The values are plotted against a diagrammatic representation of the vegetation to emphasize that the biologist must interpret the data on this basis. The design requirements were:

(1) The instrument should record the total air movement for an integrating period of not less than three minutes.

(2) The probe should be small enough to be introduced among the foliage of pasture plants without a significant effect on the air flow.

(3) The output reading should be linear with respect to wind speed over the range of 1 to 30 miles/hour and accurate to 10% of the maximum figure.

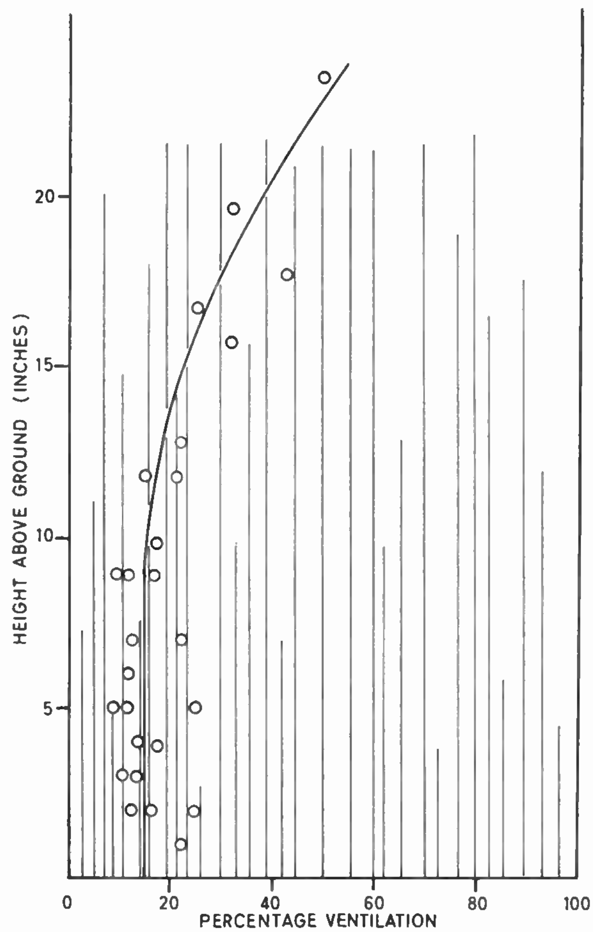

Fig. 1. Ventilation within a Lolium/Bromus/Poa pasture as a percentage of air movement 6 ft above the crop. Values are five minute averages. The diagram shows the mean number of leaves at the different heights within a 10 in cross-section of the pasture.

† Physics and Engineering Laboratory, Department of Scientific and Industrial Research, Lower Hutt, New Zealand.
‡ Plant Physiology Division, D.S.I.R., Palmerston North, New Zealand.

(4) The instrument should be sufficiently portable to enable it to be carried by one man to any location.

Other workers have described anemometers for use amongst plants (for example Penman[1]), but such instruments have operated over only a limited speed range, have not integrated the wind flow and have been insufficiently portable for the present application.

It was decided that the requirements could best be met by an instrument which relied for its action on the cooling by the wind of a heated sphere. To obtain satisfactory operation over a wide range of wind speeds this would have to be operated at a constant temperature. This type of device was first described in detail by King.[2] To reduce the effect on the readings of ambient temperature variations it would be necessary to operate the probe at a relatively high temperature and a value 150 deg C above the ambient was chosen. As it was intended to carry this instrument to altitudes of 6000 ft (2000 m) or more it had to be truly portable and powered by small dry batteries. Calculations showed that the heated probe would consume most of the power, hence it had to be as small as possible. For these reasons an unencapsulated thermistor bead with a diameter of 0·5 mm was chosen as the sensor. This was to be heated by the passage of an electric current to a constant temperature as determined by the measurement of its resistance. It was mounted on the tip of a hypodermic needle at the end of 30 ft of cable to enable it to be used in taller vegetation when required.

As shown by King[2] the heat loss from a heated wire due to a wind perpendicular to its length is given by

$$H = H_0 + K\sqrt{v}$$

where H and H_0 are in watts, K is a constant and v is the velocity. McAdam has shown that the heat loss from a sphere is described by a similar equation.[3] It is from a measurement of the quantity H that the wind speed is derived. For a bead operated at constant temperature the resistance will be constant, and it is thus sufficient to measure the voltage across it. The relation between the voltage and the velocity is a fourth-power one and it was necessary to provide the means by which a voltage with a linear relation to the wind speed could be produced to enable it to be integrated with respect to time. It was realized that it would be impossible to produce an instrument that was truly omnidirectional because of the necessity of supporting the sensing device and the inevitable shielding thereby introduced.

2. General Description

The block diagram of the instrument is shown in Fig. 2. The probe (1) consists of the bead thermistor mounted at the end of a hypodermic needle (see Fig. 8). The thermistor, which is an electrical resistor with a large negative temperature coefficient, is placed in one arm of an a.c. bridge (2). The bridge is excited by a 400 Hz oscillator with a controllable output. Sufficient excitation is applied to the bridge to maintain the temperature of the thermistor approximately 150 deg C above the ambient air temperature, the arms of the bridge being arranged to be in electrical balance, with the thermistor, at that temperature. It is the function of the a.c. amplifier (3), phase detector (4), d.c. amplifier (5), servo-motor (6), two-gang potentiometer (7) and emitter followers (8), to vary the output of the oscillator (9) in such a manner as to keep the bridge in balance as the air speed varies. The result is that the thermistor temperature is kept constant to 1 deg C. As mentioned earlier there is a fourth-power law between the oscillator voltage and the air speed. A voltage with a linear relation to the air speed is obtained from the action of the servo-motor and the two-gang potentiometer as follows:

If v = air speed

V_b = bridge voltage at speed v

V_{b0} = bridge voltage at zero wind speed

V_1 = voltage at the wiper of RV3 at angle θ and V_{10} the voltage at $\theta = 0$

V_2 = voltage at the wiper of RV2 at angle θ (Voltages V_1 and V_2 must not be loaded by the oscillator and the motor integrator.)

θ = angular rotation of the shaft of RV2 and RV3 from its position at zero wind speed.

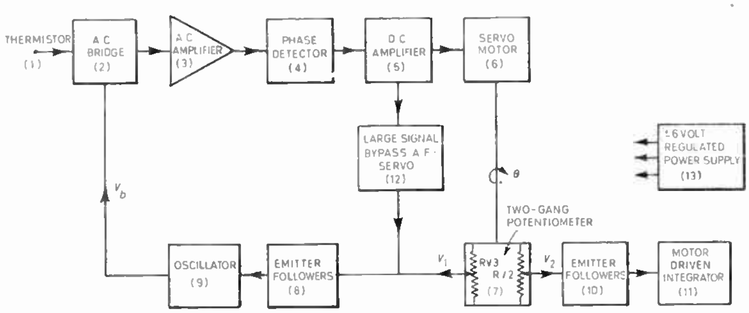

Fig. 2. Block diagram of the anemometer.

K_0 to K_6 are constants.

Then we require that $V_2 = K_0 v$.

It is assumed that

$$V_b \propto V_1$$

Now according to King,[2]

$$H = H_0 + K_1\sqrt{v}$$

or

$$V_b^2 = V_{b0}^2 + K_2\sqrt{v}$$

or

$$V_1^2 = V_{10}^2 + K_3\sqrt{v}$$

Then

$$V_1^2 - V_{10}^2 = K_3\sqrt{v}$$

If the law of RV3 is adjusted so that $V_1^2 - V_{10}^2 = K_4\theta$ then $\theta = K_5\sqrt{v}$.

The law of RV2 is adjusted so that $V_2 = K_6\theta^2$ then $V_2 = K_0 v$, satisfying our original requirement.

V_2 must be supplied from a low impedance source to drive the motor integrator (11) and the necessary transformation from the high resistance of RV2 is performed by the emitter followers (10). RV2 and RV3 are multi-tap wire-wound potentiometers and the required functions are obtained by placing fixed resistors across the taps. The calculations required to obtain the resistor values are described by Shen[4] and Merchant.[5]

A linear relation between V_1 and V_b is obtained by using a switching-type oscillator (9) with a sinusoidal output of a type described by Baxandall.[6] This is powered by the emitter follower (8) which, like (10), effects an impedance transformation.

The d.c. amplifier (5) includes a phase-correction circuit which is required to stabilize the closed loop control of thermistor temperature. The large signal by-pass a.f. servo (12), is not fundamental to the operation of the system but is required to drop the oscillator voltage more quickly than the inertia of the mechanical servo will allow when the air speed is suddenly reduced as happens, for instance, when a cap is placed over the probe. If this is not done the thermistor may reach a temperature at which damage will occur.

The power supply (13) provides two regulated rails of +6 V and −6 V with respect to ground. The primary supply is a 12 V dry battery for each regulator providing at least 12 hours of continuous operation.

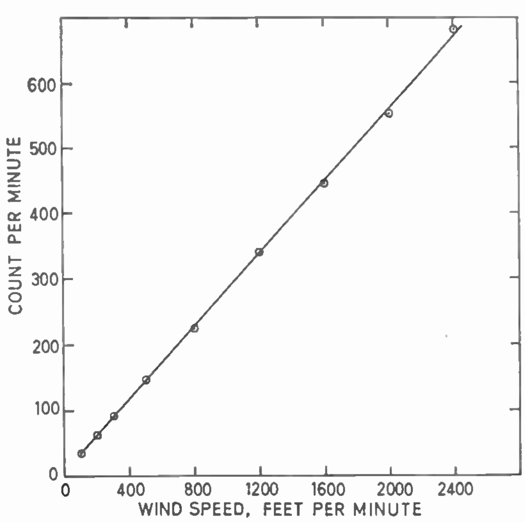

Fig. 4. A typical calibration curve for the anemometer.

3. Circuit Details

The circuit diagram of the complete instrument is given in Fig. 3. The sensing thermistor is R3 (1) with a resistance of 10 kilohms at 20°C. The sensing bridge (2) comprises a centre-tapped transformer winding T2A, and RV1 and R2 in addition to the thermistor R3. It is energized by the voltage appearing across the transformer winding which together with C2 forms one of the tuned circuits of the oscillator. RV1 is calibrated in degrees Celsius and is set by the operator to compensate for ambient temperature changes. The out-of-balance voltage of the bridge is amplified by transistors TR1, 2 and 3 (3) before rectification in the phase-sensitive detector TR4 and 5 (4). The detector derives its reference voltage from the same oscillator which powers the bridge. The direct output voltage of the rectifier, depending in sign and magnitude on the phase and amplitude of the incoming a.c. signal, is further amplified by transistors TR6, 7, 8 and 9 (5) to drive the servo-motor (6) which rotates the shaft of RV2 and RV3 (7).

It is of interest that in the development of the instrument the law of RV3 was calculated and the fixed resistors placed across the taps. This allowed the anemometer with the exception of the integrator, to be operated and its performance checked in a wind tunnel. A plot of the voltage at the wiper of RV2 versus wind speed was obtained, and from it the law required to produce a linear relation was deduced. This was found to be close to the calculated square law. A calibration curve for the complete instrument is given in Fig. 4. Transistors TR19, 20 and 21 are the compound emitter followers (10) which drive the integrating motor (11). Transistors TR24 and 25 are the emitter followers (8) which supply the oscillator TR26 and 27 (9) with V_1 the potential at the wiper of RV3. TR22 and 23 comprise the large signal by-pass circuit (12) which abruptly reduces the oscillator voltage whenever the emitter potential of TR6 rises above 2 V. This only occurs when the temperature of the thermistor is very much too high. A meter is provided to check the

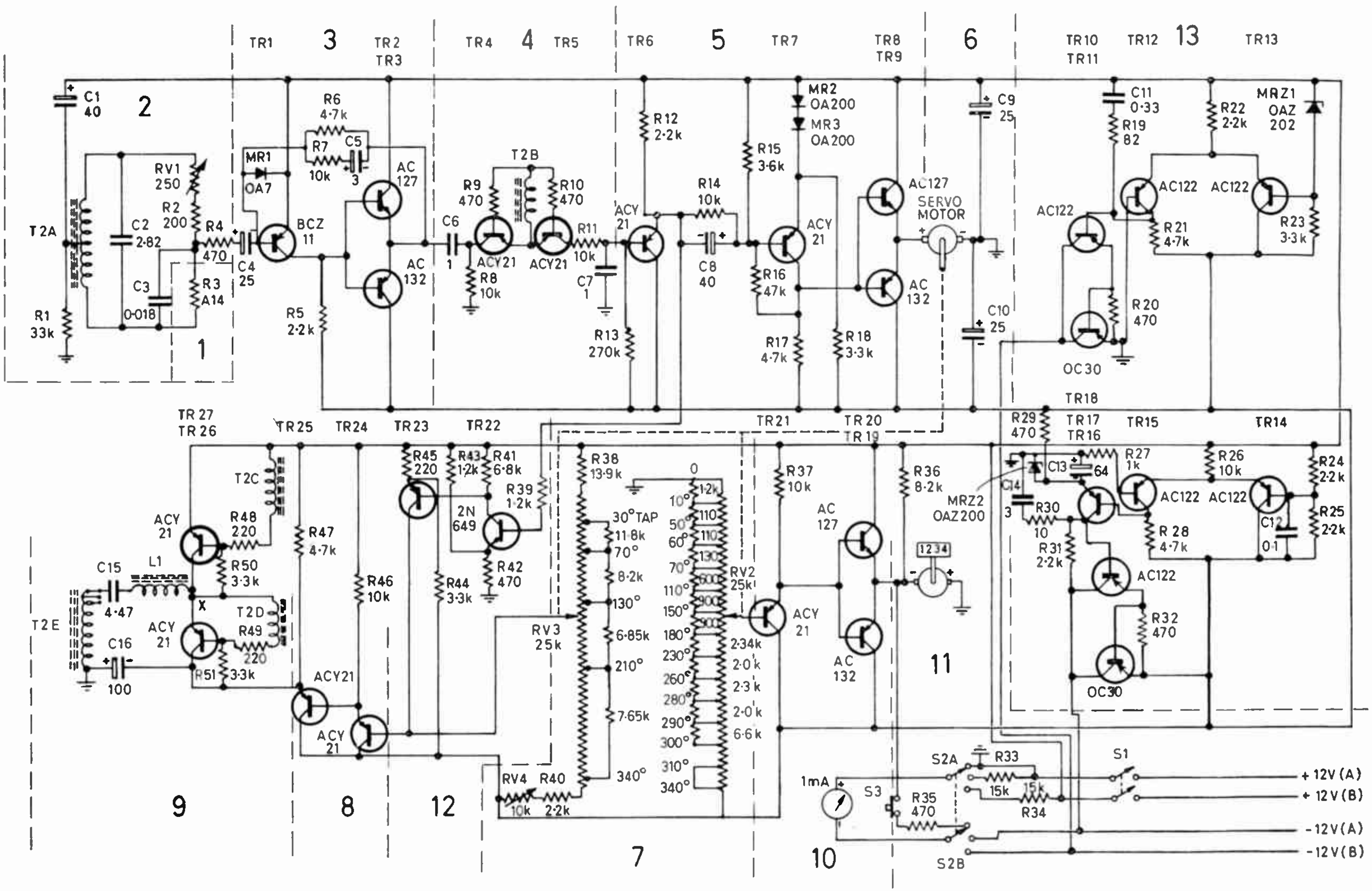

Note. TR 23 is type BCZ 11

Fig. 3. Circuit diagram.

battery voltages and bring the voltage applied to the integrator motor to zero at zero wind speed by means of the control RV4. The two series-regulated power supplies (13) which furnish the 6 V rails comprise transistors TR10 to 18 and associated components.

4. Operational Experience

The anemometer has now had a season's use in environments ranging from normal low-altitude farmland conditions to those encountered at sub-alpine altitudes. It has been used to measure the way in which wind speed varies in pastures from the ground level up to a foot or more above it. The actual measurements of wind speed will be presented elsewhere. Its use under field conditions has shown that, although the principal design requirements (with the partial exception of the omnidirectional response) have been met, the instrument is not without some weaknesses.

The fragility of the probe seems inevitable and a wire guard has been fitted to reduce risk of breakage, although this has a noticeable effect on the directional response. Fortunately, experience has shown that the directional pattern of the probe does not change significantly when the thermistor bead is replaced. It is sufficient, therefore, to recalibrate the instrument against a standard cup anemometer. Examples of typical polar plots of the directional sensitivity are given in Figs. 5 and 6.

Measurement and calculation show that the reading is unaffected by the sun shining directly on the probe, but an ambient temperature limit of 40°C does not permit the case of the instrument to be operated in direct summer sunlight when the wind speed is low. In the present anemometer this problem is overcome with an umbrella; future models would use silicon transistors.

Fig. 7. The anemometer.

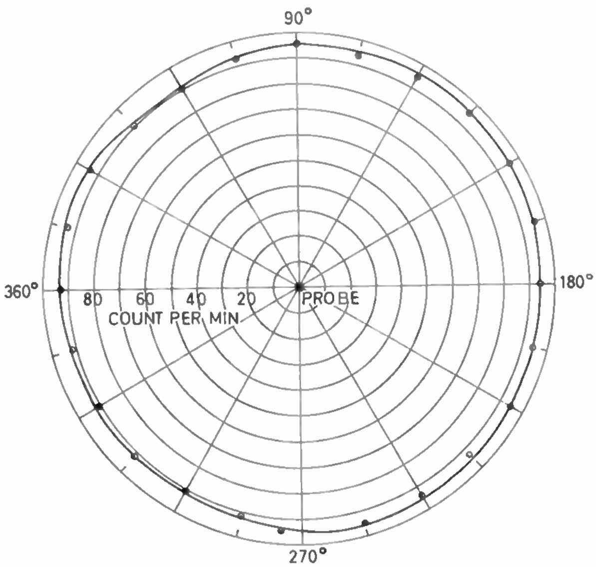

Fig. 5. Integrator count for winds of 300 ft/min normal to the axis of the probe support.

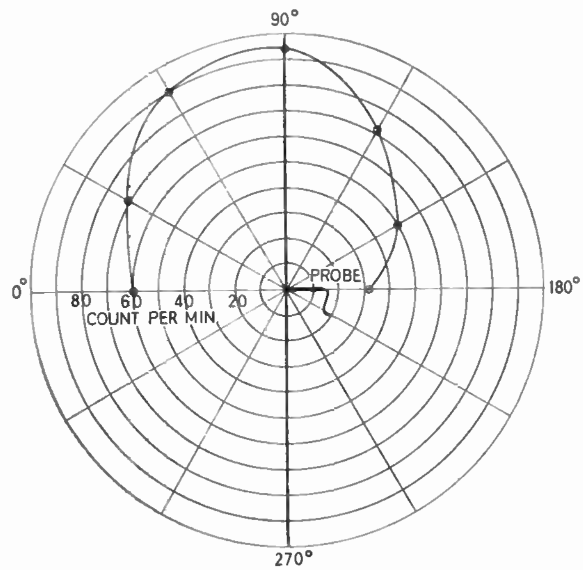

Fig. 6. Integrator count for winds of 300 ft/min in a plane containing the support.

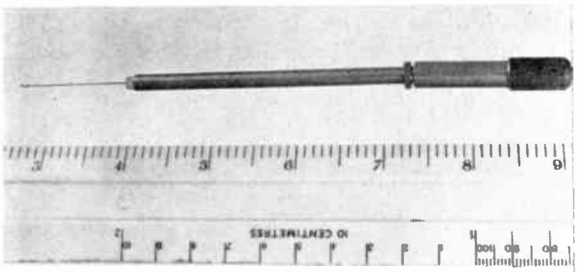

Fig. 8. The anemometer probe.

5. Conclusions

An anemometer has been described which is small (10 in × $8\frac{1}{2}$ in × 7 in) (see Fig. 7) and weighs only 17 lb. The probe, shown in Fig. 8, is very small and is sufficiently omnidirectional in its response for the intended application. The response is linear over the required range of wind speeds.

6. References

1. H. L. Penman, 'A portable thermistor bridge for micro-meteorology among growing crops', *J. Sci. Instrum. Phys. Ind.*, **26**, p. 77, March 1949.
2. L. V. King, 'On the convection of heat from small cylinders in a stream of fluid; determination of the convection constants of small platinum wires with applications to hot wire anemometry', *Phil. Trans. Roy. Soc.*, A, **214**, p. 373, November 1914.
3. W. H. McAdam, 'Heat Transmission', p. 237 (McGraw-Hill, New York, 1942).
4. D. W. C. Shen, 'Approximating non-linear functions by shunt loading tapped potentiometers in analogue computing machines', *Electronic Engng*, **29**, p. 434, September 1957.
5. J. Merchant, 'The correction of errors in potentiometer function generators', *Electronic Engng*, **32**, p. 493, August 1960.
6. P. J. Baxandall, 'Transistor sine-wave LC oscillators', *Proc. Instn Elect. Engrs*, **106B**, Suppl. No. 16, p. 748, 1959. (I.E.E. Paper No. 2978E)

Manuscript first received by the Institution on 17th May 1966 and in final form on 10th November 1966. (Paper No. 1086).

STANDARD FREQUENCY TRANSMISSIONS

(Communication from the National Physical Laboratory)

Deviations, in parts in 10^{10}, from nominal frequency for **November 1966**

November 1966	24-hour mean centred on 0300 U.T.			November 1966	24-hour mean centred on 0300 U.T.		
	GBZ 19·6 kHz	MSF 60 kHz	Droitwich 200 kHz		GBZ 19·6 kHz	MSF 60 kHz	Droitwich 200 kHz
1	− 298·3	− 300·3	+ 1·0	**16**	− 300·0	− 300·1	− 0·6
2	− 298·2	− 300·1	+ 1·6	**17**	− 300·6	− 299·7	+ 0·1
3	− 300·2	− 300·3	+ 1·6	**18**	− 298·2	− 300·4	+ 0·2
4	—	− 299·6	+ 1·7	**19**	− 301·9	− 299·8	− 0·1
5	− 295·1	− 299·5	+ 1·5	**20**	− 301·9	− 299·5	0
6	− 296·2	− 299·4	+ 1·3	**21**	− 301·8	− 299·8	+ 0·1
7	− 297·8	− 300·4	+ 0·7	**22**	− 300·5	− 300·0	+ 0·3
8	—	− 301·2	+ 0·1	**23**	− 300·9	− 300·2	+ 0·5
9	− 298·4	− 300·4	− 0·2	**24**	− 301·4	− 300·2	+ 0·7
10	− 299·3	− 300·3	+ 0·2	**25**	− 300·6	− 300·5	+ 0·4
11	− 298·2	− 300·4	+ 0·3	**26**	− 300·0	− 301·2	0
12	− 295·5	− 299·6	+ 0·4	**27**	− 299·5	− 301·4	− 0·1
13	− 297·5	− 300·3	− 0·1	**28**	− 298·3	− 301·4	− 0·4
14	− 300·4	− 300·4	− 0·6	**29**	− 298·4	− 299·8	0
15	− 300·2	− 300·5	− 0·4	**30**	− 297·8	− 299·7	− 0·2

Nominal frequency corresponds to a value of 9 192 631 770·0 Hz for the caesium F,m (4,0)–F,m (3,0) transition at zero field.

U.D.C.621.375.029.64

An S-Band Parametric Amplifier using a Balanced Idler Circuit

By

K. L. HUGHES, B.Sc., Ph.D.†

AND

J. D. PEARSON, M.Sc., C.Eng.†

Summary: The paper describes the performance of an S-band parametric amplifier pumped at J-band using a balanced idler technique where two varactor diodes are incorporated in one encapsulation. It is shown that this technique produces a simple amplifier where the idler and signal circuits can be considered to be completely separate.

Effects produced by operating the amplifier at frequencies where the circuits are not at resonance are also discussed.

List of Symbols

K diode figure of merit
$(f_c)_0$ diode cut-off frequency at zero bias voltage
C_1 maximum amplitude of change in capacitance
C_0 junction capacitance at the working voltage
r diode base resistance
f_1 signal frequency
f_2 idler frequency
G_{Ti} total conductance at f_i where $i = 1$ or 2
G_g source conductance
G_L load conductance
G_i diode conductance at f_i where $i = 1$ or 2
$\Omega = f_1/f_2$
Q_1 Q factor of input circuit
Q_2 Q factor of idler circuit
ω_{sr} diode series resonance frequency $\times 2\pi$
γ C_1/C_0
i_i source current at f_i where $i = 1$ or 2
v_i diode voltage at f_i where $i = 1$ or 2
T diode temperature
T_0 source temperature
ω_c diode angular cut-off frequency $= 2\pi f_c$

1. Introduction

The paper describes the design and performance of a simple parametric amplifier for S-band. The simplicity of the design is due to the nature of the idler circuit, which is formed by mounting two varactor diodes in juxtaposition, one inverted with respect to the other. The original amplifiers using this technique[1] incorporated pill-type diodes placed as close together as possible. In the amplifier described here, the two semiconductor diodes are mounted close together within one encapsulation so that the stray inductance may be appreciably reduced and higher idler frequencies obtained.

† Ferranti Ltd., Wythenshawe, Manchester.

2. Balanced Idler Circuit

The gain-bandwidth product of a parametric amplifier is dependent on the bandwidths of the unpumped signal and idler circuits. To obtain low noise figures for the amplifier, the signal circuit is heavily loaded by the source impedance so that it is relatively broadband. However the idler circuit is not externally loaded so that this is usually the circuit with the narrower bandwidth and hence determines the overall bandwidth of the amplifier.

The characteristics of the varactor junction determine the maximum idler bandwidth which can be achieved, but since the pump, signal and idler circuits must be isolated from each other, the stored energy associated with the idler filter reduces the idler bandwidth. However a balanced type of idler circuit restricts the idler frequency to the diodes themselves and eliminates the use of filters. Thus the theoretical maximum idler bandwidth can be achieved.

3. Noise Figure

The gain and noise figures of a parametric amplifier can be shown to be (see Appendix):

$$\text{gain} = \frac{4(G_g/G_1)^2}{(1+G_g/G_1-\Omega K^2)^2} \qquad \ldots\ldots(1)$$

$$\text{noise figure} = \left(1+\frac{G_1}{G_g}\right)(1+\Omega) \qquad \ldots\ldots(2)$$

where

$$K = \frac{1}{2}\frac{C_1}{C_0}\frac{1}{\omega_1 C_0 r} = \frac{1}{2}\frac{C_1}{C_0}\frac{\omega_c}{\omega_1} \qquad \ldots\ldots(3)$$

and

$$\Omega = \omega_1/\omega_2 \qquad \ldots\ldots(4)$$

Thus, from equation (1), the maximum over-coupling of the signal circuit for the amplifier still to

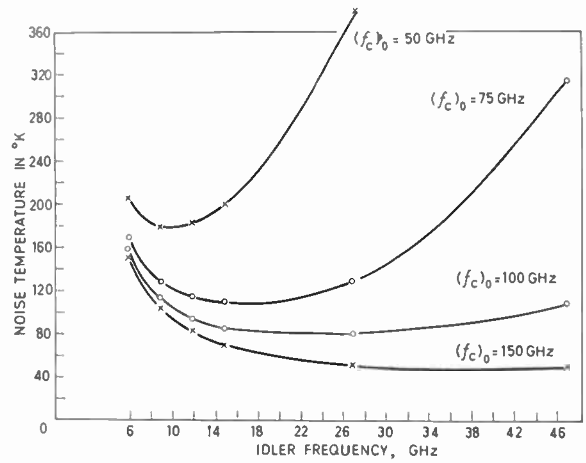

Fig. 1. Noise temperature/idler frequency for a 3 GHz parametric amplifier.

oscillate is given by

$$\frac{G_g}{G_1} = \Omega K^2 - 1 \qquad \ldots\ldots(5)$$

Thus the noise figure, F, is given by

$$F = \left(1 + \frac{1}{\Omega K^2 - 1}\right)(1+\Omega) \qquad \ldots\ldots(6)$$

From this formula a graph can be plotted of noise figure against idler frequency for a given quality of diode and a known value of C_1/C_0. The quantity C_1/C_0 has been determined[2] for diffused silicon varactor diodes as 0·5 and curves for the noise temperature/idler frequency for a 3 GHz amplifier for different values of $(f_c)_0$ are shown in Fig. 1. This indicates that the idler frequency for optimum noise performance is around 25 GHz. Further examination of Fig. 1 shows that the minimum in the curve is shallow so that considerations such as the availability and cost of klystrons may be important.

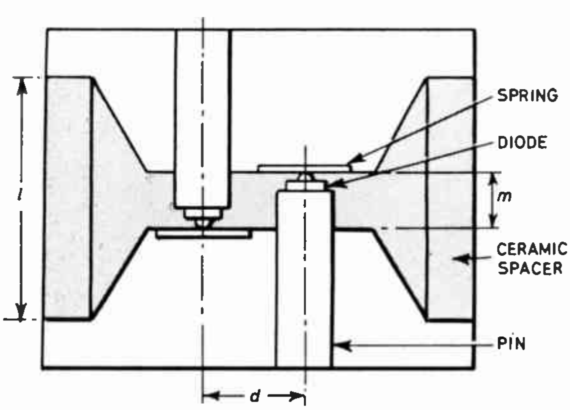

Fig. 2. Double-diode arrangement.

4. Bandwidth of Double-Diode Circuits

Figure 2 shows the double-diode arrangement using two diodes in one encapsulation and Fig. 3 shows a circuit equivalent of these diodes where C_a is the stray capacitance across the diode elements themselves, C_b is the capacitance between the ends of the encapsulation, C_c is the capacitance associated with the ceramic, L is the stray encapsulation inductance and L_1 is the internal inductance.

The idler frequency is determined by the values of C_0, L_1 and the stray capacitance C_a. Since C_a is very small (about 0·06 pF) the idler circuit is almost independent of the encapsulation stray reactances. These encapsulation strays can now be arranged to give an optimum signal circuit.

The dimensions of the encapsulation can be varied to give desired values of L and C_0. If it is made larger the value of L will increase due to the increased length of the metal end parts of the encapsulation. The signal circuit is usually completed by an inductance

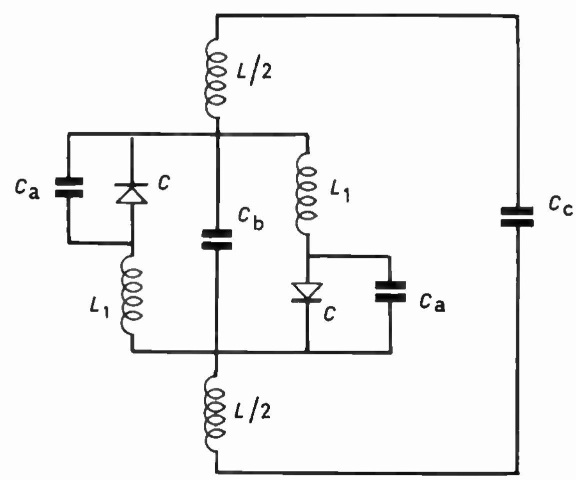

Fig. 3. Circuit equivalent of double-diode arrangement.

external to the diode encapsulation. However, the optimum condition is where the inductance of the encapsulation is arranged to make the series resonance of the diodes correspond to the desired signal frequency. This then means that the capacitance C_c does not affect the signal circuit.

The (gain)$^{\frac{1}{2}}$ bandwidth product for a parametric amplifier can be written as (see Appendix):

$$(\text{gain})^{\frac{1}{2}}\ \text{bandwidth} = \rho = \frac{2(G_g/G_1)\omega_1}{\left(Q_1 \dfrac{G_{T1}}{G_1} + \Omega^2 Q_2 K^2\right)} \qquad \ldots\ldots(7)$$

Assuming $G_{T1} \simeq G_g$, this equation reduces to

$$\rho = \frac{2\omega_1}{Q_1 + \Omega Q_2}$$

under the high gain approximation of eqn. (5).

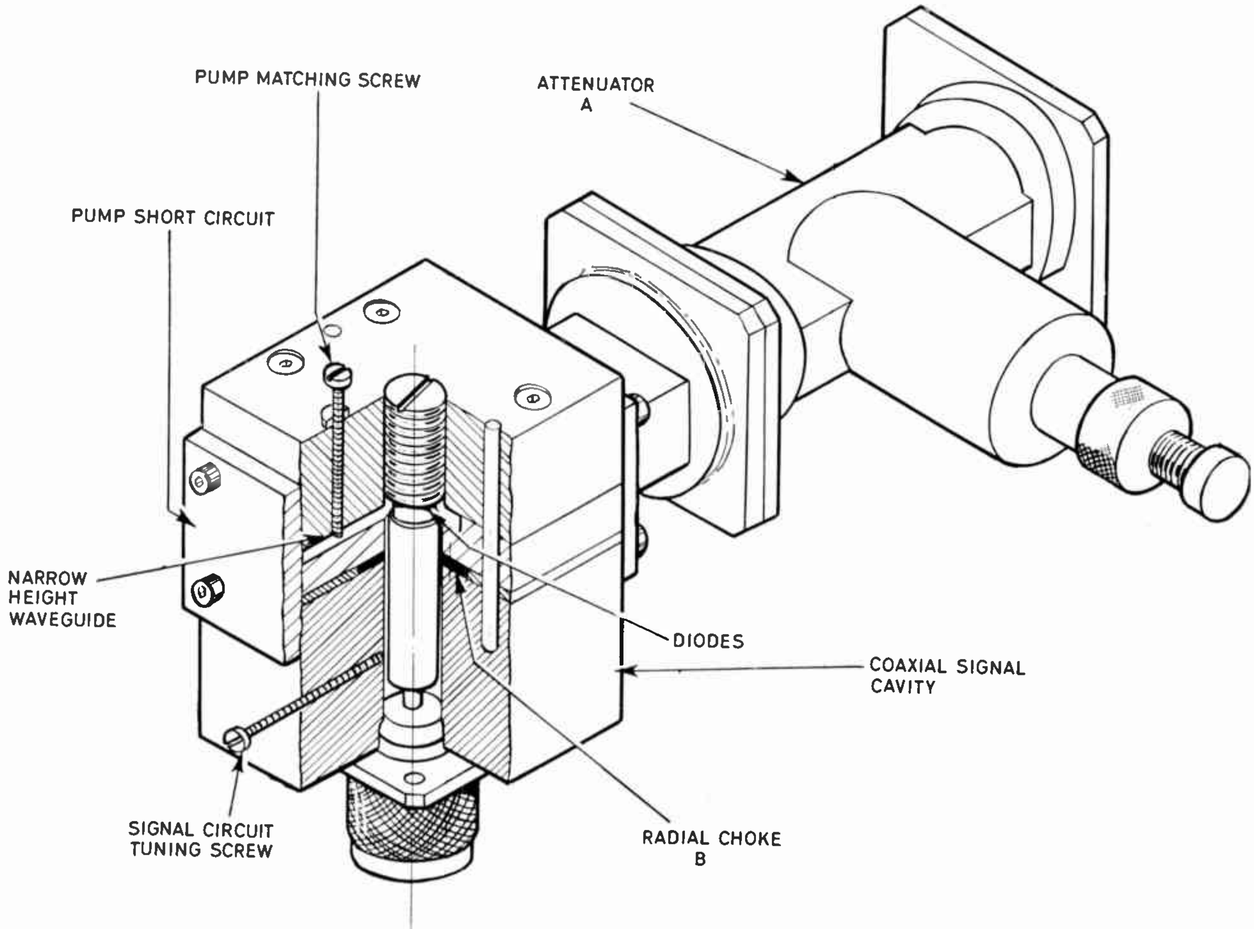

Fig. 4. Diagram of S-band parametric amplifier pumped at J-band.

The Q's of the circuits can now be calculated from expressions given by Pearson and Lunt[1] and Johnson[3]

$$Q_1 = \frac{\omega_c}{\omega_1} \cdot \frac{G_1}{G_1 + G_g} \cdot \frac{C_0 + C_a + C_b + C_c}{C_0} \qquad \ldots\ldots(8)$$

where $\omega_{sr} >> \omega_1$

$$Q_2 = \frac{\omega_c}{\omega_2} \cdot \frac{C_0 + C_a}{C_0} \qquad \ldots\ldots(9)$$

For the diodes used $C_0 \simeq 0{\cdot}38$ pF, $C_a \simeq 0{\cdot}06$ pF, $C_b \simeq 0{\cdot}29$ pF, $C_c \simeq 0{\cdot}22$ pF

so that $\rho \simeq 750$ MHz ......(10)

Thus when the gain of the amplifier is 20 dB the bandwidth is approximately 75 MHz.

5. Diode Construction

Figure 2 shows the double-diode construction in section. A number of diodes are made separately on small cylindrical pins using chips from the same slice of semiconductor material to ensure a similar capacitance/voltage relationship. The diodes are measured for cut-off frequency and capacitance and sorted into matched pairs. Each pair is then inserted into a prepared encapsulation until the diodes make contact with a low inductance spring. By suitable control of the diode capacitance and the geometry of the encapsulation it is possible to obtain a required idler frequency. The geometry may be altered by changing the separation of the pin axes, d, but it is more convenient to vary the length of the ceramic spacer, l.

6. Circuit Design

Figure 4 is a diagram of an S-band amplifier pumped at J-band. The basic problem is to separate the three frequencies present in the amplifier, namely, the signal, idler and pump. As described in Section 2, the idler circuit is complete within the diodes and effectively separated from the other circuits. Since the signal frequency is well below the cut-off frequency of the pump waveguide no leakage of signal occurs along this path. To prevent pump power passing down the coaxial signal circuit a radial bandstop filter is placed near the diode.

The dimensions of the signal cavity are chosen such that the losses in the cavity are mainly due to the series resistance of the diode, that is, the radial dimensions are chosen sufficiently large that the losses in the cavity wall can be neglected. The diodes are resonated by a length of line behind the diodes to achieve the desired signal resonance. The diode resistance is transformed by a quarter-wave transformer section to achieve the required loading. In fact, the section is not quite a quarter-wavelength long due to the presence of the radial bandstop filter. Mechanical tuning of the signal frequency is then achieved by a variable capacitance, *C*, included in the signal circuit.

The input to the signal cavity is through an N-plug and a rigid connection is made to the centre conductor of the cavity. The diameter of the inner conductor is such that the overcoupling of the signal circuit is approximately 13 : 1.

The position of the radial choke, B, is approximately a quarter-wavelength at the pump frequency from the waveguide wall so that at the pump frequency there is an effective short circuit from the diode to the waveguide wall. The pump power to the varactors is controlled by the waveguide attenuator A. A quarter-wavelength transformer connects the full height waveguide attenuator to the reduced height, 0·1 in (0·25 cm) high, waveguide in which the diodes are mounted. The waveguide beyond the diode is then completed by a short circuit.

7. Practical Considerations and Results

In Section 3 it was shown that the minimum in the noise temperature/pump frequency characteristic was very shallow, so that, although the lowest noise figure could be achieved with a pump frequency of 25 GHz, very little deterioration is incurred by pumping at 17 GHz. Furthermore a suitable pump klystron is more readily available at 17 GHz than at 26 GHz and at a more economical price.

One difficulty with the balanced idler circuit is that of measuring the flow of direct current in each of the diodes. To do this would mean affecting the simplicity of the amplifier, however it is relatively easy to measure the out-of-balance current, i.e. the difference between the currents in the two diodes. Since there are slight variations in the forward voltage/current characteristics of diodes, the two diodes do not begin to conduct current at exactly the same forward voltage. Thus for the very small currents of interest here (typically 1 μA) it is probable that the true diode current is being measured.

Figure 5 shows the behaviour of a typical pair of diodes in the amplifier shown in Fig. 4. The parametric amplifier is normally operated with a pump frequency such that the signal and idler frequencies are at the resonance of their respective circuits under pumped conditions; this corresponds to the region of zero current in Fig. 5. However amplification will still occur over a range of pump frequencies where these

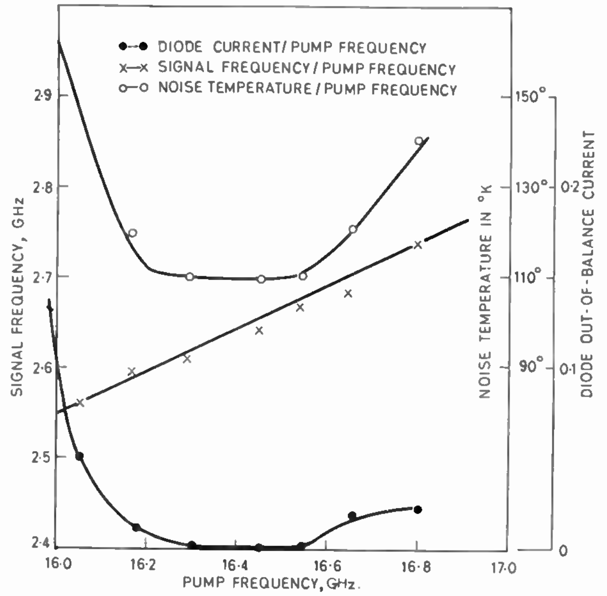

Fig. 5. Graphs of signal frequency, noise temperature, and diode current, against pump frequency for a typical diode.

circuits are not resonant. If the pump frequency is $f_p+\Delta f_p$ (where $f_p = f_{1\,res}+f_{2\,res}$) the signal frequency where maximum gain occurs is obtained from the equation

$$\frac{\Delta f_1}{f_1} = \frac{\Delta f_p}{f_2} \frac{Q_2}{Q_1+Q_2(f_1/f_2)} \qquad \ldots\ldots(11)$$

where $f_1+\Delta f_1$ is the signal frequency where maximum gain occurs. Clearly if $Q_2 \gg Q_1$, $\Delta f_1 = \Delta f_p$ and the idler frequency remains fixed, but if $Q_1 \gg Q_2$, $\Delta f_1 \ll \Delta f_p$ and the signal frequency moves very little. In the amplifiers under consideration $\Delta f_1 \simeq 1/5\ \Delta f_p$ indicating an idler bandwidth four times the signal bandwidth. When the pump frequency was such that the signal and idler circuits were near resonance increasing the pump power simply increased the gain up to oscillation. In this region where no measurable current flowed, the amplifier noise temperature alone was approximately 110°K with a bandwidth of 50 MHz at 20 dB gain.

At high pump frequencies, increasing the pump power increased the gain to a maximum value. A further increase in the pump power kept the gain at approximately the same level, but the frequency at which maximum gain occurred increased. When the pump frequency is high the signal and idler frequencies are higher than their optimum values; an increase in the pump power lowers the idler resonance, since the diode capacitance is a more integral part of the idler circuit than of the signal circuit.

The working idler frequency is therefore reduced. To maintain the relationship between the pump, signal and idler frequencies, the signal frequency must increase. The signal frequency is now further from resonance and therefore the amplifier needs the increased pump power to maintain the gain. This effect corresponds to the region in Fig. 5 where the pump frequency is above 16·6 GHz.

At pump frequencies much less than the optimum value, increasing the pump power increased the gain, as in the ideal condition, until oscillation occurred. However, the frequency of this oscillation was higher than the frequency at which gain occurred. The oscillations were maintained when the pump power was reduced, until the amplifier dropped out of oscillation at very low gain (5–6 dB). In such cases the onset of oscillations increased the voltage on the varactor, causing the idler resonant frequency to be lowered, thus increasing the operating signal frequency. From the signal circuit point of view this is a more favourable operating region, so that when the amplifier is oscillating, the extra voltage on the varactor helps to maintain the oscillations as the voltage is reduced. This effect corresponds to the region of pump frequency below 15·9 GHz in Fig. 5.

8. Conclusions

An S-band amplifier has been described using a balanced idler circuit, with the diodes contained within one encapsulation. This type of amplifier gives the theoretically maximum idler bandwidth and also produces a very simply constructed amplifier since no filtering at the idler frequency, external to the diodes, is required. The performance of the amplifier has been shown to be close to that predicted and the detuning effects associated with the amplifier have also been discussed.

9. References

1. J. D. Pearson and K. S. Lunt, 'A broadband balanced idler circuit for parametric amplifiers', *The Radio and Electronic Engineer*, **27**, p. 331, May 1964.
2. K. Kurakawa and M. Uenohara, 'Minimum noise figure of the variable-capacitance amplifier', *Bell Syst. Tech. J.*, **40**, p. 695, 1961.
3. K. M. Johnson, 'Broadband cavity-type parametric amplifier design', *Trans Inst. Radio Engrs on Microwave Theory and Techniques*, MTT-9, p. 187, 1961.
4. S. A. Schelkunoff, 'Electromagnetic Waves', p. 119 (Van Nostrand, New York, 1943).
5. H. Heffner and G. Wade, 'Gain, bandwidth and noise characteristics of the variable-parameter amplifier', *J. Appl. Phys.*, **29**, pp. 1323–31, September 1958.
6. D. G. Tucker, 'Circuits with time-varying parameters', *The Radio and Electronic Engineer*, **25**, pp. 263–271, March 1963.
7. D. G. Tucker, 'Circuits with Periodically-Varying Parameters'. (Macdonald, London 1964).

10. Appendix

Derivation of Gain, Bandwidth and Noise Figure Expressions

It has been shown by Pearson and Lunt[1] that the equations for a balanced idler circuit parametric amplifier are identical to those of a single-diode amplifier except that the standing bias capacitances of the diodes appear in parallel in the signal circuit and in series in the idler circuit. It is therefore possible to use the same basic equations as for a single-diode amplifier if Y_{T1} and Y_{T2}, the total admittances at the signal and idler frequencies, are arranged to include the effects of the standing bias capacitances of the varactors.

Thus the basic equations can be written as

$$I_1 = V_1\{Y_{T1}\}+V_2\left\{j\omega_1\frac{C_1}{2}\right\} \qquad \text{......(12)}$$

$$0 = V_1\left\{-j\omega_2\frac{C_1}{2}\right\}+V_2\{Y_{T2}\} \qquad \text{......(13)}$$

These equations are derived by Tucker[6, 7] using the time-varying analysis. In this paper these equations are derived by the use of time-varying capacitance while Tucker has made use of time-varying inductance.

10.1. *Gain*

From equations (12) and (13)

$$v_1 = \frac{i_1 Y_{T2}}{Y_{T1}Y_{T2}-\omega_1\omega_2\dfrac{C_1^2}{4}} \qquad \text{......(14)}$$

and the gain, given by $4G_1G_g\left|\dfrac{v_1}{i_1}\right|^2$ is

$$\text{gain} = \frac{4G_LG_g}{\left|Y_{T1}-\dfrac{\omega_1\omega_2C_1^2}{4Y_{T2}}\right|^2} \qquad \text{......(15)}$$

so that the gain at resonance A, becomes

$$A = \frac{4G_LG_g}{\left|G_{T1}-\dfrac{\omega_1\omega_2C_1^2}{4G_{T2}}\right|^2} \qquad \text{......(16)}$$

But

$$G_{T2} = \omega_2^2C_0^2r \qquad \text{......(17)}$$

so that

$$A = \frac{4\dfrac{G_1}{G_1}\dfrac{G_g}{G_1}}{\left|\dfrac{G_{T1}}{G_1}-\Omega K_2\right|^2} \qquad \text{......(18)}$$

Where the amplifier is fitted with a circulator, $G_L = G_g$ and the gain becomes

$$A = \frac{4(G_g/G_1)^2}{(1+G_g/G_1-\Omega K^2)^2} \qquad \text{......(19)}$$

10.2. *Bandwidth*

In the vicinity of its resonant frequency, the admittance of a circuit may be expressed in terms of the frequency and the Q of the circuit[4]

If we define

$$\Delta\omega = \omega_1 - \Omega_1 \qquad \text{......(20)}$$

and

$$\delta = \Delta\omega/\Omega_1 \qquad \text{......(21)}$$

it follows that

$$\omega_2 = \Omega_2 - \Delta\omega \qquad \text{......(22)}$$

For small values of δ, the admittances of the resonant circuits at ω_1 and ω_2 are given by

$$Y_{T1} = G_{T1}(1+2j\delta Q_1) \qquad \text{......(23)}$$

$$Y_{T2} = G_{T2}(1-2j\delta Q_2\Omega) \qquad \text{......(24)}$$

From equations (15), (16), (23) and (24), the gain falls to one-half its resonant value for values of δ given by

$$|G_{T1}(1+2j\delta Q_1)-\omega_1\omega_2 C_1^2/4G_{T2}(1+2j\delta Q_2\Omega)|^2 = 2|G_{T1}-\omega_1\omega_2 C_1^2/4G_{T2}|^2 \qquad \text{......(25)}$$

From equations (19) and (25), neglecting terms of $0(\delta^3)$, it follows that[5]

$$(\text{resonant gain})^{\frac{1}{2}} \times 2\delta = \frac{2G_g/G_1}{\left[\frac{G_{T1}}{G_1} Q_1 + \Omega^2 Q_2 K^2\right]} \qquad \text{......(26)}$$

10.3. *Noise Figure*

Consider noise currents i_{n1} and i_{n2} at frequencies ω_1 and ω_2, so that equations (12) and (13) become

$$i_{n1} = v_1\{Y_{T1}\} + v_2\left\{j\omega_1 \frac{C_1}{2}\right\} \qquad \text{......(27)}$$

$$i_{n2} = v_1\left\{-j\omega_2 \frac{C_1}{2}\right\} + v_2\{Y_{T2}\} \qquad \text{......(28)}$$

where the noise currents are given by

$$|i_{n1}|^2 = 4k\Delta f(G_g T_0 + G_1 T) \qquad \text{......(29)}$$

$$|i_{n2}|^2 = 4k\Delta f G_2 T \qquad \text{......(30)}$$

Using the definition for noise figure where

$$F = \frac{N_{out}}{kT\Delta f \times \text{gain}} \qquad \text{......(31)}$$

where

$$N_{out} = |v_1|^2 G_1 \qquad \text{......(32)}$$

It follows from eqns. (19), (29) and (30) that

$$F = 1 + \frac{G_1}{G_g}\frac{T}{T_0} + \frac{G_1}{G_g}\Omega^2 K^2 \frac{T}{T_0} \qquad \text{......(33)}$$

for the case of an amplifier with circulator.

Under the conditions where $T = T_0$

$$F = 1 + \frac{G_1}{G_g} + \frac{G_1}{G_g}\Omega^2 K^2 \qquad \text{......(34)}$$

From eqn. (19) for high gains it follows that

$$F = \left(1 + \frac{G_1}{G_g}\right)(1+\Omega) \qquad \text{......(35)}$$

Manuscript first received by the Institution on 31st May 1966 and in final form on 4th August 1966. (Paper No. 1087).

U.D.C. 681.383 : 697.93/7 : 728.98

A New System for the Digital Setting of Temperature and Humidity Controllers

By

W. P. GABRIEL, B.Sc. *(Graduate)*,†

R. A. MORRIS, B.Sc.,†

AND

R. W. ROBOTHAM†

Presented at the New Zealand National Electronics Conference sponsored jointly by the New Zealand Section of the I.E.R.E. and the New Zealand Electronics Institute, in Auckland in August 1966.

Summary: A system for programmed setting of electronic temperature or humidity controllers, which can command any of sixteen available settings, is described. The main application is to a set of controlled climate rooms which have different levels of temperature and humidity by day and by night. A defined change from one level to another is required.

Wheatstone bridges, set to give the required day and night conditions, are adjusted by transistor switches operated in binary sequence from the states of a counter. These give sixteen steps between and including the day and night settings. The selection of these steps in time is done by a train of pulses whose rate defines a period for the change between day and night levels. By operation of two switches, the counter is commanded to 'increase', 'decrease', or 'stop'. The system can be used for programs more complex than a defined change.

1. Introduction

Research at the Plant Physiology Division (D.S.I.R., Palmerston North, New Zealand) is to be assisted by the construction of twenty-five controlled climate rooms. Each room is to have controlled levels of temperature, humidity, lighting, and carbon dioxide content.

The temperature and humidity controllers each have two set points, one for 'day' and the other for 'night' levels. Since sudden transitions between the extreme set points would cause loss of control and heavy power demand, the changes are made in approximately linear steps over times varying from 30 minutes to two hours.

Controllers in earlier use were programmed by motor-driven rheostats; such a system was found unsatisfactory. To obtain reliability and defined set point change, the system here described was developed. It has the additional merit of being adaptable, if required, to programs more complex than the linear changeover described.

A brief description of the system is included in a paper by one of the authors.[1] A more recent paper by R. Shah describes the digital control of rheostats.[2]

2. General Description

A block diagram of the controller with its temperature determining input bridges is given in Fig. 1. It will be seen that there are, in effect, two Wheatstone bridges—R_1, R_4, R_3, R_6 (bridge 1) and R_2, R_5, R_3, R_6 (bridge 2). R_3 is the sensing element for temperature or humidity and with R_6 is common to both bridges. One bridge sets the day level, the other sets the night level.

Variation of the resistors R_{C1} and R_{C2} determines the working set point of the controller, between and including the balance points of bridge 1 and bridge 2. Since they perform an interpolation between the two balance points, let them be termed 'coefficient resistors'. The digital control of these coefficient resistors is the essence of this article.

If the coefficient resistor R_{C1} is made zero and R_{C2} is made infinite, then the input of the summing amplifier will depend solely on the electrical balance of bridge 1, and at some temperature T_1, R_3 will have such a value that the normal Wheatstone balance condition is

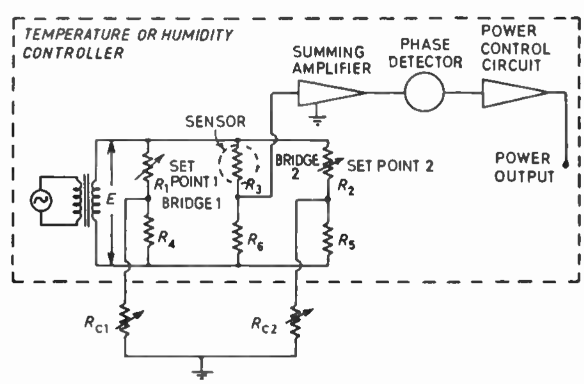

Fig. 1. Block diagram of the controller.

satisfied. The controller will try to establish and maintain this condition. In practice, the actual value of T_1 is determined by the setting of R_1. Likewise, if R_{C1} is infinite and R_{C2} is zero, there is another

† Physics and Engineering Laboratory, Department of Scientific and Industrial Research, New Zealand.

temperature T_2, determined by R_2, at which bridge 2 will be in balance and which the controller will seek to maintain.

If, instead of either zero or infinite resistance, R_{C1} and R_{C2} are given intermediate values, and these are varied in a complementary manner, then any number of control points may be established between the extreme values of T_1 and T_2. For the intended purposes a total of 16 set points, including the extreme ones, is sufficient. Given four resistors with their values in binary sequence, and four single pole switches, it is possible to obtain the 16 different values required of a coefficient resistor. In this case each switch consists of a transistor. This transistor is turned on or off, thus opening or closing the switch, by driving its base from one output terminal of one stage of a four-stage binary counter. Such a counter has 16 different states, and it is arranged that the conductance of one coefficient resistor progresses linearly with the state of the counter from state 0 to state 15. By operating the transistor switches of the other coefficient resistor from the alternate output of each stage of the counter, that resistor is made to vary in a complementary manner to the first.

Because it is desired to vary the temperature from T_1 to T_2 and back to T_2, it is necessary for the counter to be reversible. Again, because we wish to avoid a direct transition from T_1 and T_2 or vice versa, the counter is end-stopped; i.e. it can count in a forward direction from state 0 to state 15 at which point it will stop, regardless of the number of subsequent input pulses applied. Similarly it can count in a reverse direction from state 15 to state 0 and stop until it is commanded to count forward.

The counter has three inputs—a counting pulse input, an add enable terminal and a subtract enable terminal. Application of -6 volts d.c. ('1') to the add enable terminal and 0 volt d.c. ('0') to the subtract enable terminal constrains the counter to count forward, or add. The converse connection constrains the counter to subtract.

To change from one extreme set point to the other, the counter must be commanded to reverse its direction of count, as above, and a train of pulses (with a repetition rate dependent on the required changeover time) must be applied to the count input. The time taken for the set point to vary from one extreme to the other is that taken for the application of 15 input pulses.

Since to each state of the counter there corresponds an available set point, with appropriate command of the count direction and injection of a defined number of input pulses, any of the 16 available set points may be selected. This facility permits programs more complex than the linear changeover which is the primary concern of this paper.

3. Principles of Operation

A logic diagram (Fig. 2) shows the control of the coefficient resistors by the reversible counter. Control levels A and S are applied from external sources to determine whether the reversible counter adds or subtracts. For normal operation, $A = \bar{S}$. Successive states of the counter are generated by the input pulses C. These pulses are supplied from an external generator at a rate dependent on the required changeover time.

The add full state of the counter is

$$F_A = F_1.F_2.F_3.F_4 \qquad \text{......(1)}$$

Likewise, the subtract full state is

$$F_S = \bar{F}_1.\bar{F}_2.\bar{F}_3.\bar{F}_4 \qquad \text{......(2)}$$

The condition for pulses to be added is add enable

$$A_E = \bar{F}_A.A \qquad \text{......(3)}$$

and for pulses to be subtracted, subtract enable is

$$S_E = \bar{F}_S.S \qquad \text{......(4)}$$

That is to say, pulses are added or subtracted according to the control levels A and S; once the counter is at add full (1 1 1 1) no more pulses can be added, and likewise for subtract full (0 0 0 0) no more pulses can be subtracted.

The complete condition for a pulse to be entered is then

$$E = C.(A_E+S_E) = C.(\bar{F}_A.A+\bar{F}_S.S) \qquad \text{......(5)}$$

Thus if C is a regular train of pulses and $A = 1$, the counter will step progressively from subtract full to add full and stop; if the control levels are changed to $S = 1$, the counter will step back to subtract full and stop. Further, if at any point there is set up $A = S = 0$, the counter will be stopped—a facility which is available for extending the system to complex programs.

The states of the reversible counter are inverted by the buffer amplifiers I. These amplifiers control the switches S11, S12, S13, S14, S21, S22, S23, S24. A state 0 at the input of an amplifier gives a state 1 at its output and closes the associated switch. Calling a closed switch 1 and an open switch 0, the switch states form a set of binary numbers corresponding to the states of the counter. The switches are suitably biased p-n-p transistors.

The coefficient resistors are made up of resistors in binary proportion, switched by the switches S11 to S24. The correspondence between switches and flip-flops is:

$$S11 = FF_1 \qquad S21 = \overline{FF}_1$$
$$S12 = FF_2 \qquad S22 = \overline{FF}_2$$
$$S13 = FF_3 \qquad S23 = \overline{FF}_3$$
$$S14 = FF_4 \qquad S24 = \overline{FF}_4$$

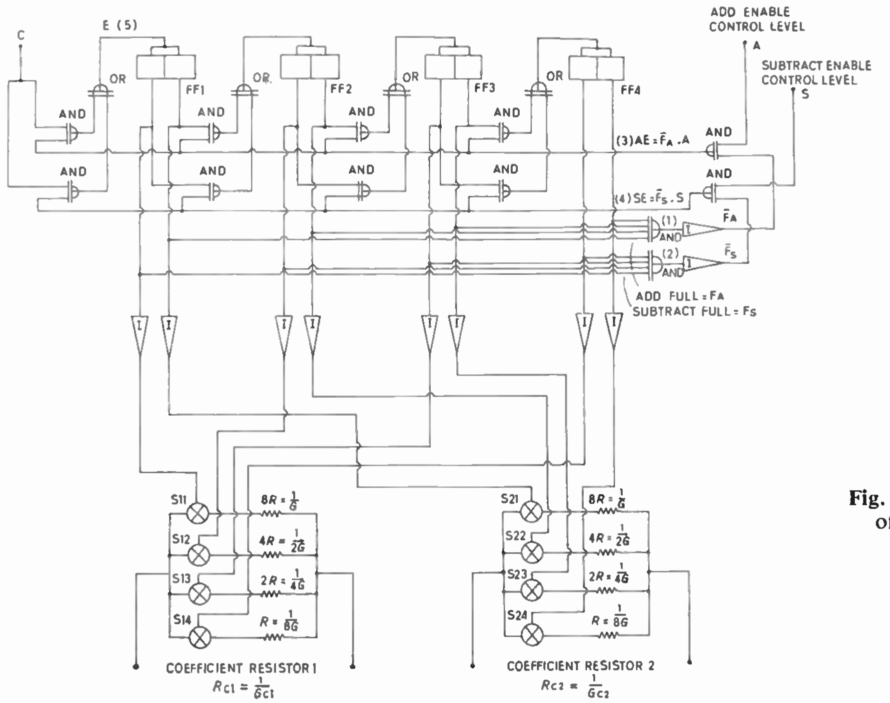

Fig. 2. Logic diagram of the controller.

The coefficient resistors vary as in Table 1 below. Conductances are indicated:

Table 1

	Counter state		Coefficient conductance	
	Pulse	Binary	G_{C1}	G_{C2}
Subtract full	= 0	0000	0	15G
	1	0001	G	14G
	2	0010	2G	13G
	3	0011	3G	12G
	4	0100	4G	11G
	5	0101	5G	10G
	6	0110	6G	9G
	7	0111	7G	8G
	8	1000	8G	7G
	9	1001	9G	6G
	10	1010	10G	5G
	11	1011	11G	4G
	12	1100	12G	3G
	13	1101	13G	2G
	14	1110	14G	G
Add full	= 15	1111	15G	0

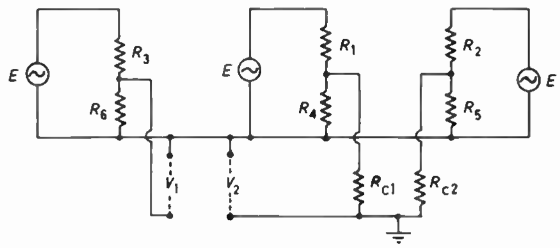

Fig. 3. Equivalent circuit of the bridge.

The programming of a controller by switching its bridge was shown in Fig. 1. The extreme set points are entered by the bridge arms $R_1 R_4$, $R_2 R_5$ whose junctions are returned to ground by the coefficient resistors R_{C1} and R_{C2}. The input of the summing amplifier is taken to be a virtual earth.

The humidity controllers have automatic quadrature suppression applied to their bridges, but this neither affects nor is affected by the switching action.

Bridge balance ($V_1 = V_2$) may be found from the equivalent circuit of Fig. 3.

$$V_1 = \frac{ER_6}{R_3+R_6} \qquad \text{......(6}$$

$$\frac{V_2}{R_{C1}+\dfrac{R_1 R_4}{R_1+R_4}} + \frac{V_2}{R_{C2}+\dfrac{R_2 R_5}{R_2+R_5}} = \frac{ER_4}{\left(R_{C1}+\dfrac{R_1 R_4}{R_1+R_4}\right)(R_1+R_4)} + \frac{ER_5}{\left(R_{C2}+\dfrac{R_2 R_5}{R_2+R_5}\right)(R_2+R_5)} \qquad \text{......(7)}$$

Note that if R_{C1} is infinite, $$V_2=\frac{R_5}{R_2+R_5}$$

and that if R_{C2} is infinite, $$V_2=\frac{R_4}{R_1+R_4}$$

These are the extreme set points, as would be expected.

For balance, $$V_1=V_2$$

Rearranging terms in eqn. (7),

$$V_2\left(R_{C1}+R_{C2}+\frac{R_1R_4}{R_1+R_4}+\frac{R_2R_5}{R_2+R_5}\right)=\frac{ER_4}{R_1+R_4}\left(R_{C2}+\frac{R_2R_5}{R_2+R_5}\right)+\frac{ER_5}{R_2+R_5}\left(R_{C1}+\frac{R_1R_4}{R_1+R_4}\right)\quad\ldots\ldots(8)$$

from which can be found the general balance condition

$$\frac{R_6}{R_3+R_6}=\frac{R_4}{R_1+R_4}\left(\frac{R_{C2}+\dfrac{R_2R_5}{R_2+R_5}}{R_{C1}+R_{C2}+\dfrac{R_1R_4}{R_1+R_4}+\dfrac{R_2R_5}{R_2+R_5}}\right)+\frac{R_5}{R_2+R_5}\left(\frac{R_{C1}+\dfrac{R_1R_4}{R_1+R_4}}{R_{C1}+R_{C2}+\dfrac{R_1R_4}{R_1+R_4}+\dfrac{R_2R_5}{R_2+R_5}}\right)\quad\ldots\ldots(9)$$

While this expression appears complicated, most of the terms are constant for a given pair of extreme set points, the variables being R_{C1} and R_{C2}.

By substitution of the successive values of R_{C1} and R_{C2} in eqn. (9), the intermediate set points can be found.

The use of transistors as a.c. switches is successful provided that the reverse base-emitter voltage when off is greater than the peak voltage to be switched and that the forward base current when on is greater than the peak current to be switched.

4. Circuit Details

The circuitry of the scheme is shown in Fig. 4. Programming of a temperature controller is illustrated; the same circuitry (but for different values of bridge and coefficient resistors) is used with the humidity controllers.

The enable logic of the reversible counter (eqns. (1) to (5)) is performed by the circuit section indicated.

n–p–n silicon transistors are used for the inverting amplifiers to simplify biasing while satisfying the loading requirements of the flip-flops in the reversible

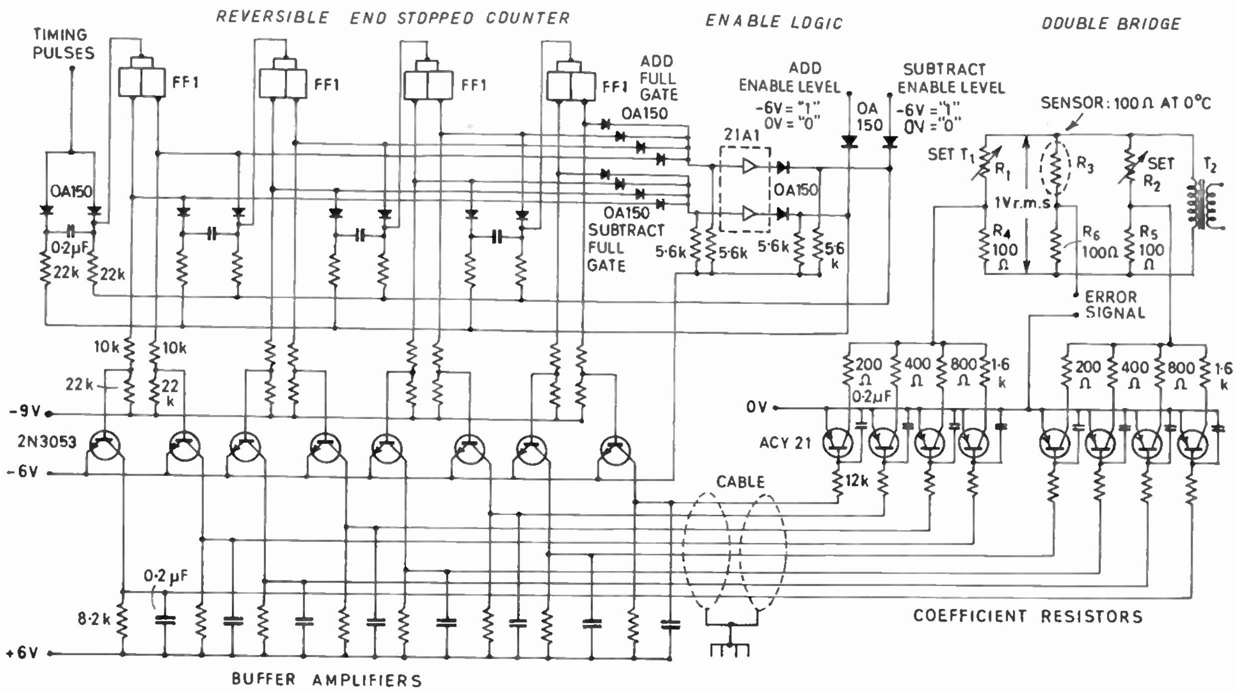

Fig. 4. Circuit diagram of the controller.

Table 2

Pulse number	Set point °C
0	41·1
1	37·0
2	34·0
3	30·8
4	27·1
5	24·6
6	22·6
7	20·2
8	18·7
9	16·6
10	14·1
11	11·5
12	9·0
13	6·4
14	3·6
15	0

counter and to ensure reliable switching of the transistors associated with the coefficient resistors.

The bases of these transistors are driven from the inverting amplifiers through 12 kilohm limiting resistors. The ACY21 transistors used as coefficient resistor switches show 'closed' resistances of the order of 10 ohms and 'open' resistances of megohms.

Because the system operates in an environment of severe electrical noise and because cable runs between counters and controllers may be of up to 50 feet, by-pass capacitors (0·2 μF) are connected to the collectors of the inverting transistors and the bases of the switching transistors. The switching system has an inherent noise immunity of several volts on the interconnecting lines, and this is augmented by the by-pass capacitors.

Philips' circuit blocks are used in the reversible counter-flip-flops type FF1 (B892000), and an inverter block 21A1 (B894002) for the enable logic.

Table 2 shows a typical transition of bridge set points between two extremes, obtained by test on an existing unit. Figure 5 is a graphical representation

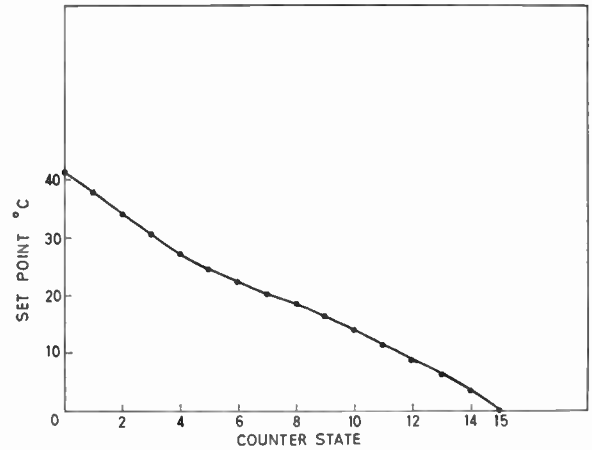

Fig. 5. Graph showing the linearity of change-over between two extreme set points.

of Table 2, from which it will be seen that the system gives useful linearity of changeover between the two extreme set points.

The buffer amplifiers of the reversible counter are able to drive 10 sets of bridge coefficient resistor switches.

5. Performance and Conclusions

The system has been operating without any fault for some twelve months. It is considered to be greatly superior to mechanical methods which use rheostats for changing bridge set points. It has the great advantage that it can be used to program conventional transistorized controllers with modification only to their bridge circuits.

6. References

1. W. P. Gabriel, 'Some applications of digital electronics in science and industry', *Radio, Electronics and Communications (N.Z.)*, 20, No. 6, pp. 11–15, August 1965.
2. R. Shah, 'The characteristics of digital rheostats', *Control Engineering*, 13, No. 2, pp. 68–70, February 1966.

Manuscript first received by the Institution on 27th May 1966 and in the final form on 28th November 1966. (Paper No. 1088.)

Radio Engineering Overseas . . .

The following abstracts are taken from Commonwealth, European and Asian journals received by the Institution's Library. Abstracts of papers published in American journals are not included because they are available in many other publications. Members who wish to consult any of the papers quoted should apply to the Librarian giving full bibliographical details, i.e. title, author, journal and date, of the paper required. All papers are in the language of the country of origin of the journal unless otherwise stated. Translations cannot be supplied.

TELEMETRY TIMING

An Australian paper describes how events recorded at a remote missile station in Australia were connected to a manned station by a time-division multiplex telemetry link. One channel of the multiplex was available to indicate the occurrence of remote events and to enable them to be accurately timed. The paper describes an electronic system which has been developed to meet this need and: (*a*) produces a code whereby events recorded remotely can be subsequently correlated with the telemetry signals; (*b*) produces a coded voltage ramp waveform per event which is telemetered (the telemetry sender periodically samples this ramp and from the samples the ramp can be extrapolated back to its beginning which marks the actual time of the event); (*c*) produces a coded output to mark the remote record.

The system developed is of special interest in that it is based upon the use of available micro-electronic integrated networks.

'The timing of remote events using periodic telemetry samples', N. E. Burrowes, *Proceedings of the Institution of Radio and Electronics Engineers Australia*, **27**, No. 9, pp. 244–53, September 1966.

ANALOGUE INFORMATION TRANSMISSION SYSTEMS

A Soviet paper giving analysis of the conditional *a posteriori* probability density suggests that the noise immunity of different broadband analogue information-transmission methods should be assessed according to two criteria: the normal r.m.s. error δ_n (the transmission accuracy criterion) and the probability of the occurrence of an anomalous error P_{an} (the transmission reliability criterion). Calculation methods are given, and formulae are presented. The analysis provides a framework for determining threshold signals and optimum modulation parameters.

'Information-transmission accuracy and reliability of analogue wide-band modulation systems in the presence of fluctuation noise', A. F. Fomin, *Telecommunications and Radio Engineering* (English edition of *Elektrosvyaz* and *Radiotekhnika*), **21**, No. 4, pp. 65–71, April 1966.

TRANSISTOR RELIABILITY

A very important cause of failures is believed to be the thermal action: low allowable temperature and small heat capacity are the primary causes of this difficulty.

A Japanese paper investigates the failure mechanism of transistors under steady (d.c.) electrical power and also under pulsed conditions. A method is proposed to use forward-potential sampling of the junction as a means of obtaining the transient junction temperature rise. The conditions for secondary breakdown are studied in connection with the transient thermal resistance.

'Transient junction temperature rise and failure energy of transistors', Keiji Takagi and Kunio Mano, *Electronics and Communications in Japan* (English edition of *Denki Tsushin Gakkai Zasshi*), **48**, No. 10, pp. 33–41, October 1965.

NON-LINEAR THEORY FOR DISTRIBUTED AMPLIFIERS

A general non-linear theory of travelling-wave amplifiers using non-linear susceptances and negative non-linear conductances, is presented. The theory is constructed for the case of weak growth of the wave along the system, and then its results are sharpened by the method of successive approximations. The theory is extended to the case of tunnel-circuit travelling-wave amplifiers up to the first approximations. Tunnel circuits are considered whose oscillatory characteristics belong to soft body and hard excitation conditions. The effect of line losses is taken into account in the calculations.

'Non-linear theory of negative-conductance travelling-wave amplifiers', Yu. P. Voloshchenko and V. A. Malyshev, *Radio Engineering and Electronic Physics* (English edition of *Radiotekhnika i Elektronika*), **11**, No. 4, pp. 598–606, April 1966.

ATMOSPHERIC DUCTS AND MICROWAVE FADING

A Japanese paper describes radiometeorological observations of the vertical structure of the lower atmosphere made by the use of the remote recording mercury thermometers installed along a 300 m high tower. Variations with time of ducts and the refractive index gradient of the atmosphere were measured as well as the fine structure of the occurrence and disappearance of ducts. Measurement of microwave fading was made in parallel to the radiometeorological observations. Fading occurred with very close relation to the atmospheric duct and particularly remarkable effects of duct and path height on fading were observed. The analyses of the measured data presented detailed information for the analysis of the fading occurrence mechanism.

'Experimental studies on atmospheric ducts and microwave fading', Fumio Ikegami, Minoru Haga, Takayuki Fukuda and Haruhiko Yoshida, *Review of the Electrical Communication Laboratory, N.T.T.*, **14**, Nos. 7–8, pp. 505–33, July–August 1966.

SUBJECT INDEX

Papers and major articles are denoted by printing the page numbers in bold type.

INDEX OF PERSONS

Names of authors of papers published in the volume are indicated by bold numerals for the page reference.
Authors of papers which are given in abstract form are denoted by A.
Biographical references are denoted by B.
Contributors to discussion are indicated by D.

INDEX OF ABSTRACTS

This index classifies under subject headings the abstracts published throughout the volume in "Radio Engineering Overseas" and the summaries of papers scheduled for presentation at the Conference on Electronic Engineering in Oceanography.

Navigational Aids

Propagation

Radar

Reliability

Semiconductors

Sonar and Acoustical Measurements

Telemetry

Television

JOURNALS FROM WHICH ABSTRACTS HAVE BEEN TAKEN DURING THE SECOND HALF OF 1966

Archiv der Elektrischen Übertragung (Germany)
E.B.U. Review (Switzerland)
Electronics and Communications in Japan
(English language edition of *Denki Tsushin Gakkai Zasshi*)
Nachrichtentechnische Zeitschrift (Germany)
L'Onde Electrique (France)
Proceedings of the Institution of Radio and Electronics Engineers, Australia
Radio Engineering and Electronic Physics
English language edition of *Radiotekhnika i Elektronika* (U.S.S.R.)
Review of the Electrical Communication Laboratory, N.T.T. (Japan)
Slaboproudý Obzor (Czechoslovakia)
Telecommunications and Radio Engineering
(Translation of *Elektrosvyaz i Radiotekhnika*) (U.S.S.R.)